To be submitted to ApJ, 2017 January 02
Preprint typeset using LaTeX style AASTeX6 v. 1.0

arXiv:1701.00490v1 [astro-ph.SR] 2 Jan 2017

PHOTOMETRY AND PROPER MOTIONS OF M, L, AND T DWARFS FROM THE Pan-STARRS1 3π SURVEY

William M. J. Best[1], Eugene A. Magnier[1], Michael C. Liu[1], Kimberly M. Aller[1], Zhoujian Zhang[1], W. S. Burgett[2], K. C. Chambers[1], P. Draper[3], H. Flewelling[1], N. Kaiser[1], R.-P. Kudritzki[1], N. Metcalfe[3], J. L. Tonry[1], R. J. Wainscoat[1], C. Waters[1]

[1]Institute for Astronomy, University of Hawaii, 2680 Woodlawn Drive, Honolulu, HI 96822, USA; wbest@ifa.hawaii.edu

[2]GMTO Corporation, 465 N. Halstead St., Suite 250, Pasadena, CA 91107, USA

[3]Department of Physics, Durham University, South Road, Durham DH1 3LE, UK

ABSTRACT

We present a catalog of 9,938 M, L and T dwarfs detected in the Pan-STARRS1 3π Survey (PS1), covering three-quarters of the sky. Our catalog contains nearly all known objects of spectral types L0–T2 in the PS1 field, with objects as early as M0 and as late as T9, and includes PS1, 2MASS, and AllWISE photometry. We have rigorously vetted the association of PS1 measurements to previously identified objects, in particular to detections in the 2MASS and AllWISE surveys. We analyze the different types of photometry reported by PS1, and use two types in our catalog to maximize both depth and accuracy. We systematically assess the quality of the photometry to ensure that the faintest detections in our catalog are real. Using parallaxes from the literature, we construct empirical SEDs for field ultracool dwarfs spanning $0.5 - 12$ μm. We determine typical colors of M0–T9 dwarfs, and we highlight the distinctive colors of subdwarfs and young objects. Our catalog includes 492 L dwarfs detected in $r_{\rm P1}$, the largest sample of L dwarfs detected at such blue wavelengths. We combine astrometry from PS1 (a multi-epoch survey), 2MASS, and Gaia when available to calculate new proper motions for our catalog, achieving a median precision of 3.5 mas yr^{-1}. Our method enables us to merge the PS1 epochs of fast-moving objects ($\mu \gtrsim 200$ mas yr^{-1}) whose detections are split among more than one object in the PS1 database, Overall our catalog contains proper motions for 2,394 M6–T9 dwarfs and includes the largest set of homogeneous proper motions for L and T dwarfs published to date, 409 objects for which there were no previous measurements, and 1,140 objects for which we improve upon previous literature values. We analyze the kinematics of ultracool dwarfs in our catalog and find evidence that bluer but otherwise generic late-M and L field dwarfs (i.e., not subdwarfs) tend to have higher tangential velocities compared to typical field objects. With the public release of the PS1 data, this survey will continue to be an essential tool for characterizing the ultracool dwarf population.

Keywords: brown dwarfs — stars: late-type

1. INTRODUCTION

Ultracool dwarfs (spectral types M6 and later) are the lowest-mass members of the stellar population, encompassing the coolest stars, brown dwarfs, and planetary-mass objects. The discovery of brown dwarfs over 20 years ago launched an understanding of the complex properties and evolution of ultracool atmospheres (e.g., Burrows et al. 2006), and allowed us to constrain the low-mass end of the stellar mass and luminosity functions in the solar neighborhood (Marocco et al. 2015, and references therein). In addition, the youngest (≈10–100 Myr) ultracool dwarfs in the field appear to be our best analogs to directly-imaged giant planets (e.g., Liu et al. 2013b), and they are far easier to observe without the drowning glare of host stars. The major drivers for ultracool discoveries, which now include ≈2,000 L and T dwarfs and many thousands of late-M dwarfs, have been wide-field imaging surveys such as the Deep Near Infrared Survey of the Southern Sky (DENIS, Epchtein et al. 1999), the Sloan Digital Sky Survey (SDSS; York et al. 2000), the Two Micron All Sky Survey (2MASS; Skrutskie et al. 2006), the UKIRT Infrared Deep Sky Survey (UKIDSS; Lawrence et al. 2007), and the Wide-Field Infrared Survey Explorer (*WISE*; Wright et al. 2010).

Large photometric samples obtained from these imaging surveys have provided much of our fundamental knowledge about ultracool dwarfs. Samples of L dwarfs have revealed a surprising diversity of near-IR colors (e.g. Leggett et al. 2002; Knapp et al. 2004; Gizis et al. 2012) which are believed to be caused by variations in surface gravity and/or dusty

clouds (e.g. Kirkpatrick et al. 2008; Allers & Liu 2013a) or thermo-chemical instabilities (Tremblin et al. 2016). Objects transitioning from L to T spectral types undergo a dramatic shift to bluer near-IR colors thought to be driven by the clearing of clouds and the formation of methane (e.g., Burgasser et al. 2002; Chiu et al. 2006; Saumon & Marley 2008). UKIDSS and *WISE* have illustrated the diversity of late-T and Y dwarf near- and mid-IR colors (e.g., Burningham et al. 2010a; Kirkpatrick et al. 2011; Mace et al. 2013), and *WISE* has enabled us to discover the coolest known substellar objects (e.g., Cushing et al. 2011; Kirkpatrick et al. 2012; Luhman 2014). Large samples have revealed the mass and luminosity functions of the local ultracool population (e.g., Allen et al. 2005; Cruz et al. 2007; Burningham et al. 2010a), while measurements of the space density of brown dwarfs (e.g. Reid et al. 2008; Metchev et al. 2008) have identified a relative paucity of L/T transition dwarfs indicating that this evolutionary phase is short-lived and have given us contraints on the birth history of substellar objects (e.g., Day-Jones et al. 2013; Marocco et al. 2015). The surveys have also enabled brown dwarf searches in star-forming regions (e.g., Lodieu et al. 2009; Martín et al. 2010), important for determination of the substellar IMF. Photometric samples encompassing more than one survey have enabled us to determine well-constrained ultracool colors across a broad range of wavelengths (e.g., Schmidt et al. 2015; Skrzypek et al. 2015), and to measure bolometric luminosities that give us effective temperatures and constraints on atmospheric and evolutionary models (e.g. Leggett et al. 2002; Golimowski et al. 2004).

Similarly, large samples of proper motions have contributed significantly to our discovery and understanding of the ultracool population. Proper motions have enabled searches to distinguish ultracool dwarfs from distant luminous red objects such as giants and galaxies (e.g., Kirkpatrick et al. 2000; Theissen et al. 2016) and to detemine whether individual discoveries are members of star-forming regions (e.g., Lodieu et al. 2007a, 2012a). Proper motions have helped to find objects in crowded areas of the sky such as the Galactic plane (e.g., Luhman 2013; Smith et al. 2014b). and to identify ultracool dwarfs with atypical colors that were missed by color cuts used in photometry-only searches (e.g., Kirkpatrick et al. 2010). Several studies have found clear evidence for cold (slow-moving) and hot (fast-moving) dynamical populations of ultracool dwarfs that are consistent with the thin disk and and thick disk/halo populations (e.g., Faherty et al. 2009; Schmidt et al. 2010; Dupuy & Liu 2012), implying that ultracool dwarfs form in the same manner as hotter stars. Searches for high-proper motion objects, often using surveys with shorter time baselines, have identified rare fast-moving objects that are typically members of the older, low-metallicity populations (e.g., Jameson et al. 2008; Smith et al. 2014a; Kirkpatrick et al. 2014) or very nearby, previously overlooked objects (e.g., Luhman & Sheppard 2014; Luhman 2014; Schneider et al. 2016a; Kirkpatrick et al. 2016). Proper motions measured from the large surveys have enabled us to identify the substellar members of nearby young moving groups (e.g., Gagné et al. 2015b,c; Faherty et al. 2016; Liu et al. 2016), a population crucial to our understanding of brown dwarf evolution over their first few hundred million years. Proper motions from large catalogs have also identified wide comoving companions to higher-mass stars whose ages and metallicities can more easily be determined (e.g., Zhang et al. 2013; Luhman et al. 2012; Burningham et al. 2013; Smith et al. 2014b), making the ultracool companions important benchmarks for constraining atmospheric and evolutionary models.

The Panoramic Survey Telescope And Rapid Response System (Pan-STARRS1) is a large multi-epoch, multi-wavelength, optical imaging survey using a 1.8-m wide-field telescope on Haleakala, Maui (Kaiser et al. 2010). The Pan-STARRS1 3π Survey (PS1; K. C. Chambers et al., 2017, in prep) observed the entire sky north of $\delta = -30°$ (three-quarters of the sky) in five filters ($g_{\rm P1}r_{\rm P1}i_{\rm P1}z_{\rm P1}y_{\rm P1}$) over four years (2010 May – 2014 March), imaging the survey area ≈12 times in each filter. PS1 images are ∼1 mag deeper in z-band than the most comparable optical survey to date (SDSS), and the novel $y_{\rm P1}$ filter (0.918−1.001 μm) extends further toward the near-infrared than previous optical surveys. This long-wavelength sensitivity allows PS1 to better detect and characterize red objects such as ultracool dwarfs. In addition, the multi-epoch astrometry of PS1 enables precise measurement of proper motions and parallaxes that help to distinguish faint, nearby ultracool dwarfs from reddened background stars and galaxies.

Significant ultracool discoveries from PS1 include many wide ultracool companions to main sequence stars (Deacon et al. 2012a,b, 2014) and young stars (Aller et al. 2013), L/T transition dwarfs that are difficult to identify with near-IR photometry alone (Deacon et al. 2011; Best et al. 2013, 2015), new low-mass members of the Hyades (Goldman et al. 2013) and Praesepe (Wang et al. 2014a), and new brown dwarf members of nearby young moving groups (Liu et al. 2013b; Aller et al. 2016). PS1 has also enabled studies with large samples of more massive stars, including fiducial sequences of Galactic star clusters (Bernard et al. 2014), proper motions and wide binaries in the *Kepler* field (Deacon et al. 2016, who also present SEDs for spectral types B9V through M9V in the PS1 photometric system), and photometric distances and reddening for all stars detected by PS1 (Green et al. 2014; Schlafly et al. 2014). PS1 can detect ultracool dwarfs at larger distances than SDSS and 2MASS, so its optical photometry helps to create a rich multi-color catalog that will enable even bigger searches based solely on photometry, a precursor to LSST science. In addition, the proper motions and parallaxes in PS1 should be fertile ground for identifying more ultracool dwarfs that

have eluded detection due to their locations in crowded areas of the sky (e.g., Liu et al. 2011), or are too red to be measured by *Gaia*.

In this paper we present a comprehensive catalog of ultracool dwarfs observed by PS1, including photometry, proper motions, spectral types, gravity classifications, and multiplicity. Section 2 describes the contents and assembly of our catalog. The PS1 photometry and proper motions are discussed in detail in Sections 3 and 4, respectively. We briefly describe a binary M7 dwarf newly identified by PS1 in Section 5. We summarize our catalog and its features in Section 6.

2. CATALOG

Our catalog of ultracool dwarfs in Pan-STARRS1 contains photometry and proper motions from PS1 for 9,938 M, L, and T dwarfs, along with photometry from 2MASS and AllWISE whenever available. The catalog includes all published L and T dwarfs as of 2015 December with photometry in at least one of the five PS1 bands ($g_{\rm P1}r_{\rm P1}i_{\rm P1}z_{\rm P1}y_{\rm P1}$). The catalog does not contain all known M dwarfs, but includes a large sample in order to accurately represent the colors and kinematics of M dwarfs in PS1.

We describe the construction of our catalog in Section 2.1. In Sections 2.2 and 2.3, we provide more details about our selection of L+T and M dwarfs, respectively. In Section 2.4, we discuss the spectral types used in our catalog. We describe our identification of young objects in Section 2.5 and our treatment of binaries in Section 2.6. In Section 2.7 we assess the completeness of our catalog.

2.1. *Construction*

To create our catalog, we compiled a list of late-M, L and T dwarfs from DwarfArchives[1], M dwarfs from West et al. (2008), and numerous literature sources from 2012–2016. We included positions, proper motions, spectral types, and photometry from 2MASS (Cutri et al. 2003) and AllWISE (Cutri et al. 2014) when available. We also tracked objects identified as binaries and those with spectroscopic or other indications of youth. The catalog includes new discoveries through 2015 December and a handful of updates to photometry, astrometry, and spectral types from 2016.

In order to ensure that every object in our catalog is a bona fide M, L, or T dwarf, we included only published objects with spectroscopic classification. We have therefore excluded objects with only photometric spectral types. Our catalog also does not include close substellar companions to main sequence stars detected by high-angular resolution imaging and/or radial velocity because these objects are not resolved in PS1.

We cross-matched our list with the full PS1 Processing Version 3 database (PV3, August 2016, the final reprocessing of PS1 data prior to public release) by position using a 3" matching radius, retaining the closest object matched in PV3. In order to maximize the number of accurate matches, we used PS1 positions published in the literature (from earlier processing versions) or AllWISE positions (nearly contemporaneous with PS1) whenever possible for the objects in our list. If neither of those were available, we used the most recent positions reported in the literature (frequently these came from 2MASS, SDSS, or UKIDSS). If these objects had reported proper motions, we used the proper motions to project expected PS1 coordinates and used those for our cross-match.

To ensure that our catalog contains only secure PS1 measurements of real astrophysical objects, we applied photometric quality cuts described in detail in Section 3.1.1. Briefly, we required our PS1 matches to have photometric errors less than 0.2 mag in at least one PS1 band, with detections at two or more epochs in that band, and we exclude objects likely to be saturated in all bands. In addition, we excluded any sources marked as quasars, transients, periodic variables, or solar system objects in the PS1 database, as well as any sources flagged as having poor PSF fits (`psf_qf` < 0.85). Any object without a PS1 match within 3" of the expected coordinates was removed from our catalog.

To check for incorrect matches, we calculated colors using the 2MASS and AllWISE photometry from our list and the PS1 photometry for our matches (Section 3.2). We sorted our list into bins of one spectral sub-type, and inspected every object with a $g_{\rm P1}-y_{\rm P1}$, $r_{\rm P1}-i_{\rm P1}$, $r_{\rm P1}-z_{\rm P1}$, $r_{\rm P1}-y_{\rm P1}$, $i_{\rm P1}-z_{\rm P1}$, $i_{\rm P1}-y_{\rm P1}$, $z_{\rm P1}-y_{\rm P1}$, $y_{\rm P1}-J_{\rm 2MASS}$, or $y_{\rm P1}-W1$ color differing from the median for its spectral type by more than 3 times the rms color for that spectral type bin. We also inspected every T dwarf with a reported $g_{\rm P1}$, $r_{\rm P1}$, or $i_{\rm P1}$ detection. In addition, since the cool temperatures of M, L, and T dwarfs necessitate reddish PS1 (optical) colors, we inspected all objects having a secure detection in a bluer band but not in a redder band (e.g., in $i_{\rm P1}$ but not in $z_{\rm P1}$). To inspect an object, we examined stacked images from PS1, 2MASS, and AllWISE, and searched in all three surveys within a 60" radius around the PS1 position for other

[1] Hosted at http://DwarfArchives.org. Last updated 2013-05-29.

possible matches. We discarded PS1 matches for which the detection was clearly contaminated by an image artifact, a nearby brighter star, or a blue or extended background object. In cases where contamination affected some but not all of the PS1 bands, we retained the object in our catalog and rejected photometry only from the contaminated bands (all g_{P1} and r_{P1} detections of T dwarfs were discarded in this manner). We corrected a match when the images and colors clearly pointed to a different PS1 source, but we did not make corrections in ambiguous cases in order to minimize rejection of objects with naturally-occurring unusual photometry.

For most outliers we found nothing to indicate the object was anything other than an object with unusual colors. Many red outliers were young objects in star-forming regions and/or with low gravity spectral classifications, both associated with redder-than-typical colors for L dwarfs (e.g., Faherty et al. 2013). We discovered a few cases in which the 2MASS or AllWISE photometry was for a different nearby object, often a brighter source with which the ultracool object was blended. In the case of blends we rejected the 2MASS or AllWISE photometry; otherwise we corrected the photometry to the right object.

2.2. *L and T Dwarfs*

Although ultracool dwarfs are normally brightest in the near-infrared, the depth and red-optical sensitivity of Pan-STARRS1 have allowed PS1 to detect 1,607 L and T dwarfs, including spectral types as late as T9. Barring unintentional omissions, our catalog contains all spectroscopically confirmed L and T dwarfs published through 2015 December and meeting our detection standards in PS1. The L and T dwarfs in our catalog are primarily drawn from DwarfArchives and Mace (2014), supplemented by other literature sources. The final catalog includes 1,257 L dwarfs and 350 T dwarfs.

2.3. *M Dwarfs*

M dwarfs comprise the majority of the stars in our galaxy, so a clear understanding of M dwarf properties is essential for characterizing the local stellar population and constraining models of star formation and evolution. In addition, M dwarfs provide context for the photometric and kinematic properties of L and T dwarfs, and more massive brown dwarfs younger than ∼200 Myr will have late-M spectral types. Compiling a complete list of known M dwarfs would require an effort far beyond what is needed to accurately characterize the PS1 photometry and proper motions of the nearby field population. Instead, we built a representative sample of the field population from two sub-samples.

The first sub-sample comprises objects with well-studied and/or potentially distinctive photometry and kinematics from the recent literature, and contains 457 M6–M9 dwarfs. These objects were included in order to sample the diversity of colors and kinematics in late-M dwarfs. We included M dwarfs from the proper motion and parallax compilations of Faherty et al. (2009, 2012) and Dupuy & Liu (2012), the young object list from Allers & Liu (2013a), the young moving group members and non-members from Gagné et al. (2015c), the SpeX-observed catalog of Bardalez Gagliuffi et al. (2014, identifying spectral blends), and wide ultracool companions to main sequence stars from Deacon et al. (2014).

The second sub-sample is a large set of M dwarfs with high-quality photometry, representative of the generic field population. We cross-matched all M0–M9 dwarfs listed in the catalog of West et al. (2008) with PS1, 2MASS, and AllWISE using a matching radius of 5″. We required sources to have photometric errors < 0.05 mag in at least five of the eight total PS1 and 2MASS bands ($grizyJHK$), and at least two detections in individual exposures in each PS1 band. To avoid saturated objects, we rejected any sources brighter than the limits listed in Section 3.1.2 or flagged by PS1 for poor PSF fits (`psf_qf` < 0.85). In addition, we excluded any sources marked by PS1 as quasars, transients, periodic variables, or solar system. We then removed objects with non-zero confusion, saturation, extendedness, or de-blending flags in either 2MASS or AllWISE. These cuts are more stringent than for the late-M, L and T dwarfs in our catalog in order to ensure a very clean field M dwarf sample with high-quality photometry. This sub-sample contains 7,874 M dwarfs from West et al. (2008), bringing the total for M dwarfs in our catalog to 8,331.

2.4. *Spectral Types*

For the objects in our catalog, we use spectral types from the literature. These spectral types were determined by a variety of methods, based on visual or numerical analysis of red-optical ($\approx 0.65 - 1$ μm) or near-infrared ($\approx 1 - 2.5$ μm) spectra. In cases where an object has both an optical and a near-IR spectral type, we adopt the optical type for M and L dwarfs and the near-IR type for T dwarfs. The spectral types for the M dwarfs drawn from West et al. (2008) were all derived from optical spectra.

There are seven objects in our catalog with an optical L type and a near-IR T type. For these we use the T spectral type (all T0–T1). All seven objects show clear methane absorption at 1.6 μm and/or 2.2 μm in their near-IR spectra, a

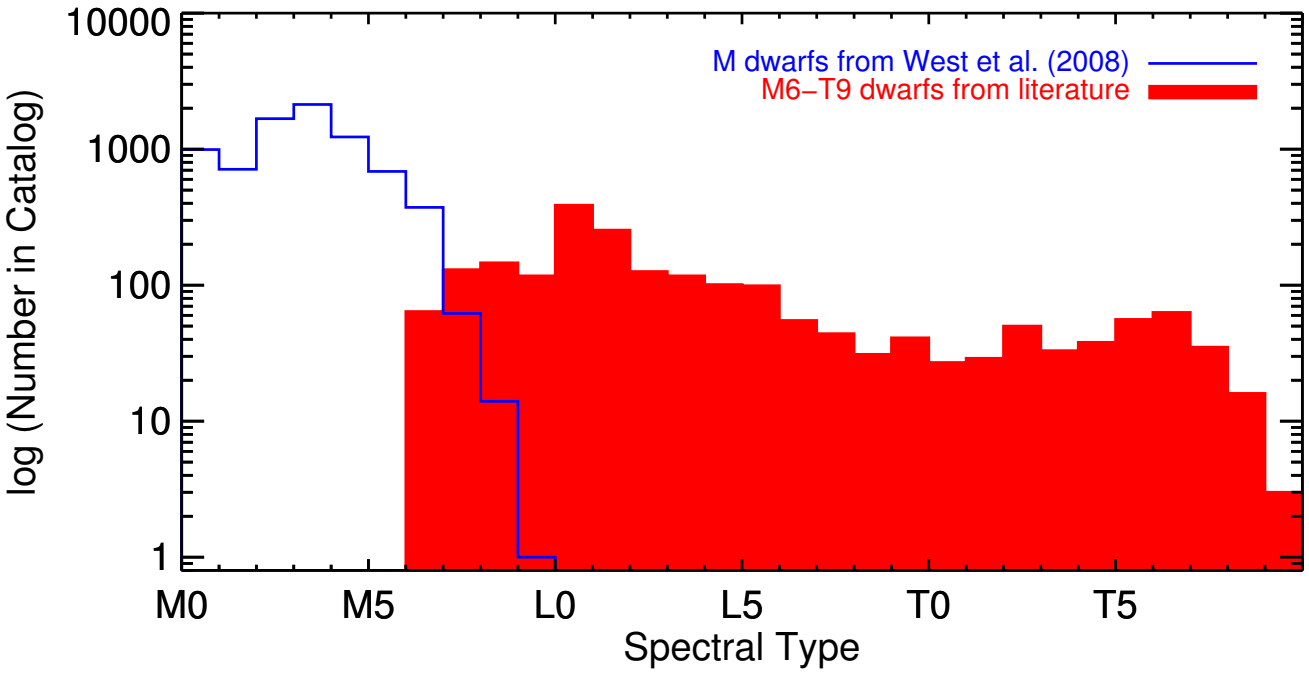

Figure 1. The distribution of spectral types in our catalog. The late-M, L and T dwarfs compiled from the literature are shown in solid red, while the M dwarfs from West et al. (2008) are shown with a blue outline. The catalog robustly samples the temperature range of all but the coolest brown dwarfs, and includes objects with spectral types as late as T9.

hallmark of T dwarfs. We note that these objects are all confirmed binaries (by high-resolution imaging) or candidate binaries (based on peculiar spectra) with components spanning the L/T transition. The spectral types are therefore based on unresolved spectral blends, explaining the disagreement between the optical and near-IR types.

We show the distribution of all spectral types in our catalog in Figure 1. The earliest type in our catalog is M0 (by construction), and the latest spectral type detected by PS1 in T9. Our catalog contains more than 20 objects of each spectral sub-type through T7, robustly sampling the brown dwarf population for all but the coolest objects. We compare the distribution of L and T dwarfs in our catalog to all L and T dwarfs in the PS1 field (north of $\delta = -30°$) in Figure 2. The known objects not present in our catalog are mostly later-T dwarfs too faint to be detected by PS1. These have chiefly been discovered by deeper near-IR searches over narrower fields (e.g., Albert et al. 2011; Burningham et al. 2013) or by searches for late-T and Y dwarfs using *WISE* (e.g., Kirkpatrick et al. 2011). The ≈30 L dwarfs not detected by PS1 are mostly unresolved companions to higher-mass stars or discoveries from deep imaging of star-forming regions.

2.5. *Young Objects*

Our catalog includes many young objects (ages $\lesssim$ 200 Myr), which are known to have distinctive colors and kinematics (e.g., Kirkpatrick et al. 2008; Faherty et al. 2009). We identify young objects primarily by low-gravity classifications reported in the literature: β, γ, and δ classes based on optical (Kirkpatrick 2005; Cruz et al. 2009) or near-IR (Gagné et al. 2015c) spectra, and INT-G and VL-G based on near-IR spectra (Allers & Liu 2013a). We also identify any object known to be in a star-forming region as young. In addition, we include objects in our young sample that lack formal low-gravity classifications but have other evidence for youth: NLTT 13728, LP 423-31, and 2MASS J19303829−1335083 (Shkolnik et al. 2009), 2MASS J06195260−2903592 (Allers & Liu 2013a), LSPM J1314+1320 (Schlieder et al. 2014), 2MASS J17081563+2557474 (Kellogg et al. 2015), and 2MASS J22344161+4041387 (Allers et al. 2009) show spectroscopic signs of low gravity; SDSSp J111010.01+011613.1 (Gagné et al. 2015a) and WISEA J114724.10−204021.3 (Schneider et al. 2016b) are members of young moving groups; and 2MASSW J0951054+355801 (Reid & Walkowicz 2006) and Gl 417BC (Kirkpatrick et al. 2001a) are wide companions to young stars.

2.6. *Binaries*

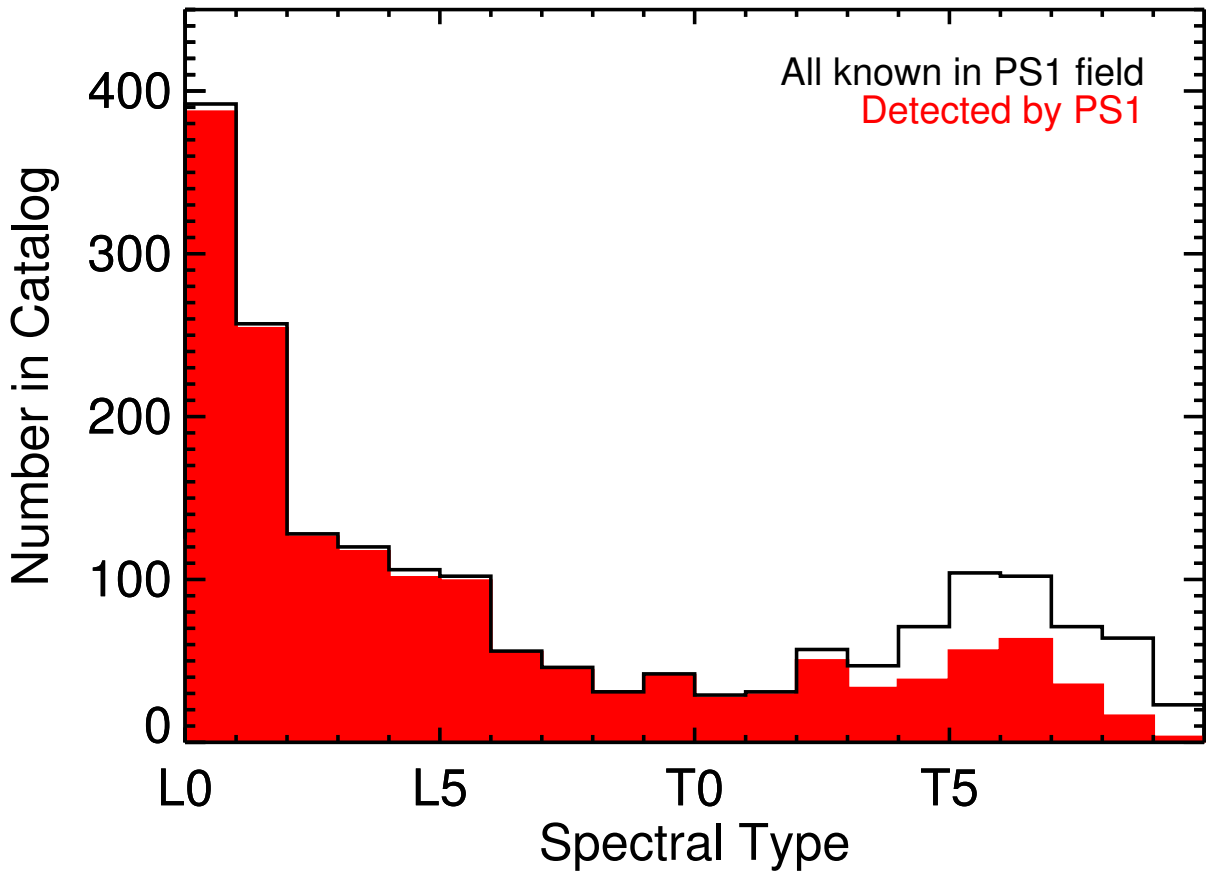

Figure 2. The distribution of L and T spectral types in our catalog, compared to all known L and T dwarfs in the PS1 field. PS1 has detected nearly all previously-known L dwarfs; the handful of non-detections are mostly faint objects in star-forming regions or unresolved companions to higher-mass stars. The T dwarfs (mostly later-type) not detected by PS1 have primarily been discovered by deeper near-IR searches over narrower fields or in the mid-IR using the *WISE* survey.

Our catalog naturally includes ultracool binaries with separations wide enough to be resolved in PS1, as well as many that are unresolved. For resolved binaries, we report the photometry and proper motion for each component individually. We treat unresolved binaries as single objects, reporting their blended photometry. Our catalog contains a single instance of a binary resolved in PS1 and 2MASS, but not in AllWISE: UScoCTIO 108 and UScoCTIO 108b. For this pair, we report AllWISE photometry (blended) only for the primary, and no AllWISE photometry for the secondary.

In our catalog, we identify only binaries confirmed by high-resolution imaging or radial velocity measurements. Peculiar spectral features have been used to identify candidate unresolved binaries (Burgasser et al. 2010a; Bardalez Gagliuffi et al. 2014), but this technique has not been demonstrated to robustly distinguish actual blends from single objects with unusual atmospheric properties. Given our conservative approach, we expect our catalog to contain some unidentified binaries.

2.7. *Completeness*

Our catalog is a combination of discoveries from many searches for M, L, and T dwarfs, conducted using a variety of methods and instruments and therefore containing a variety of biases. Our selection of a representative sample of M dwarfs means that our catalog will be far from complete for this spectral type, especially for types M0–M5 for which we include only bright objects. While we have included all known L and T dwarfs observed by PS1, there are some L and T dwarfs beyond the detection limit or angular resolution of PS1 (Figure 2), and there are sure to be undiscovered objects remaining in the PS1 field.

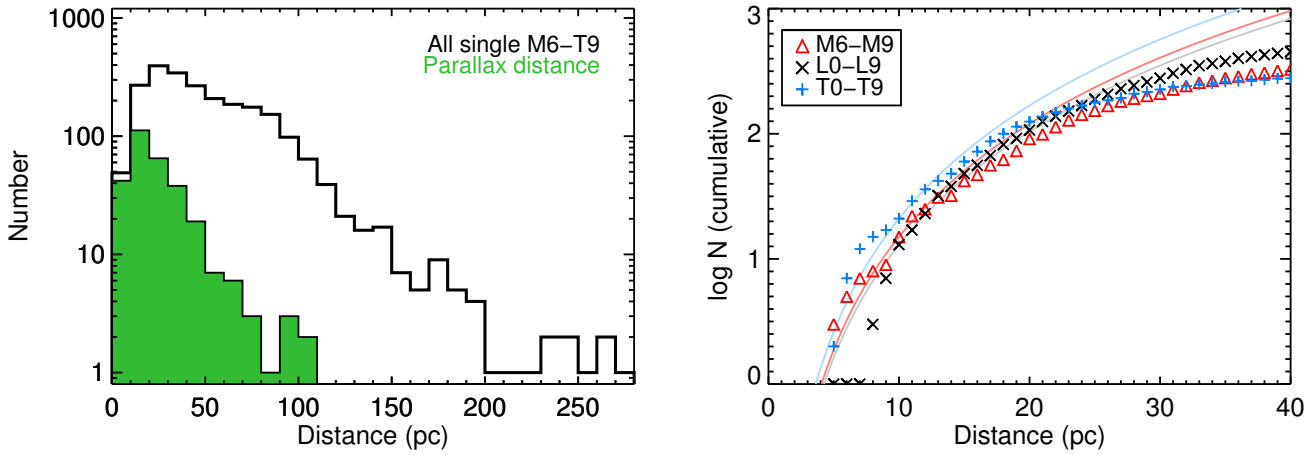

Figure 3. *Left*: Distribution of the distances of single M6–T9 dwarfs in our catalog (black outline). Where available, we use a parallax distance from the literature (solid green); for other objects we use $W2$-based photometric distances. *Right*: Cumulative distribution of these distances for M (red triangles), L (black × symbols), and T (blue + symbols) dwarfs, using a format similar to Figure 5 in Faherty et al. (2009). The curves indicate constant density distributions ($N \propto d^3$) normalized at 10 pc, with light red, grey, and blue lines for M, L, and T dwarfs, respectively. Our catalog is not consistent with a constant density distribution beyond 10 pc for late-M and T dwarfs and 20 pc for L dwarfs, implying that our catalog is incomplete beyond these distances.

We assess the completeness of our catalog for spectral types M6–T9 by examining the number of objects as a function of distance, shown in Figure 3. We use trigonometric parallax distances when available from the literature. For the remaining objects we used photometric distances calculated from $W2$ magnitudes and the spectral type-absolute magnitude polynomial from Dupuy & Liu (2012). Photometric distances for binaries are not expected to be accurate, so we exclude known binaries from our assessment. Figure 3 also compares the cumulative distributions of late-M, L, and T dwarf distances to constant density distributions ($N \propto d^3$) normalized at 10 pc. The distances begin to deviate from constant density distributions beyond ≈10 pc for late-M and T dwarfs and ≈20 pc for L dwarfs, implying that our catalog is not volume-complete beyond these distances. However, given the comprehensiveness of our catalog, the properties of colors and proper motions we present in this paper should still be illustrative of local ultracool dwarfs.

3. PHOTOMETRY

We present the PS1, 2MASS, and AllWISE photometry for our catalog in Table 1. PS1 photometry is on the AB magnitude scale (Tonry et al. 2012), calibrated using the procedures outlined in Schlafly et al. (2012) and (Magnier et al. 2013). 2MASS and AllWISE photometry are calibrated on the Vega magnitude scale (Cohen et al. 2003; Wright et al. 2010, respectively).

The full table contains 46 columns, and is available for download in electronic form in the online journal. Table 1 is arranged in two parts: (1) the late-M, L, and T dwarfs compiled from the literature, followed by (2) the M dwarfs from West et al. (2008). For reference, Table 1 includes spectral types (with notation for subdwarfs), and indicates whether an object has been classified as a low-gravity object based on its optical or near-IR spectrum, identified as a young object (due to low gravity or other reasons), or identified as a binary. Table 2 shows a sample of the rows and columns of Table 1 for guidance regarding format and content.

Table 1. Photometry of M, L, and T Dwarfs in the Pan-STARRS1 3π Survey

Column	Label	Description
1	Name	Name used in the object's discovery or spectral confirmation paper
2	Spectral Type: Opt	Optical spectral type[a,b]
3	Spectral Type: NIR	Near-infrared spectral type[a,b]
4	Spectral Type: Adopted	Adopted spectral type[a,b]
5	Gravity: Opt	Low-gravity classification from an optical spectrum[b]

Table 1 continued on next page

Table 1 *(continued)*

Column	Label	Description
6	Gravity: NIR	Low-gravity classification from a near-infrared spectrum[b]
7	Binary	"Y" or "triple" for known binary or triple systems not resolved in PS1
8	Young	"Y" for known young objects[c]
9	Pan-STARRS1 Name	PS1 Designation[d], rrr.rrrr+dd.dddd (J2000)
10	$g_{\rm P1}$	PS1 g magnitude
11	$\rm err_{g_{P1}}$	Error in PS1 g magnitude
12	N_g	Number of measurements used in the $g_{\rm P1}$ photometry
13	$\rm S_g$	Source of the $g_{\rm P1}$ photometry: chip (C), recalculated chip[e] (R), or forced warp (W)
14	$r_{\rm P1}$	PS1 r magnitude
15	$\rm err_{r_{P1}}$	Error in PS1 r magnitude
16	N_r	Number of measurements used in the $r_{\rm P1}$ photometry
17	$\rm S_r$	Source of the $r_{\rm P1}$ photometry: chip (C), recalculated chip[e] (R), or forced warp (W)
18	$i_{\rm P1}$	PS1 i magnitude
19	$\rm err_{i_{P1}}$	Error in PS1 i magnitude
20	N_i	Number of measurements used in the $i_{\rm P1}$ photometry
21	$\rm S_i$	Source of the $i_{\rm P1}$ photometry: chip (C), recalculated chip[e] (R), or forced warp (W)
22	$z_{\rm P1}$	PS1 z magnitude
23	$\rm err_{z_{P1}}$	Error in PS1 z magnitude
24	N_z	Number of measurements used in the $z_{\rm P1}$ photometry
25	$\rm S_z$	Source of the $z_{\rm P1}$ photometry: chip (C), recalculated chip[e] (R), or forced warp (W)
26	$y_{\rm P1}$	PS1 y magnitude
27	$\rm err_{y_{P1}}$	Error in PS1 y magnitude
28	N_y	Number of measurements used in the $y_{\rm P1}$ photometry
29	$\rm S_y$	Source of the $y_{\rm P1}$ photometry: chip (C), recalculated chip[e] (R), or forced warp (W)
30	2MASS Name	2MASS catalog designation
31	J	J magnitude or upper limit (2MASS)
32	$\rm err_J$	Error in J magnitude
33	H	H magnitude or upper limit (2MASS)
34	$\rm err_H$	Error in H magnitude
35	K_S	K_S magnitude or upper limit (2MASS)
36	$\rm err_{K_S}$	Error in K_S magnitude
37	AllWISE Name	AllWISE catalog designation
38	$W1$	$W1$ magnitude or upper limit (AllWISE)
39	$\rm err_{W1}$	Error in $W1$ magnitude
40	$W2$	$W2$ magnitude or upper limit (AllWISE)
41	$\rm err_{W2}$	Error in $W2$ magnitude
42	$W3$	$W3$ magnitude or upper limit (AllWISE)
43	$\rm err_{W3}$	Error in $W3$ magnitude
44	$W4$	$W4$ magnitude or upper limit (AllWISE)
45	$\rm err_{W4}$	Error in $W4$ magnitude
46	References	References: Discovery, Spectral Type, Gravity, Binarity, 2MASS photometry, AllWISE photometry

Table 1 continued on next page

Table 1 *(continued)*

Column	Label	Description

[a] Spectral types taken from the literature (Section 2.4). When both optical and near-IR types are available, we adopt the optical type for M and L dwarfs and the near-IR type for T dwarfs. Most spectral types have an uncertainty of ±0.5 subtypes; ":" = ±1 subtype; "::" = ±2 or more subtypes. "sd" = subdwarf; "esd" = extreme subdwarf (Gizis 1997).

[b] β, γ, and δ indicate classes of increasingly low gravity based on optical (Kirkpatrick 2005; Cruz et al. 2009) or near-infrared (Gagné et al. 2015c) spectra. FLD-G indicates near-infrared spectral signatures of field-age gravity, INT-G indicates intermediate gravity, and VL-G indicates very low gravity (Allers & Liu 2013a).

[c] Young objects identified by low-gravity classifications or other spectroscopic evidence for youth, membership in star-forming regions or young moving groups, or companionship to a young star (Section 2.5).

[d] Pan-STARRS names are from the 3π Survey, Processing Version 3 (PV3), unless the object has a previously published Pan-STARRS designation. Photometry listed here is from PV3 and supersedes values given in previous publications.

[e] Chip photometry recalculated by combining the measurements for an object that is split into two or more "partial objects" in PS1 (Sections 3.1.5 and 4.1.3).

[f] Although classified as FLD-G, the spectrum shows hints of intermediate gravity (as described in Aller et al. 2016).

[g] Photometry rejected for this band after visual inspection of stack images found no detection at the PS1 coordinates.

[h] Photometry rejected for this band after visual inspection of stack images found obvious contamination by a background object.

[i] Photometry rejected for this band after visual inspection of stack images found an image processing artifact at the PS1 coordinates.

[j] Photometry rejected for this band after visual inspection of stack images found obvious contamination from a nearby bright star.

[k] UScoCTIO 108 and UScoCTIO 108b are not resolved in AllWISE. For this binary, we report AllWISE photometry (blended) only for the primary, and no AllWISE photometry for the secondary.

[l] $W3$ photometry for SDSS J004930.00+010704.4 rejected because it is dominated by a diffraction spike.

Note—This table is available in its entirety in machine-readable form in the online journal. A sample of the rows and columns is shown in Table 2.

3.1. *PS1 Photometry*

3.1.1. *Chip and Forced Warp Photometry*

Our catalog uses two types of PSF photometry from the PS1 database: chip and forced warp. These types are described in detail in Magnier et al. (2017, in prep), and we explain them briefly here.

During PS1 data processing, each raw image was individually detrended and calibrated to create a "chip" image, and each detected object on a chip was fitted with a PSF model to determine its photometry and astrometry. The chip pixels were geometrically transformed onto a grid with uniform pixel scale representing pre-defined sky coordinates (R.A. and Decl.), creating "warp" images. The warps for each filter matching the same portions of the sky were then summed together, forming "stack" images. Detections in the stacks were again fit with PSFs to measure photometry and astrometry.

Chip photometry is the mean measurement from all chips in which an object was detected, and is likely to be the most accurate photometry for a well-detected object due to the individual calibration of each chip. Stack photometry is measured from the single fit to a stack detection. Stack photometry will generally be less accurate because individual images forming a stack were taken in varying conditions and at different locations on the Pan-STARRS1 detector, creating poorly-defined PSFs. However, the stacks can identify objects too faint to be detected in indivdual images, as long as the objects do not move significantly over the 4-year time baseline of the survey. To take advantage of the greater depth of the stacks without sacrificing too much of the calibration of the chip images, the PS1 data pipeline force-fit a model PSF on every warp image at the location of each object detected in a stack. This "forced warp photometry" (hereinafter "warp photometry") reported by PS1 is the mean of the fluxes from the force-fit PSF at a given location, excluding cases where the warp pixels were excessively masked. Warp photometry will not have the full accuracy of the chip measurements, but achieves the depth of the stack photometry with more accuracy than the stack image alone. Warp photometry is therefore most useful, at least in theory, for slow-moving objects with magnitudes comparable to or fainter than the chip detection limit.

To quantify where PS1 chip and warp photometry differ significantly, we examined the photometry of a large sample of well-detected objects in PS1 chip images. For each of the five PS1 bands, we extracted the chip and warp magnitudes for all objects having at least three chip detections in a 4 deg^2 patch of sky (centered at $\alpha = 80°$, $\delta = 5°$)

Table 2. Sample of columns in Table 1

Discovery Name	Spectral Type[a,b]			Binary	Young[c]	Pan-STARRS1												References
	Opt	NIR	Adopted			i_{P1} (mag)	$\mathrm{err}_{i_{P1}}$ (mag)	N_i	S_i	z_{P1} (mag)	$\mathrm{err}_{z_{P1}}$ (mag)	N_z	S_z	y_{P1} (mag)	$\mathrm{err}_{y_{P1}}$ (mag)	N_y	S_y	(Disc; SpT; Grav; Bin;) (2MASS; AllWISE)
SDSS J000013.54+255418.6	T5	T4.5	T4.5	···	···	···	···	···	···	19.17	0.01	10	C	17.42	0.01	11	C	168; 236,48; –; –; 84; –
SDSS J000112.18+153535.5	···	L3.7 INT-G	L3.7 INT-G	···	Y	20.37	0.01	13	C	18.85	0.02	7	C	17.81	0.01	10	C	168; 117; 117; –; 84; 85
WISEA J000131.93−084126.9	···	L1 pec (blue)	L1 pec (blue)	···	···	20.21	0.03	7	C	18.57	0.01	12	C	17.57	0.01	10	C	208; 208; –; –; 84; 85
SDSS J000250.98+245413.8	···	L5.5	L5.5	···	···	22.30	0.08	11	W	20.30	0.04	9	W	19.31	0.03	16	W	70; 70; –; –; 84; 85
2MASSI J0003422−282241	M7.5	M7: FLD-G	M7.5	···	···	16.77	0.01	7	C	15.43	0.01	6	C	14.67	0.01	6	C	79; 79,11; 11; –; 84; 85
2MASS J00044144−2058298	M8	···	M8	···	···	16.41	0.01	8	C	14.94	0.01	5	C	14.06	0.01	7	C	153; 154; –; –; 84; 85
2MASS J00054844−2157196	M9	···	M9	···	···	17.11	0.01	3	C	15.69	0.01	10	C	14.84	0.01	8	C	260; 258; –; –; 84; 85
ULAS J000613.24+154020.7	···	L9	L9	···	···	···	···	···	···	21.05	0.08	5	C	19.87	0.06	9	C	90; 90; –; –; –; 85
SDSS J000614.06+160454.5	L0	···	L0	···	···	20.75	0.02	18	W	19.23	0.01	9	C	18.30	0.01	9	C	321; 321; –; –; 84; 85

References—(1) This work, (2) Aberasturi et al. (2014), (3) Aganze et al. (2016), (4) Albert et al. (2011), (5) Allen et al. (2007), (6) Allen et al. (2012), (7) Aller et al. (2013), (8) Aller et al. (2016), (9) Allers et al. (2009), (10) Allers et al. (2010), (11) Allers & Liu (2013a), (12) Allers & Liu (2013b), (13) Alves de Oliveira et al. (2013), (14) Artigau et al. (2006), (15) Artigau et al. (2011), (16) Bardalez Gagliuffi et al. (2014), (17) Bardalez Gagliuffi et al. (2015), (18) Baron et al. (2015), (19) Barrado Y Navascués et al. (2002), (20) Basri et al. (2000), (21) Beamín et al. (2013), (22) Becklin & Zuckerman (1988), (23) Béjar et al. (2008), (24) Bessell (1991), (25) Best et al. (2013), (26) Best et al. (2015), (27) Bihain et al. (2010), (28) Bihain et al. (2013), (29) Boeshaar (1976), (30) Boudreault & Lodieu (2013), (31) Bouvier et al. (2008), (32) Bouy et al. (2003), (33) Bowler et al. (2010), (34) Bowler et al. (2013), (35) Burgasser et al. (1999), (36) Burgasser et al. (2000b), (37) Burgasser et al. (2000a), (38) Burgasser et al. (2002), (39) Burgasser et al. (2003a), (40) Burgasser et al. (2003e), (41) Burgasser et al. (2003c), (42) Burgasser et al. (2003b), (43) Burgasser et al. (2003d), (44) Burgasser (2004), (45) Burgasser et al. (2004), (46) Burgasser et al. (2005b), (47) Burgasser et al. (2005a), (48) Burgasser et al. (2006a), (49) Burgasser & Kirkpatrick (2006), (50) Burgasser et al. (2006b), (51) Burgasser & McElwain (2006), (52) Burgasser (2007), (53) Burgasser et al. (2007), (54) Burgasser et al. (2008a), (55) Burgasser et al. (2008b), (56) Burgasser et al. (2009b), (57) Burgasser et al. (2009a), (58) Burgasser et al. (2010b), (59) Burgasser et al. (2010a), (60) Burgasser et al. (2011), (61) Burgasser et al. (2012), (62) Burgasser et al. (2015), (63) Burgasser et al. (2016), (64) Burningham et al. (2010a), (65) Burningham et al. (2010b), (66) Burningham et al. (2011), (67) Burningham et al. (2013), (68) Castro & Gizis (2012), (69) Castro et al. (2013), (70) Chiu et al. (2006), (71) Chiu et al. (2008), (72) Close et al. (2002a), (73) Close et al. (2002b), (74) Close et al. (2003), (75) Crifo et al. (2005), (76) Cruz & Reid (2002), (77) Cruz et al. (2003), (78) Cruz et al. (2004), (79) Cruz et al. (2007), (80) Cruz et al. (2009), (81) Cushing & Vacca (2006), (82) Cushing et al. (2011), (83) Cushing et al. (2014), (84) Cutri et al. (2003), (85) Cutri et al. (2014), (86) Dahn et al. (1986), (87) Dahn et al. (2002), (88) Dahn et al. (2008), (89) Dawson et al. (2014), (90) Day-Jones et al. (2013), (91) Deacon et al. (2005), (92) Deacon & Hambly (2007), (93) Deacon et al. (2009), (94) Deacon et al. (2011), (95) Deacon et al. (2012a), (96) Deacon et al. (2012b), (97) Deacon et al. (2014), (98) Delfosse et al. (1997), (99) Delfosse et al. (1999), (100) Delorme et al. (2008), (101) Dobbie et al. (2002), (102) Dupuy et al. (2009), (103) Dupuy et al. (2010), (104) Dupuy & Liu (2012), (105) Dupuy et al. (2015), (106) Dupuy et al. (2016), (107) Faherty et al. (2009), (108) Faherty et al. (2010), (109) Faherty et al. (2012), (110) Faherty et al. (2013), (111) Faherty et al. (2016), (112) Fan et al. (2000), (113) Folkes et al. (2012), (114) Forveille et al. (2005), (115) Freed et al. (2003), (116) Gagné et al. (2014a), (117) Gagné et al. (2015c), (118) Gauza et al. (2012), (119) Gauza et al. (2015), (120) Geballe et al. (2002), (121) Geißler et al. (2011), (122) Gelino et al. (2011), (123) Gelino et al. (2014), (124) Giampapa & Liebert (1986), (125) Giclas et al. (1967), (126) Gillon et al. (2016), (127) Gilmore et al. (1985), (128) Gizis (1997), (129) Gizis & Reid (1997), (130) Gizis et al. (2000a), (131) Gizis et al. (2000b), (132) Gizis et al. (2001), (133) Gizis (2002), (134) Gizis et al. (2003), (135) Gizis et al. (2011b), (136) Gizis et al. (2011a), (137) Gizis et al. (2012), (138) Gizis et al. (2013), (139) Gizis et al. (2015), (140) Goldman et al. (2010), (141) Gomes et al. (2013), (142) Hall (2002), (143) Hawley et al. (2002), (144) Henry & Kirkpatrick (1990), (145) Henry et al. (2004), (146) Henry et al. (2006), (147) Huelamo et al. (2015), (148) Irwin et al. (1991), (149) Kellogg et al. (2015), (150) Kellogg et al. (2016), (151) Kendall et al. (2003), (152) Kendall et al. (2004), (153) Kendall et al. (2007a), (154) Kendall et al. (2007b), (155) Kirkpatrick et al. (1991), (156) Kirkpatrick et al. (1993), (157) Kirkpatrick et al. (1994), (158) Kirkpatrick et al. (1995), (159) Kirkpatrick et al. (1997b), (160) Kirkpatrick et al. (1997a), (161) Kirkpatrick et al. (1999), (162) Kirkpatrick et al. (2000), (163) Kirkpatrick et al. (2001b), (164) Kirkpatrick et al. (2008), (165) Kirkpatrick et al. (2010), (166) Kirkpatrick et al. (2011), (167) Kirkpatrick et al. (2014), (168) Knapp et al. (2004), (169) Koerner et al. (1999), (170) Kraus & Hillenbrand (2009), (171) Lachapelle et al. (2015), (172) Law et al. (2006), (173) Leggett (1992), (174) Leggett et al. (1996), (175) Leggett et al. (2000), (176) Leinert et al. (1994), (177) Lépine et al. (2002b), (178) Lépine et al. (2002a), (179) Lépine et al. (2003a), (180) Lépine et al. (2003b), (181) Lépine et al. (2003c), (182) Lépine & Shara (2005), (183) Lépine et al. (2009), (184) Liebert et al. (1979), (185) Liebert et al. (2003), (186) Liebert & Gizis (2006), (187) Liu et al. (2002), (188) Liu & Leggett (2005), (189) Liu et al. (2006), (190) Liu et al. (2010), (191) Liu et al. (2011), (192) Liu et al. (2013b), (193) Lodieu et al. (2002), (194) Lodieu et al. (2005), (195) Lodieu et al. (2007b), (196) Lodieu et al. (2008), (197) Lodieu et al. (2010), (198) Lodieu et al. (2012c), (199) Lodieu et al. (2012b), (200) Lodieu et al. (2014), (201) Looper et al. (2007), (202) Looper et al. (2008), (203) Loutrel et al. (2011), (204) Lucas et al. (2010), (205) Luhman et al. (2007), (206) Luhman et al. (2009), (207) Luhman et al. (2012), (208) Luhman & Sheppard (2014), (209) Luyten (1979), (210) Mace et al. (2013), (211) Manjavacas et al. (2013), (212) Marocco et al. (2013), (213) Marocco et al. (2015), (214) Marshall (2008), (215) Martín et al. (1994), (216) Martín et al. (1998), (217) Martín et al. (1999b), (218) Martín et al. (1999a), (219) Martín et al. (2000), (220) Martín et al. (2010), (221) Matsuoka et al. (2011), (222) McCarthy et al. (1964), (223) McCaughrean et al. (2002), (224) McElwain & Burgasser (2006), (225) McGovern et al. (2004), (226) Metchev et al. (2008), (227) Mohanty & Basri (2003), (228) Montagnier et al. (2006), (229) Mugrauer et al. (2006), (230) Murray et al. (2011), (231) Muzic et al. (2012), (232) Phan-Bao et al. (2001), (233) Phan-Bao & Bessell (2006), (234) Phan-Bao et al. (2006), (235) Phan-Bao et al. (2008), (236) Pineda et al. (2016), (237) Pinfield et al. (2008), (238) Pokorny et al. (2004), (239) Pope et al. (2013), (240) Probst & Liebert (1983), (241) Radigan et al. (2008), (242) Radigan et al. (2013), (243) Rebolo et al. (1998), (244) Reid & Gilmore (1981), (245) Reid et al. (1995), (246) Reid et al. (2000), (247) Reid et al. (2001), (248) Reid & Cruz (2002), (249) Reid et al. (2002), (250) Reid et al. (2003a), (251) Reid et al. (2003b), (252) Reid (2003), (253) Reid et al. (2004), (254) Reid & Gizis (2005), (255) Reid et al. (2006b), (256) Reid et al. (2006a), (257) Reid et al. (2007), (258) Reid et al. (2008), (259) Reiners & Basri (2006), (260) Reylé & Robin (2004), (261) Rice et al. (2010), (262) Rodono et al. (1980), (263) Rodriguez et al. (2013), (264) Ruiz et al. (1997), (265) Ruiz et al. (2001), (266) Sahlmann et al. (2015), (267) Salim et al. (2003), (268) Schmidt et al. (2007), (269) Schmidt et al. (2010), (270) Schmidt et al. (2015), (271) Schneider et al. (1991), (272) Schneider et al. (2002), (273) Schneider et al. (2011), (274) Schneider et al. (2014), (275) Schneider et al. (2016a), (276) Schneider et al. (2016b), (277) Scholz et al. (2001), (278) Scholz & Meusinger (2002), (279) Scholz et al. (2004a), (280) Scholz et al. (2004b), (281) Scholz et al. (2009), (282) Scholz (2010a), (283) Scholz (2010b), (284) Scholz et al. (2011), (285) Scholz et al. (2012), (286) Scholz (2014), (287) Scholz et al. (2014), (288) Schweitzer et al. (1999), (289) Seifahrt et al. (2010), (290) Sheppard & Cushing (2009), (291) Shkolnik et al. (2009), (292) Siegler et al. (2003), (293) Siegler et al. (2005), (294) Siegler et al. (2007), (295) Silvestri et al. (2007), (296) Sivarani et al. (2009), (297) Skrutskie et al. (2006), (298) Stern et al. (2007), (299) Stone et al. (2016), (300) Strauss et al. (1999), (301) Stumpf et al. (2009), (302) Stumpf et al. (2010), (303) Stumpf et al. (2011), (304) Thompson et al. (2013), (305) Thorstensen & Kirkpatrick (2003), (306) Tinney (1993a), (307) Tinney (1993b), (308) Tinney et al. (1993), (309) Tinney (1996), (310) Tinney et al. (1998), (311) Tinney et al. (2005), (312) Tsvetanov et al. (2000), (313) van Biesbroeck (1961), (314) West et al. (2008), (315) Wilson et al. (2001), (316) Wilson et al. (2003), (317) Wright et al. (2013), (318) Zapatero Osorio et al. (1999), (319) Zapatero Osorio et al. (2000), (320) Zhang et al. (2009), (321) Zhang et al. (2010), (322) Zhang et al. (2013).

NOTE—Table 1 is published in its entirety in machine readable format in the online journal. A portion is shown here for guidance regarding its form and content. The full table contains 46 columns and 9,938 rows.

at moderate galactic latitude ($\approx -18°$) and away from regions of significant reddening. This gave us a sample of more than 60,000 objects in each band, $\gtrsim$99% having proper motions less than 100 mas yr^{-1}. Figure 4 plots the differences between $y_{\rm P1}$ chip and warp magntudes for each object, normalized by the quadrature sum of the chip and warp errors, as a function of magnitude. For brighter unsaturated objects ($y_{\rm P1} \approx 13 - 19$ mag), the difference between chip and warp magnitudes is nearly always less than 2σ. For objects fainter than $y_{\rm P1} \approx 19$ mag, however, the chip photometry becomes significantly brighter for many objects, due to a flux overestimation bias for objects near the chip detection threshold. This well-known bias is discussed in depth in the context of 2MASS in Cutri et al. (2006) and Kellogg et al. (2015), and is important for detections with S/N $\lesssim 10$. Briefly, since the chips have brighter detection limits than the warps, mean chip photometry may not include the fainter measurements that are present in the warp photometry. For example, an object near the chip detection limit may have 10 forced warp measurements but only 3 chip detections due to noise at the detection threshold. Those chip detections will be the 3 brightest measurements of the object, so the mean chip magnitude will be brighter than the mean warp magnitude. Warp photometry is therefore more likely to be accurate for faint objects near the chip detection limits in each band. We list the magnitudes at which the flux overestimation bias becomes significant for chip photometry in each PS1 band in Table 3. We note that for even fainter objects, flux overestimation bias will also impact the warp photometry, but for those objects there is no deeper PS1 photometry available.

Table 3. Flux overestimation bias thresholds for PS1 chip photometry

Band	Threshold (mag)
$g_{\rm P1}$	21.0
$r_{\rm P1}$	21.0
$i_{\rm P1}$	20.5
$z_{\rm P1}$	20.0
$y_{\rm P1}$	19.0

Note—PS1 chip magnitudes fainter than these thresholds may be significantly affected by flux overestimation bias. For slow-moving objects (<100 mas yr^{-1}), warp photometry is more likely to be accurate.

Objects that moved significantly over the four years of PS1 observations will be smeared on the stack images. This smearing will also impact the warp photometry, because the warp PSF force-fits are applied at the same location on each warp, but a moving object will not be centered at that location in every warp. To assess the impact of proper motion on warp photometry, we examined the difference between chip and warp magnitudes for objects brighter than the faint thresholds in Table 3, sorted into bins of PS1-measured proper motion. We determined that nearly all objects for which chip and warp photometry are $>2\sigma$ different have proper motions exceeding 100 mas yr^{-1} (Figure 4), so we do not use warp photometry for objects moving faster than 100 mas yr^{-1}.

3.1.2. *PS1 Photometry Reported in Our Catalog*

For each object and PS1 band ($g_{\rm P1}r_{\rm P1}i_{\rm P1}z_{\rm P1}y_{\rm P1}$) in our catalog, we report a single magnitude, either chip or warp. By default, we use the chip photometry for objects with chip errors < 0.2 mag and detected in at least two chip exposures. We use the warp photometry only in specific cases, when either:

1. Chip photometry is fainter than the thresholds listed in Table 3, to avoid flux overestimation bias in the chip photometry.

2. Chip photometry is either not measured or of insufficient quality (i.e., fewer than two detections or error $\geq$ 0.2 mag).

However, since warp photometry degrades for faster-moving objects, we only use warp photometry when both of the following are true:

1. A proper motion has not been measured (in PS1 or the literature) at $\mu > 100$ mas yr^{-1} with $\frac{\mu}{\sigma_\mu} > 3$, to avoid fast-moving objects.

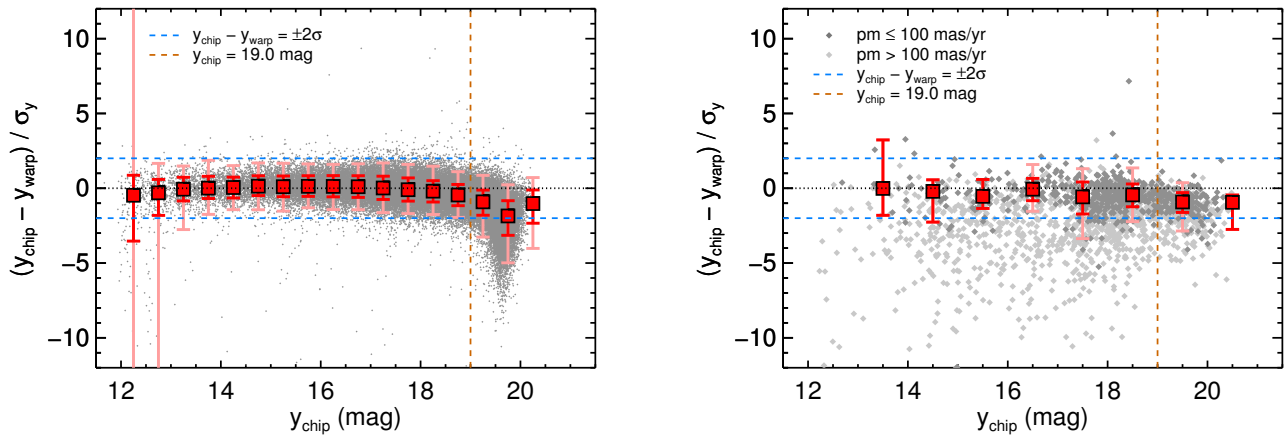
y_chip − y_warp = ±2σ
y_chip = 19.0 mag
(y_chip − y_warp) / σ_y
y_chip (mag)
pm ≤ 100 mas/yr
pm > 100 mas/yr
y_chip − y_warp = ±2σ
y_chip = 19.0 mag
(y_chip − y_warp) / σ_y
y_chip (mag)

Figure 4. *Left*: Differences in $y_{\rm P1}$ chip and warp mean magnitudes (gray dots) for objects in an arbitrary 4 deg^2 patch of sky, normalized by the uncertainties. >99% of these objects have proper motions less than 100 mas yr^{-1}. The red boxes show the median differences for objects in bins of 0.5 mag; the dark and light red error bars indicate 68% and 95% confidence limits, respectively. For reference, the blue dashed lines mark $y_{\rm chip} - y_{\rm warp}$ differences of $\pm 2\sigma$, and the dotted black line indicates no difference. For objects of moderate brightness, the differences between chip and warp magnitudes are nearly always less than 2σ significance. At the bright end, saturation causes significant scatter in magnitudes. At the faint end, many chip magnitudes become significantly brighter due to flux overestimation bias. The vertical brown dashed line at $y = 19$ mag marks the onset of this bias. *Right*: The same plot for objects from our ultracool catalog, with those having proper motions less than 100 mas yr^{-1} plotted in dark grey and faster moving objects in light grey. The red boxes indicate the median $y_{\rm chip} - y_{\rm warp}$ differences only for the slower (proper motion $\leq$ 100 mas yr^{-1}) objects. Warp photometry is significantly fainter than chip photometry for most of the faster moving objects because an object is not at the same force-fit position in all warps. We use chip photometry in our catalog as our default, but use warp photometry for objects with $y_{\rm chip} > 19.0$ mag and proper motion $<$ 100 mas yr^{-1}. Analogous plots for the other four PS1 bands show similar results.

2. A proper motion has not been measured (in PS1 or the literature) with $\mu - \sigma_\mu > 100$ mas yr^{-1}, to avoid most fast-moving objects with poorly-measured proper motions.

Finally, we only use warp photometry with errors < 0.2 mag and calculated from at least two successful warp fits, equivalent to the criteria for chip photometry.

On the bright end, we rejected any photometry with $g_{\rm P1} < 14.5$ mag, $r_{\rm P1} < 14.5$ mag, $i_{\rm P1} < 14.5$ mag, $z_{\rm P1} < 13.5$ mag, or $y_{\rm P1} < 12.5$ mag to avoid saturation.

For many objects in our catalog we use chip photometry for some bands and warp for the others, depending on the value and quality of the chip photometry. If neither the chip nor the warp photometry are of sufficient quality in a given band, we report no photometry for that band. Objects with no chip or forced warp photometry of sufficient quality in any of the five PS1 bands are not included in our catalog.

3.1.3. *False Warp Detections of Faint Objects*

While inspecting the PS1 colors of our catalog objects, we discovered a few dozen instances where very faint objects near the stack detection limit (e.g., $y_{\rm P1} > 21$ mag) had warp photometry with surprisingly small errors (as small as 0.01 mag) despite only two or three warps contributing to the mean photometry. In particular, we found T dwarfs with low-error warp photometry reported for $g_{\rm P1}$ and $r_{\rm P1}$. T dwarfs are much too faint in these visual bands to be detected. We confirmed that the g and r stack images showed no objects at the locations of these false detections.

We traced the source of these false high-S/N detections to the method used to calculate PS1 photometry errors. This method is described in detail in Magnier et al. (2017, in prep); here we offer a brief summary. Each individual photometry measurement (chip, warp, or stack) includes a measurement uncertainty, which naturally is large for faint objects. Mean chip and warp magnitudes are computed using an iterative reweighting process to reject outliers, and the errors for the mean photometry are calculated by bootstrap resampling of the individual non-outlier measurements. Bootstrapping uses the individual measurements but not their uncertainties, instead sampling the outlier-cleaned photometry measurements to determine the error. For well-detected objects with multiple measurements, bootstrapping is demonstrated to calculate errors consistent with standard errors on the mean photometry while effectively clipping outliers such as transient image artifacts (Magnier et al., 2017, in prep). However, in cases where photometry was measured only a few times for an object, and those measurements are very similar (a statistical possibility even for

objects at the detection limit), the bootstrapping process will find a very small error, even if the individual measurements had large uncertainties. The false g and r warp detections in our catalog were the result of ≈2–3 low-S/N forced warp measurements of background noise that happened to find similar values, resulting in errors < 0.2 mag (from bootstrapping) on the mean warp photometry.

To identify and remove these false detections from our catalog in a systematic fashion, we extracted from PS1 the individual warp flux measurements used to calculate the mean warp photometry for each object in our catalog. For each object and band, we calculated a weighted-mean warp magnitude (using inverse variance weighting) and the standard error on this weighted mean. If the reported warp error in PS1 was less than 0.2 mag but the standard error was greater than 0.2 mag, we discarded the warp photometry for that object and band. This occurred for 12% of the PS1-reported warp measurements passing our criteria for inclusion in the catalog (Section 3.1.2), affecting 255 objects and implying that false detections in the warps at the faint end can be a significant source of contamination. Specifically, we discarded 129 out of 199 measurements in $g_{\rm P1}$, 123 out of 410 in $r_{\rm P1}$, 27 out of 601 in $i_{\rm P1}$, 19 out of 677 in $r_{\rm P1}$, and 0 out of 698 in $y_{\rm P1}$, consistent with the red nature of the objects in our sample (nearly all have strong $y_{\rm P1}$ detections). If the reported warp error in PS1 and the standard error were both less than 0.2 mag, we retained the PS1-reported photometry and error for our catalog. We use our re-calculated standard errors only to assess the reliability of small warp photometry errors reported by PS1, and do not report them in our catalog.

3.1.4. *Precision*

The photometric errors reported in the PS1 database are formal errors that do not include systematics. Given the sensitivity of the Pan-STARRS1 camera and the multiple epochs of photometry, these formal errors can be very small, less than 0.0005 mag in some cases. A full assessment of the systematic photometry errors for PV3 has not yet been completed, but a calibration of the first 1.5 years of PS1 photometry performed by Schlafly et al. (2012) found per-image zeropoints had rms scatter of ≈ 10 mmag in all five PS1 filters, so we adopt this value (0.01 mag) as a floor for our catalog.

3.1.5. *Fast-Moving Objects*

As discussed in detail in Section 4.1.3, we found that objects with proper motions $\gtrsim 200$ mas yr^{-1} were often split into two or more distinct "partial objects" in the PS1 database. In these cases we use the photometry from the partial object with the chip photometry in the most PS1 bands, giving preference to the redder bands if no partial object had photometry in all bands. In a few dozen cases where a chosen partial object had no photometry or photometry of insufficient quality in some PS1 band, we used photometry recalculated by combining the measurements from the partial objects into a single object (Section 4.1.3) for that band.

3.2. *Colors and SEDs*

We show multiple colors from our catalog in Figures 5–8, spanning $g_{\rm P1}$ through $W3$. We include 11 colors using at least one PS1 bands, and four more ($(J-K_S)_{\rm 2MASS}$, $J_{\rm 2MASS}-W1$, $W1-W2$, and $W2-W3$) that have been used in many previous studies. To create these figures, we have extracted all objects known to be young, subdwarfs, or binaries, and used these to form a sample of "unusual" objects. The remaining objects are our "normal field" sample. Figure 5 shows colors as a function of spectral type for the normal field sample, and Figure 6 shows the same colors for the unusual sample. In both plots, we use large symbols and error bars to indicate the median colors and 68% confidence intervals for the normal field sample in bins of two spectral subtypes. In Figures 7 and 8, we use the same format to show colors vs. colors for the normal field and unusual samples, respectively. We only use 2MASS and AllWISE photometry with errors ≤ 0.2 mag, the same criterion we use for PS1 photometry (Section 3.1.2), for the figures and analysis presented in this section. (Table 1 includes 2MASS and AllWISE photometry with larger errors.)

Our catalog contains 492 L dwarfs with $r_{\rm P1}$ detections, including 427 in the normal field sample. With these we present the largest set of r-band colors of L dwarfs to date, a tenfold increase over the sample presented by Liebert & Gizis (2006) and the compilation of Koen (2013). Most PS1 colors become redder through the M dwarfs, plateau for the L dwarfs and become redder again for T dwarfs (when detected), but the L dwarfs show a different behavior with $r_{\rm P1}$. $r_{\rm P1}-i_{\rm P1}$ shows a blueward turn at spectral type ≈M8, becoming ≈0.8 mag bluer by spectral type L5 where the objects become too faint for $r_{\rm P1}$ detection, robustly confirming previous findings using much smaller samples (Hawley et al. 2002; Liebert & Gizis 2006). $r_{\rm P1}-z_{\rm P1}$ and $r_{\rm P1}-y_{\rm P1}$ show a similar but less amplified feature. $y_{\rm P1}-W1$ also peaks at spectral type ≈L7, and becomes more than 1.5 mag bluer through spectral type T5.

We also note in Figure 5 that early-M dwarfs have few detections and redder colors in $W2-W3$. M dwarfs are relatively faint in $W3$, and the early-M dwarfs in our catalog are more distant than other spectral types, so most were

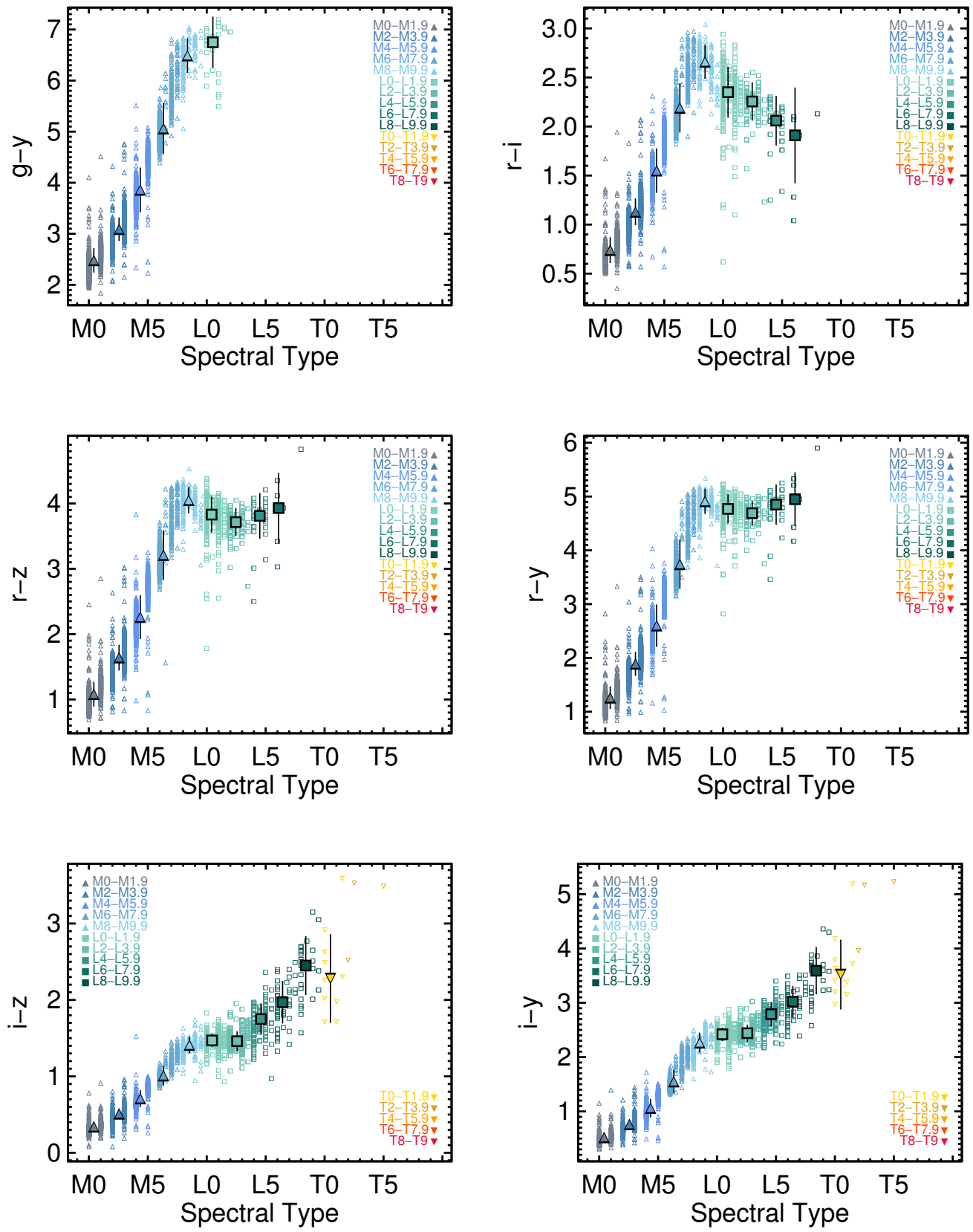

Figure 5. Color vs. spectral type plots for the M, L, and T dwarfs in our PS1-detected catalog, excluding objects known to be binaries, subdwarfs, or young. We use only photometry with errors ≤ 0.2 mag. For objects having both optical and near-IR spectral types, we use the optical type for M and L dwarfs and the near-IR type for T dwarfs. Colors of individual objects are shown with small open symbols, while median colors for bins of two spectral subtypes are shown with large filled symbols (see legend in each figure). The error bars on the median symbols represent rms. Median symbols are not plotted for bins with fewer than three objects. Most PS1 colors plateau through the L dwarfs but become redder for T dwarfs (when detected), with $r_{\rm P1} - i_{\rm P1}$ and $y_{\rm P1} - W1$ being notable exceptions.

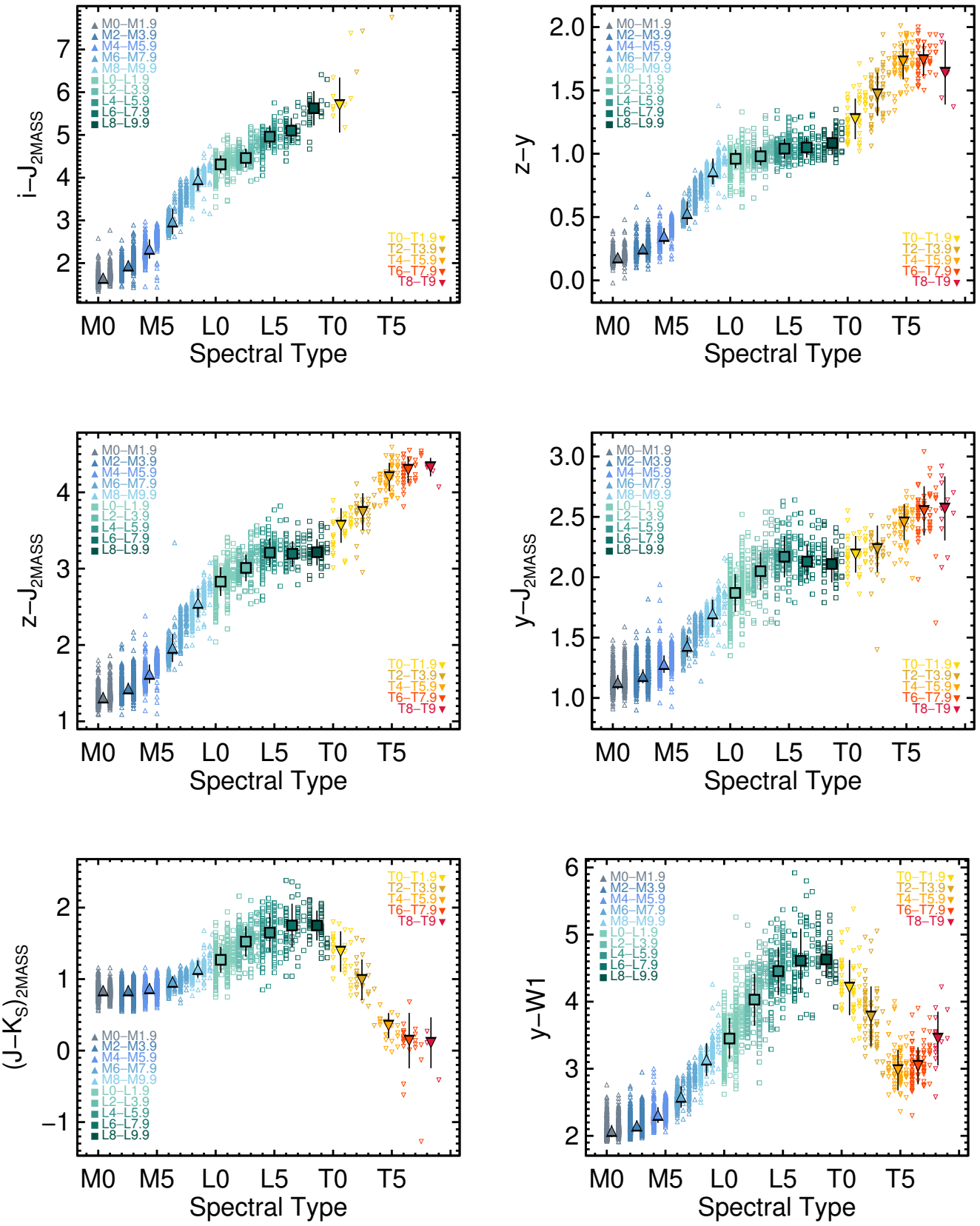

Figure 5. continued.

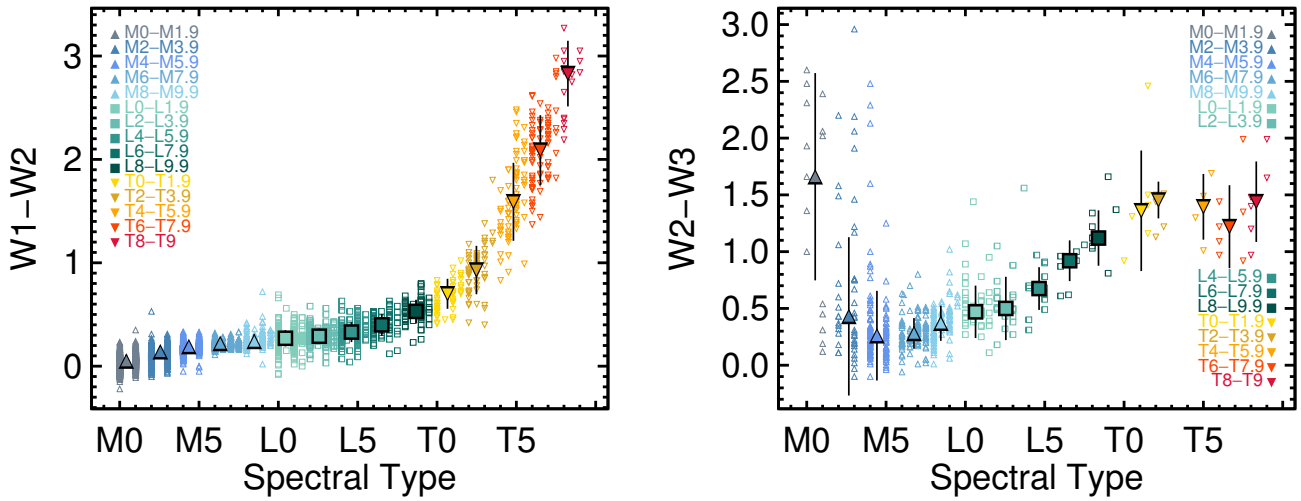

Figure 5. continued.

not detected in $W3$. In contrast, all are detected with errors ≤ 0.05 mag in $W2$. The few early-M dwarfs that have $W3$ detections are the brightest ones in that band in our catalog, so the observed colors are redder than the overall population. The source of the $W3$ emission for the reddest objects is most likely to be debris disks or contamination from background objects, and we note that the $W2-W3$ colors are consistent with those of other debris disks (e.g., Theissen & West 2014). We therefore do not interpret the $W2-W3$ colors as representative of stellar luminosities for spectral types earlier than M5 in our catalog.

We use the photometry in our catalog to calculate median colors of field M0–T9 dwarfs spanning ≈0.55 to 12 μm. As with Figures 5 and 7, we have excluded all known binaries, young objects, and subdwarfs from these calculations in order to produce colors representative of the field population. Table 4 presents these colors in single steps of adjacent filter pairs from $g_{\rm P1}$ to $W3$ (excluding spectral types M0–M4 for $W2-W3$ as explained in the preceding paragraph. Table 5 presents five additional colors ($i_{\rm P1}-y_{\rm P1}$, $i_{\rm P1}-J_{\rm 2MASS}$, $z_{\rm P1}-J_{\rm 2MASS}$, $(J-K_S)_{\rm 2MASS}$, and $y_{\rm P1}-W1$) previously used to study ultracool dwarfs. For both tables, we list the median and rms colors for single spectral subtypes, along with the number of objects used to calculate each color.

We construct empirical spectral energy distributions for field ultracool dwarfs using the photometry in our catalog and parallaxes from the literature. Excluding binaries, subdwarfs, and young objects, our catalog contains 246 objects (spectral types M6–T9) with reported parallaxes and $J_{\rm 2MASS}$ photometry. We calculate absolute $J_{\rm 2MASS}$ magnitudes for these objects, and determine the weighted mean and rms $M_{J_{\rm 2MASS}}$ magnitude for bins of one spectral subtype. We then use our catalog to detemine median colors and rms relative to $J_{\rm 2MASS}$ for all other bands from $g_{\rm P1}$ to $W3$, and use these to calculate absolute magnitudes, adding the rms color for each band in quadrature with the $M_{J_{\rm 2MASS}}$ rms magnitude to determine errors. We present our SEDs for each spectral subtype between M6 and T9 in Table 6.

Recently, Deacon et al. (2016, hereinafter D16) published empirical SEDs for the Pan-STARRS1 photometric system for spectral types B8V–M9V. Our two sets of SEDs have only spectral types M6–M9 in common. For these late-M types, the SEDs are consistent within our uncertainties, but we note that our absolute magnitudes are mostly $\approx 0.1-0.3$ mag fainter. In Figure 9 we compare our PS1 colors for M dwarfs from Table 4 to the PS1 colors from D16. The colors are generally quite consistent, but we note that our $g_{\rm P1}-r_{\rm P1}$ colors are slightly ($\approx 0.5\sigma-1\sigma$) bluer and our $z_{\rm P1}-y_{\rm P1}$ colors are $\approx 1\sigma-2\sigma$ redder than those of D16. The differences in colors are likely due to differences in our input samples (DL16 uses ≈500 M dwarfs, while our sample has over 8000 M dwarfs) and the earlier processing version (PV2) of PS1 data used by D16. We also find a significant blueward turn in the $r_{\rm P1}-i_{\rm P1}$ colors of M9 dwarfs (that continues into the L dwarfs) that D16 do not identify. D16 converted spectral types into absolute magnitudes using bolometric magnitudes and a series of color transformations fitted with smoothing splines. In particular, D16 used $g_{\rm P1}-i_{\rm P1}$ as a proxy for spectral type, and this relation does not clearly distinguish M9 dwarfs from M6–M8 dwarfs, so the sudden turn for M9 in $r_{\rm P1}-i_{\rm P1}$ could not be detected by their method.

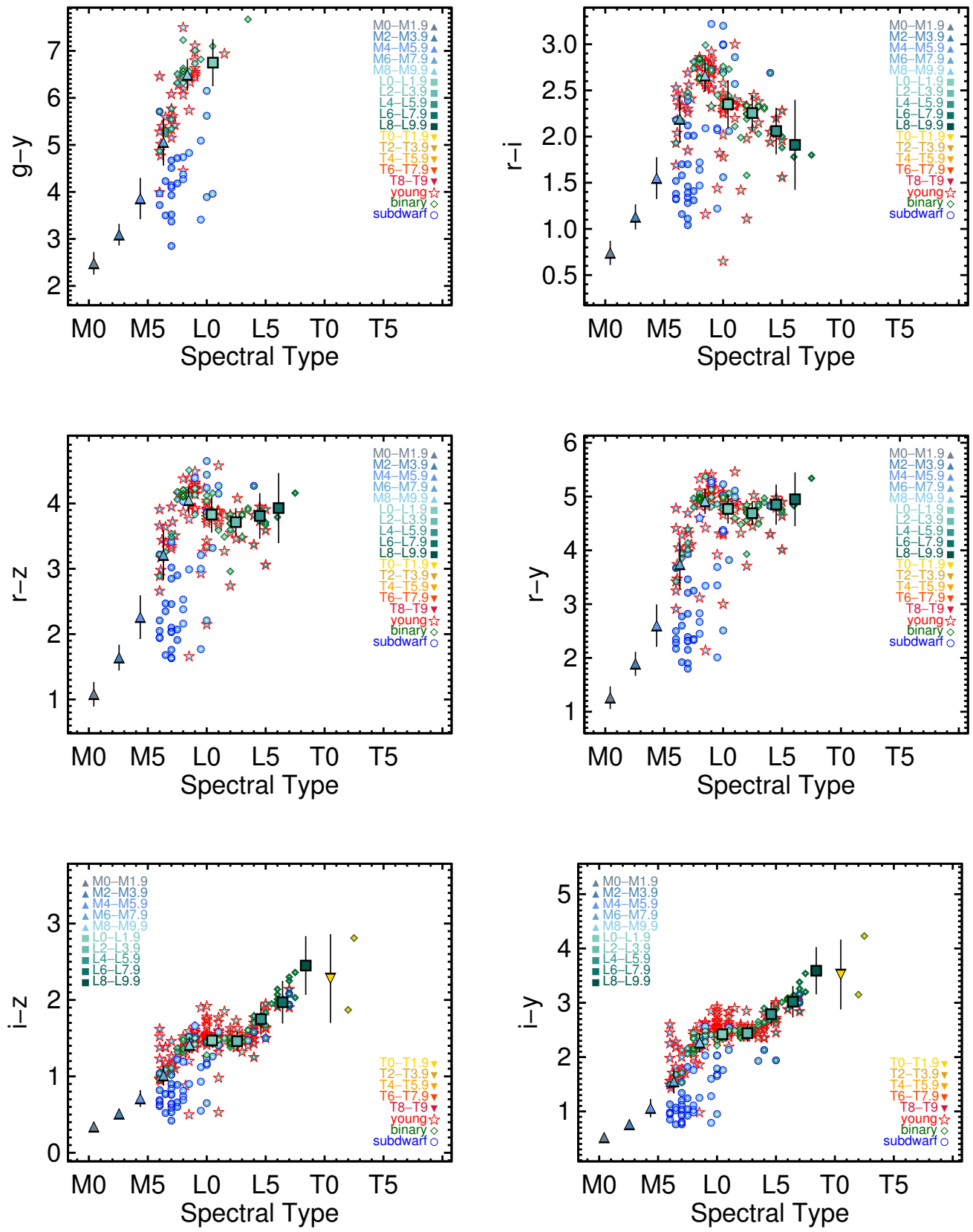

Figure 6. Color vs. spectral type plots for known young objects (outlined with red stars), binaries (green diamonds), and subdwarfs (blue circles) in our PS1-detected catalog. Interiors of the symbols use the same color scheme as in Figure 5 (see legends). Median colors and error bars for normal field objects from Figure 5 are overplotted for reference. Typically the young objects have field-like or redder colors while the subdwarfs have bluer-than-field colors, but the $r_{\rm P1}-i_{\rm P1}$, $r_{\rm P1}-z_{\rm P1}$, and $r_{\rm P1}-y_{\rm P1}$ vs. SpT plots show a number of exceptions to both of these norms.

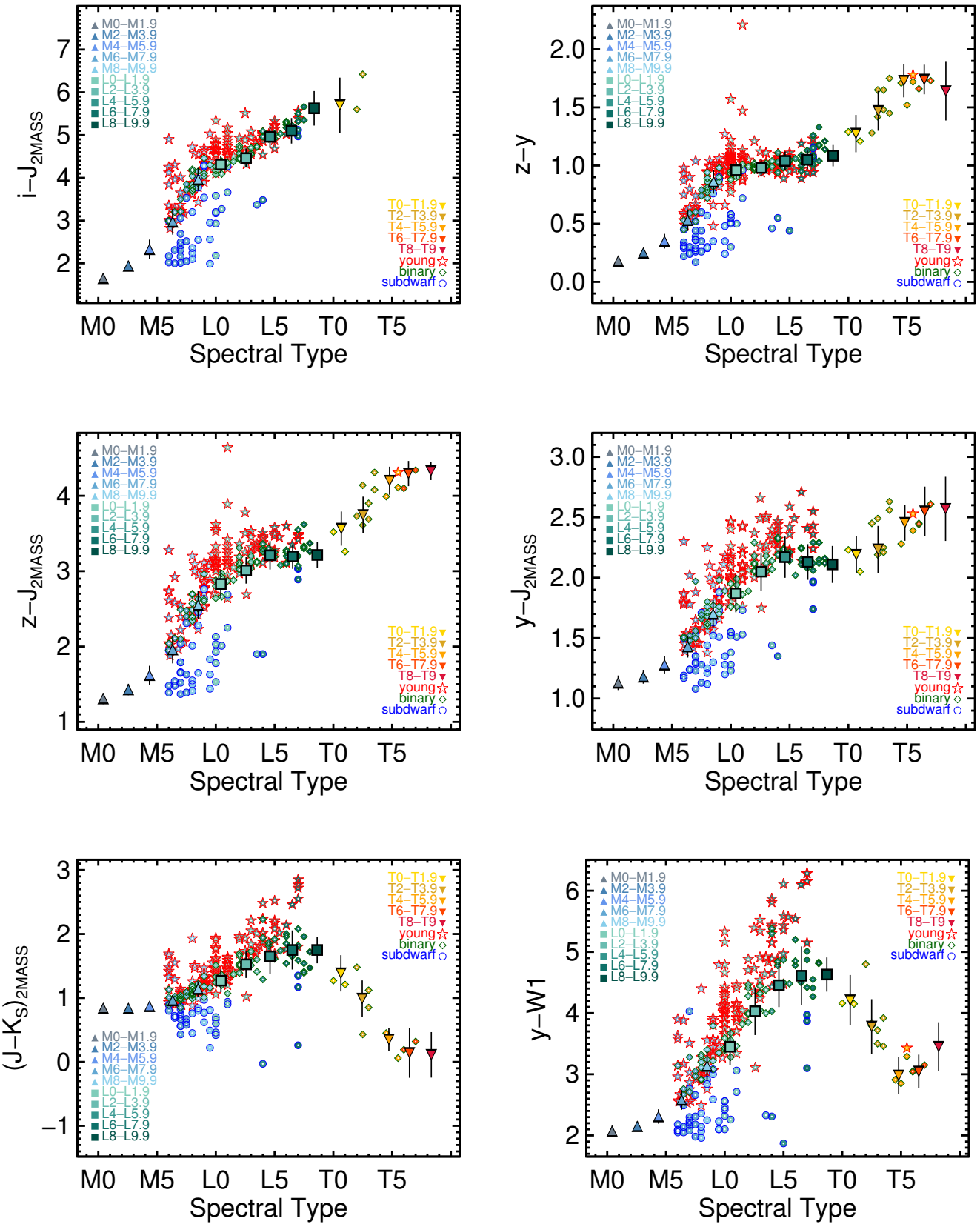

Figure 6. continued.

Table 4. Median Colors

SpT	$g_{P1} - r_{P1}$			$r_{P1} - i_{P1}$			$i_{P1} - z_{P1}$			$z_{P1} - y_{P1}$			$y_{P1} - J_{2MASS}$			$(J-H)_{2MASS}$			$(H-K_S)_{2MASS}$			$K_{S,2MASS} - W1$			$W1 - W2$			$W2 - W3$		
	Median (mag)	rms (mag)	N	Median (mag)	rms (mag)	N	Median (mag)	rms (mag)	N	Median (mag)	rms (mag)	N	Median (mag)	rms (mag)	N	Median (mag)	rms (mag)	N	Median (mag)	rms (mag)	N	Median (mag)	rms (mag)	N	Median (mag)	rms (mag)	N	Median (mag)	rms (mag)	N
M0–M0.9	1.19	0.05	993	0.67	0.10	993	0.31	0.05	993	0.17	0.03	993	1.12	0.06	993	0.66	0.06	993	0.18	0.07	993	0.10	0.07	993	0.02	0.06	993	···	···	0
M1–M1.9	1.22	0.05	711	0.85	0.10	711	0.39	0.05	711	0.20	0.03	711	1.14	0.06	711	0.64	0.06	711	0.21	0.06	711	0.12	0.07	711	0.07	0.06	711	···	···	0
M2–M2.9	1.21	0.05	1675	1.02	0.08	1675	0.46	0.04	1675	0.23	0.03	1675	1.16	0.05	1675	0.62	0.07	1675	0.22	0.07	1675	0.12	0.07	1675	0.12	0.05	1675	···	···	0
M3–M3.9	1.21	0.05	2130	1.22	0.10	2130	0.55	0.05	2130	0.27	0.03	2130	1.20	0.06	2129	0.60	0.06	2129	0.24	0.06	2130	0.14	0.06	2130	0.16	0.05	2130	···	···	0
M4–M4.9	1.23	0.06	1229	1.46	0.11	1229	0.67	0.06	1229	0.32	0.03	1229	1.25	0.06	1229	0.59	0.06	1228	0.26	0.06	1228	0.16	0.06	1229	0.18	0.04	1229	···	···	0
M5–M5.9	1.31	0.05	686	1.88	0.13	686	0.87	0.06	686	0.44	0.04	686	1.34	0.05	686	0.59	0.06	686	0.31	0.07	686	0.19	0.06	686	0.21	0.03	686	0.21	0.17	47
M6–M6.9	1.33	0.07	405	2.13	0.16	394	0.98	0.06	393	0.51	0.04	393	1.40	0.06	399	0.60	0.06	410	0.33	0.06	410	0.21	0.06	409	0.22	0.03	409	0.23	0.14	49
M7–M7.9	1.40	0.12	155	2.55	0.19	153	1.20	0.10	155	0.67	0.08	155	1.54	0.08	155	0.63	0.05	158	0.39	0.05	158	0.22	0.05	156	0.23	0.03	157	0.32	0.10	67
M8–M8.9	1.53	0.17	92	2.70	0.15	110	1.38	0.09	121	0.81	0.08	122	1.66	0.08	118	0.68	0.06	119	0.43	0.05	119	0.26	0.06	112	0.23	0.05	112	0.35	0.12	62
M9–M9.9	1.79	0.22	35	2.58	0.18	59	1.44	0.12	86	0.92	0.09	86	1.77	0.12	70	0.71	0.08	68	0.48	0.11	69	0.31	0.10	59	0.26	0.09	68	0.44	0.17	35
L0–L0.9	1.87	0.21	15	2.35	0.27	199	1.47	0.07	343	0.95	0.06	346	1.82	0.14	316	0.76	0.14	286	0.48	0.14	287	0.33	0.12	272	0.27	0.08	322	0.51	0.27	20
L1–L1.9	2.00	0.71	11	2.35	0.24	112	1.48	0.11	225	0.97	0.09	232	1.93	0.15	184	0.80	0.14	173	0.52	0.14	175	0.36	0.12	166	0.26	0.08	208	0.46	0.16	19
L2–L2.9	2.30	···	1	2.28	0.17	50	1.45	0.12	108	0.97	0.06	111	2.01	0.12	95	0.91	0.14	94	0.59	0.12	94	0.42	0.15	90	0.29	0.07	105	0.51	0.20	14
L3–L3.9	···	···	0	2.22	0.23	30	1.49	0.14	96	1.01	0.08	101	2.13	0.17	79	0.95	0.16	77	0.64	0.17	78	0.52	0.16	77	0.30	0.08	94	0.50	0.20	10
L4–L4.9	···	···	0	2.10	0.26	16	1.64	0.18	70	1.02	0.07	84	2.15	0.18	57	1.06	0.18	54	0.62	0.19	56	0.62	0.15	50	0.32	0.10	76	0.68	0.24	6
L5–L5.9	···	···	0	2.00	0.24	13	1.78	0.21	68	1.05	0.08	86	2.18	0.14	62	1.05	0.18	60	0.64	0.14	62	0.67	0.15	54	0.33	0.09	78	0.66	0.15	8
L6–L6.9	···	···	0	1.91	0.49	5	1.89	0.26	34	1.05	0.07	45	2.09	0.14	34	0.99	0.16	32	0.67	0.23	37	0.71	0.17	33	0.39	0.09	41	0.74	0.18	4
L7–L7.9	···	···	0	···	···	0	2.09	0.29	15	1.04	0.10	28	2.19	0.16	23	1.16	0.25	19	0.72	0.19	22	0.75	0.15	19	0.45	0.13	26	1.00	0.07	3
L8–L8.9	···	···	0	2.13	···	1	2.45	0.37	17	1.05	0.07	27	2.13	0.17	22	1.13	0.14	23	0.66	0.15	27	0.85	0.10	25	0.53	0.10	26	1.12	0.12	6
L9–L9.9	···	···	0	···	···	0	2.46	0.40	8	1.15	0.10	41	2.11	0.14	31	1.07	0.17	30	0.58	0.16	31	0.79	0.20	27	0.56	0.12	36	1.09	0.40	2
T0–T0.9	···	···	0	···	···	0	2.38	0.44	6	1.21	0.13	25	2.20	0.15	14	0.93	0.14	14	0.55	0.14	14	0.76	0.16	12	0.58	0.12	23	0.92	···	1
T1–T1.9	···	···	0	···	···	0	2.14	0.83	4	1.39	0.17	27	2.19	0.11	16	0.88	0.14	14	0.30	0.21	14	0.64	0.19	14	0.72	0.14	27	1.41	0.18	3
T2–T2.9	···	···	0	···	···	0	3.02	0.71	2	1.45	0.16	39	2.23	0.21	24	0.80	0.14	16	0.24	0.21	16	0.64	0.26	16	0.91	0.15	43	1.45	0.16	6
T3–T3.9	···	···	0	···	···	0	···	···	0	1.55	0.18	23	2.27	0.14	12	0.59	0.17	7	0.17	0.21	7	0.53	0.34	7	1.08	0.32	19	···	···	0
T4–T4.9	···	···	0	···	···	0	···	···	0	1.71	0.15	31	2.43	0.13	22	0.33	0.18	12	0.11	0.19	10	0.21	0.19	8	1.35	0.26	30	1.30	···	1
T5–T5.9	···	···	0	···	···	0	3.49	···	1	1.74	0.13	32	2.50	0.16	30	0.19	0.20	10	0.03	0.13	6	0.39	0.31	6	1.85	0.33	43	1.25	0.34	2
T6–T6.9	···	···	0	···	···	0	···	···	0	1.73	0.13	32	2.54	0.17	38	0.05	0.25	21	0.06	0.32	14	0.40	0.36	15	2.06	0.31	51	1.16	0.20	4
T7–T7.9	···	···	0	···	···	0	···	···	0	1.80	0.10	14	2.55	0.27	21	0.08	0.17	12	0.01	0.54	7	0.31	0.13	5	2.26	0.32	29	1.35	0.54	3
T8–T8.9	···	···	0	···	···	0	···	···	0	1.76	0.23	4	2.57	0.29	9	0.09	···	1	···	···	0	···	···	0	2.75	0.33	13	1.30	0.23	4
T9–T9.9	···	···	0	···	···	0	···	···	0	1.37	···	1	2.61	0.12	2	0.24	···	1	···	···	0	···	···	0	2.95	0.11	3	1.82	0.24	2

Note—For each spectral type and color, this table lists the median and rms color followed by the number of objects (N) used to determine the median and rms.

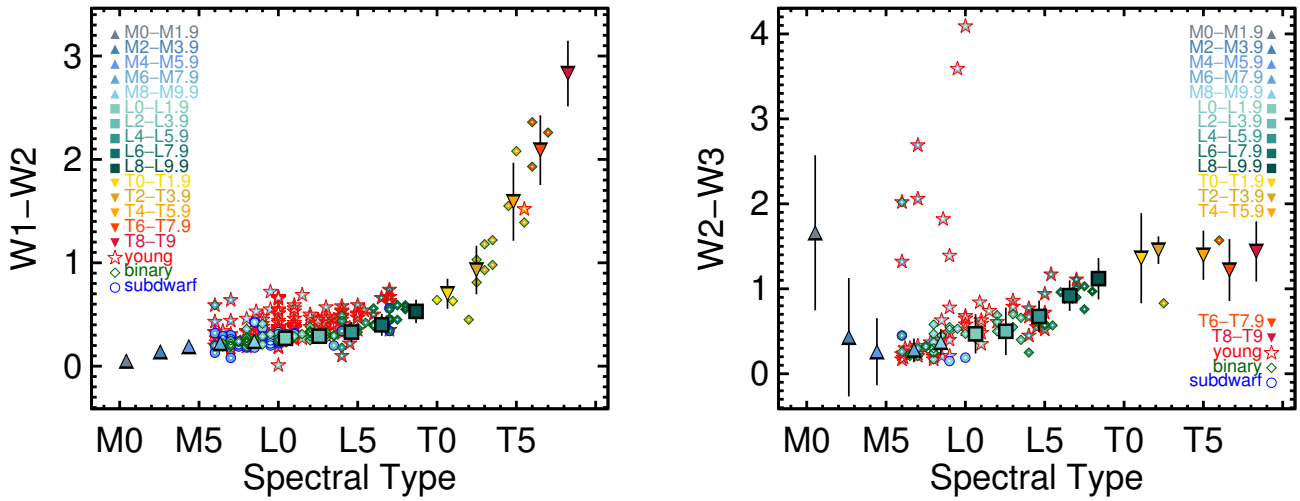

Figure 6. continued.

Table 5. More Median Colors

SpT	$i_{P1} - y_{P1}$			$i_{P1} - J_{2MASS}$			$z_{P1} - J_{2MASS}$			$(J - K_S)_{2MASS}$			$y_{P1} - W1$		
	Median (mag)	rms (mag)	N	Median (mag)	rms (mag)	N	Median (mag)	rms (mag)	N	Median (mag)	rms (mag)	N	Median (mag)	rms (mag)	N
M0–M0.9	0.48	0.06	993	1.61	0.10	993	1.29	0.07	993	0.84	0.07	993	2.05	0.09	993
M1–M1.9	0.59	0.06	711	1.74	0.10	711	1.34	0.07	711	0.85	0.07	711	2.10	0.08	711
M2–M2.9	0.69	0.05	1675	1.85	0.08	1675	1.39	0.07	1675	0.84	0.07	1675	2.12	0.08	1675
M3–M3.9	0.82	0.07	2130	2.02	0.10	2129	1.46	0.07	2129	0.84	0.07	2129	2.17	0.08	2130
M4–M4.9	0.99	0.08	1229	2.24	0.12	1229	1.57	0.08	1229	0.86	0.07	1229	2.26	0.09	1229
M5–M5.9	1.31	0.09	686	2.66	0.13	686	1.78	0.08	686	0.91	0.07	686	2.44	0.08	686
M6–M6.9	1.48	0.11	395	2.89	0.15	395	1.91	0.12	394	0.93	0.07	410	2.54	0.10	399
M7–M7.9	1.87	0.18	156	3.41	0.25	154	2.20	0.16	153	1.02	0.08	158	2.79	0.16	154
M8–M8.9	2.19	0.16	122	3.84	0.22	118	2.45	0.15	117	1.12	0.09	119	3.03	0.16	113
M9–M9.9	2.35	0.16	86	4.16	0.24	70	2.71	0.16	70	1.19	0.13	68	3.29	0.23	73
L0–L0.9	2.41	0.10	343	4.24	0.19	316	2.77	0.17	316	1.24	0.16	285	3.35	0.25	327
L1–L1.9	2.45	0.15	225	4.38	0.20	182	2.90	0.18	184	1.32	0.19	173	3.61	0.31	217
L2–L2.9	2.41	0.13	108	4.41	0.15	95	2.99	0.13	95	1.50	0.20	94	3.91	0.33	107
L3–L3.9	2.51	0.18	96	4.63	0.25	78	3.12	0.20	79	1.59	0.22	77	4.26	0.43	97
L4–L4.9	2.68	0.21	70	4.84	0.26	52	3.15	0.19	57	1.64	0.28	55	4.37	0.38	76
L5–L5.9	2.88	0.21	68	5.04	0.20	57	3.24	0.15	62	1.67	0.26	60	4.56	0.31	78
L6–L6.9	2.97	0.27	34	5.09	0.28	29	3.17	0.15	34	1.62	0.31	32	4.55	0.41	41
L7–L7.9	3.09	0.31	15	5.15	0.32	12	3.24	0.18	22	1.87	0.26	19	4.70	0.54	26
L8–L8.9	3.44	0.41	16	5.54	0.38	15	3.20	0.17	23	1.79	0.17	23	4.76	0.27	25
L9–L9.9	3.59	0.44	8	5.71	0.39	7	3.22	0.17	31	1.67	0.22	30	4.55	0.26	36
T0–T0.9	3.52	0.43	6	5.66	0.35	5	3.43	0.20	14	1.45	0.22	13	4.34	0.34	22
T1–T1.9	3.55	0.92	4	5.78	0.95	4	3.62	0.17	16	1.18	0.29	14	4.10	0.44	27
T2–T2.9	4.57	0.86	2	6.95	0.68	2	3.72	0.26	23	1.06	0.25	16	3.85	0.40	44
T3–T3.9	...	...	0	...	...	0	3.81	0.19	11	0.82	0.27	7	3.65	0.51	21
T4–T4.9	...	...	0	...	...	0	4.12	0.16	22	0.38	0.16	10	3.07	0.36	31
T5–T5.9	5.23	...	1	7.75	...	1	4.26	0.19	27	0.17	0.19	6	2.93	0.23	42
T6–T6.9	...	...	0	...	...	0	4.29	0.17	27	0.16	0.31	15	3.02	0.28	52
T7–T7.9	...	...	0	...	...	0	4.36	0.14	9	0.08	0.54	7	3.07	0.26	29
T8–T8.9	...	...	0	...	...	0	4.34	0.04	4	...	...	0	3.40	0.41	13
T9–T9.9	...	...	0	...	...	0	4.07	...	1	...	...	0	3.66	0.30	2

NOTE—For each spectral type and color, this table lists the median and rms color followed by the number of objects (N) used to determine the median and rms.

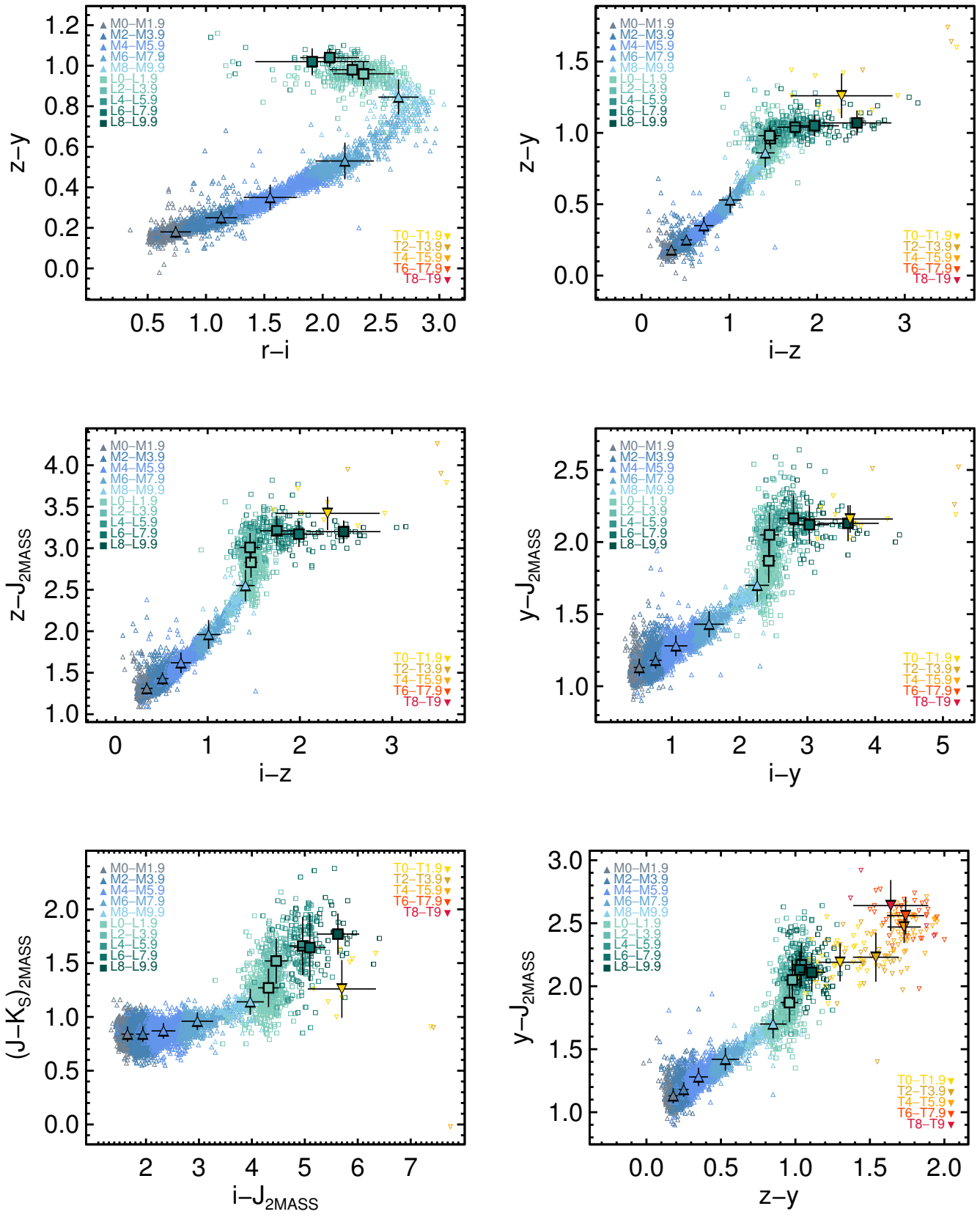

Figure 7. Color-color plots for the M, L, and T dwarfs in our PS1-detected catalog, using the same format as in Figure 5. The L dwarf color plateau is especially evident for $z_{\rm P1} - y_{\rm P1}$ and $z_{\rm P1} - J_{\rm 2MASS}$.

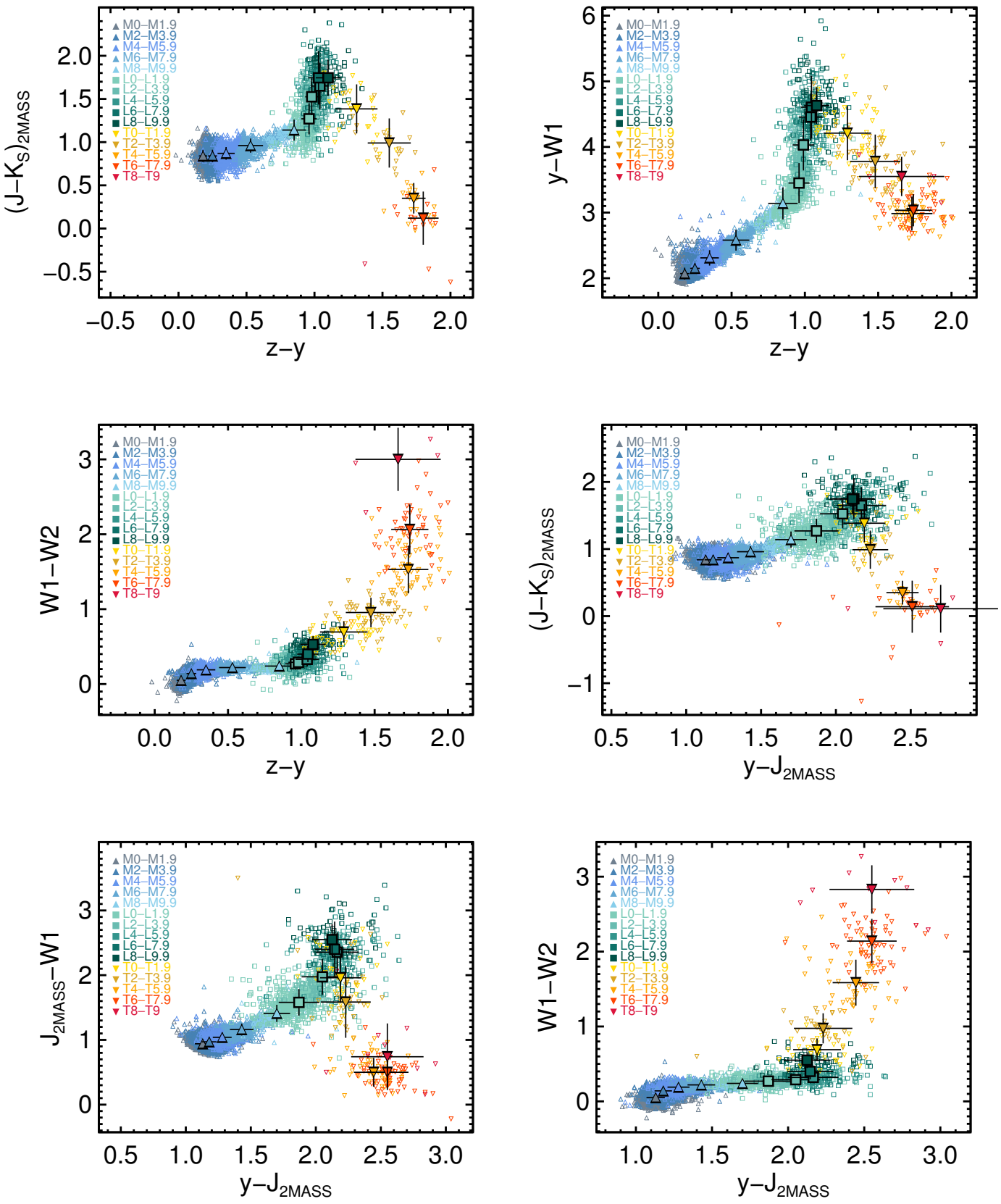

Figure 7. continued.

Table 6. Spectral Energy Distributions for Field Ultracool Dwarfs

SpT	N	$M_{g_{P1}}$		$M_{r_{P1}}$		$M_{i_{P1}}$		$M_{z_{P1}}$		$M_{y_{P1}}$		$M_{J_{2MASS}}$		$M_{H_{2MASS}}$		$M_{K_{S,2MASS}}$		M_{W1}		M_{W2}		M_{W3}	
		Mean (mag)	σ (mag)	Mean (mag)	σ (mag)	Mean (mag)	σ (mag)	Mean (mag)	σ (mag)	Mean (mag)	σ (mag)	Mean (mag)	σ (mag)	Mean (mag)	σ (mag)	Mean (mag)	σ (mag)	Mean (mag)	σ (mag)	Mean (mag)	σ (mag)	Mean (mag)	σ (mag)
M6–M6.9	33	16.65	0.49	15.31	0.47	13.19	0.39	12.21	0.38	11.70	0.36	10.30	0.36	9.70	0.36	9.37	0.37	9.16	0.37	8.95	0.36	8.66	0.40
M7–M7.9	27	18.11	0.56	16.75	0.50	14.18	0.39	12.97	0.34	12.31	0.31	10.77	0.30	10.14	0.31	9.75	0.31	9.52	0.31	9.30	0.31	8.96	0.33
M8–M8.9	22	19.16	0.58	17.70	0.51	14.95	0.47	13.56	0.44	12.77	0.43	11.11	0.42	10.43	0.42	9.99	0.43	9.74	0.43	9.51	0.43	9.15	0.46
M9–M9.9	12	19.95	0.43	18.15	0.42	15.63	0.42	14.19	0.38	13.25	0.37	11.48	0.35	10.77	0.36	10.29	0.37	9.97	0.37	9.71	0.37	9.26	0.43
L0–L0.9	18	20.40	0.43	18.41	0.35	16.04	0.29	14.57	0.28	13.62	0.26	11.80	0.22	11.04	0.26	10.56	0.28	10.26	0.29	9.98	0.29	9.36	0.34
L1–L1.9	22	20.86	0.78	18.75	0.31	16.42	0.26	14.94	0.24	13.97	0.23	12.04	0.17	11.24	0.22	10.72	0.25	10.37	0.27	10.12	0.28	9.65	0.32
L2–L2.9	12	21.25	···	19.03	0.29	16.74	0.26	15.32	0.25	14.34	0.25	12.33	0.21	11.42	0.26	10.83	0.29	10.42	0.34	10.15	0.35	9.63	0.37
L3–L3.9	5	···	···	19.72	0.32	17.53	0.26	16.02	0.22	15.03	0.20	12.90	0.10	11.95	0.19	11.31	0.24	10.79	0.30	10.52	0.32	10.04	0.32
L4–L4.9	8	···	···	20.46	0.65	18.25	0.49	16.56	0.46	15.56	0.45	13.41	0.42	12.35	0.46	11.77	0.51	11.11	0.53	10.77	0.55	10.17	0.56
L5–L5.9	8	···	···	20.66	0.37	18.74	0.32	16.94	0.29	15.87	0.29	13.70	0.25	12.65	0.31	12.03	0.36	11.28	0.37	10.98	0.41	10.13	0.52
L6–L6.9	10	···	···	21.20	0.77	19.26	0.65	17.34	0.60	16.26	0.60	14.17	0.58	13.18	0.61	12.54	0.66	11.84	0.69	11.48	0.73	10.30	0.78
L7–L7.9	4	···	···	···	···	20.11	0.36	18.20	0.25	17.15	0.24	14.96	0.18	13.80	0.30	13.09	0.32	12.44	0.49	12.01	0.58	10.37	0.83
L8–L8.9	9	···	···	22.87	···	20.43	0.39	18.09	0.21	17.02	0.21	14.89	0.12	13.76	0.18	13.10	0.21	12.20	0.26	11.67	0.27	10.64	0.36
L9–L9.9	4	···	···	···	···	20.64	0.50	18.15	0.36	17.04	0.35	14.93	0.32	13.85	0.36	13.26	0.38	12.41	0.39	11.89	0.43	11.15	0.43
T0–T0.9	1	···	···	···	···	20.22	···	17.99	···	16.76	···	14.56	···	13.63	···	13.11	···	12.43	···	11.87	···	11.02	···
T1–T1.9	4	···	···	···	···	21.03	0.96	18.87	0.21	17.44	0.17	15.25	0.13	14.37	0.19	14.07	0.32	13.41	0.37	12.68	0.33	11.26	0.76
T2–T2.9	5	···	···	···	···	21.50	0.70	18.27	0.31	16.78	0.27	14.55	0.16	13.75	0.22	13.49	0.30	12.95	0.56	12.05	0.47	10.62	0.43
T3–T3.9	2	···	···	···	···	···	···	18.07	0.25	16.52	0.22	14.26	0.16	13.67	0.24	13.44	0.32	12.78	0.60	11.71	0.43	···	···
T4–T4.9	7	···	···	···	···	···	···	18.11	0.41	16.41	0.40	13.98	0.38	13.66	0.42	13.60	0.41	13.36	0.42	11.94	0.41	10.79	···
T5–T5.9	7	···	···	···	···	22.69	···	19.20	0.22	17.43	0.20	14.94	0.12	14.75	0.24	14.77	0.23	14.46	0.26	12.67	0.25	11.54	0.27
T6–T6.9	11	···	···	···	···	···	···	19.82	0.32	18.07	0.32	15.53	0.27	15.48	0.37	15.37	0.41	15.08	0.35	13.03	0.41	11.61	0.37
T7–T7.9	8	···	···	···	···	···	···	21.14	0.78	19.33	0.81	16.78	0.77	16.70	0.79	16.70	0.94	16.27	0.80	14.11	0.83	12.25	0.77
T8–T8.9	4	···	···	···	···	···	···	21.52	0.52	19.75	0.59	17.18	0.51	17.09	···	···	···	16.50	0.77	13.90	0.94	12.27	0.64
T9–T9.9	1	···	···	···	···	···	···	21.82	···	20.37	···	17.75	···	17.51	···	···	···	16.70	···	13.81	···	11.97	···

Note—SEDs constructed using parallaxes from the literature to determine absolute J_{2MASS} magnitudes, for which we report the weighted mean and rms for each spectral subtype bin. The number of objects used to determine $M_{J_{2MASS}}$ for each spectral subtype is listed in the second column (N). Binaries, subdwarfs, and young objects were excluded from these SEDs. We use median colors from our catalog to calculate absolute magnitudes in other bands.

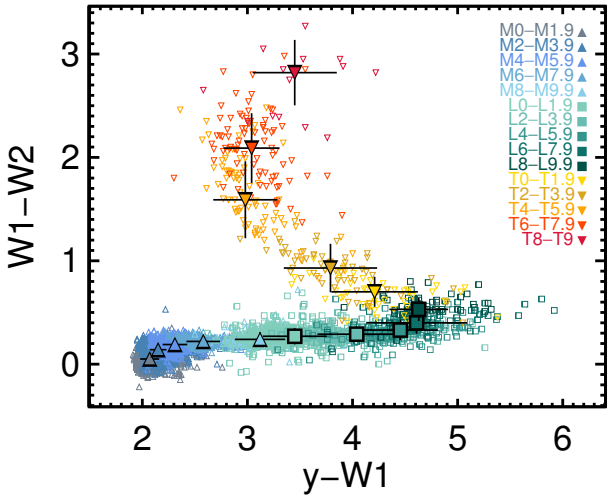

Figure 7. continued.

4. PROPER MOTION

In Table 7 we present our proper motions for 9,813 M, L, and T dwarfs based on PS1 astrometry, along with parallaxes from the literature or photometric distances, tangential velocities, and proper motions from the literature for comparison. The full table is available for download in electronic form in the online journal. Like Table 1, Table 7 is arranged in two parts: (1) the late-M, L, and T dwarfs compiled from the literature, followed by (2) the M dwarfs from West et al. (2008). For reference, Table 7 also includes spectral types (Section 2.4), and indicates whether an object has been identified as a binary or young object, or classified as low-gravity based on its optical or near-IR spectrum.

4.1. *Method*

4.1.1. *PS1 database proper motions*

The procedure used to calculate the proper motions and errors for the objects in the PS1 database will be described in detail in Magnier et al. (2017, in prep). Briefly, all detections for an object in all filters were fit simultaneously for proper motion and parallax using iteratively-reweighted least-squares regression with outlier clipping. The detections retained in the fit were then bootstrap-resampled to determine the errors on the proper motion and parallax. For objects having a 2MASS or Gaia DR1 (Lindegren et al. 2016) counterpart within 1" of the mean PS1 position, the PS1 proper motion calculation includes these positions. (The parallaxes will be presented in Magnier et al., 2017, in prep). For this paper we also convert the PS1-measured $\mu_\alpha \cos\delta$ and μ_δ to a combined proper motion μ and position angle PA, and we calculate errors for these in a Monte Carlo fashion. To establish a minimum quality for our PS1 proper motions, if either $\mu_\alpha \cos\delta$ or μ_δ for an object has an error greater than 100 mas yr^{-1} and $\mu/\sigma_\mu < 3$, we do not report a proper motion for the object. This rejects large but very uncertain proper motions that may erroneously identify fast-moving objects (e.g., 500 ± 300 mas yr^{-1}), but preserves high-precision measurements of very small proper motions that have a formal S/N < 3 (e.g., 5 ± 3 mas yr^{-1}).

4.1.2. *PS1 mean positions and epoch*

Table 7 includes a mean PS1 position and epoch for each object. To determine these, the PS1 astrometric pipeline calculates a weighted mean epoch t_0, in which the epochs are weighted by the rms of the R.A. and Decl. astrometric uncertainties. The mean position (α_0, δ_0) is calculated (in simple terms) by fitting the positions (α, δ) at each epoch t to

$$\begin{aligned} \alpha(t) &= \alpha_0 + \pi p_\alpha(t) + \mu_\alpha (t - t_0)/\cos(\delta) \\ \delta(t) &= \delta_0 + \pi p_\delta(t) + \mu_\delta (t - t_0) \end{aligned} \quad (1)$$

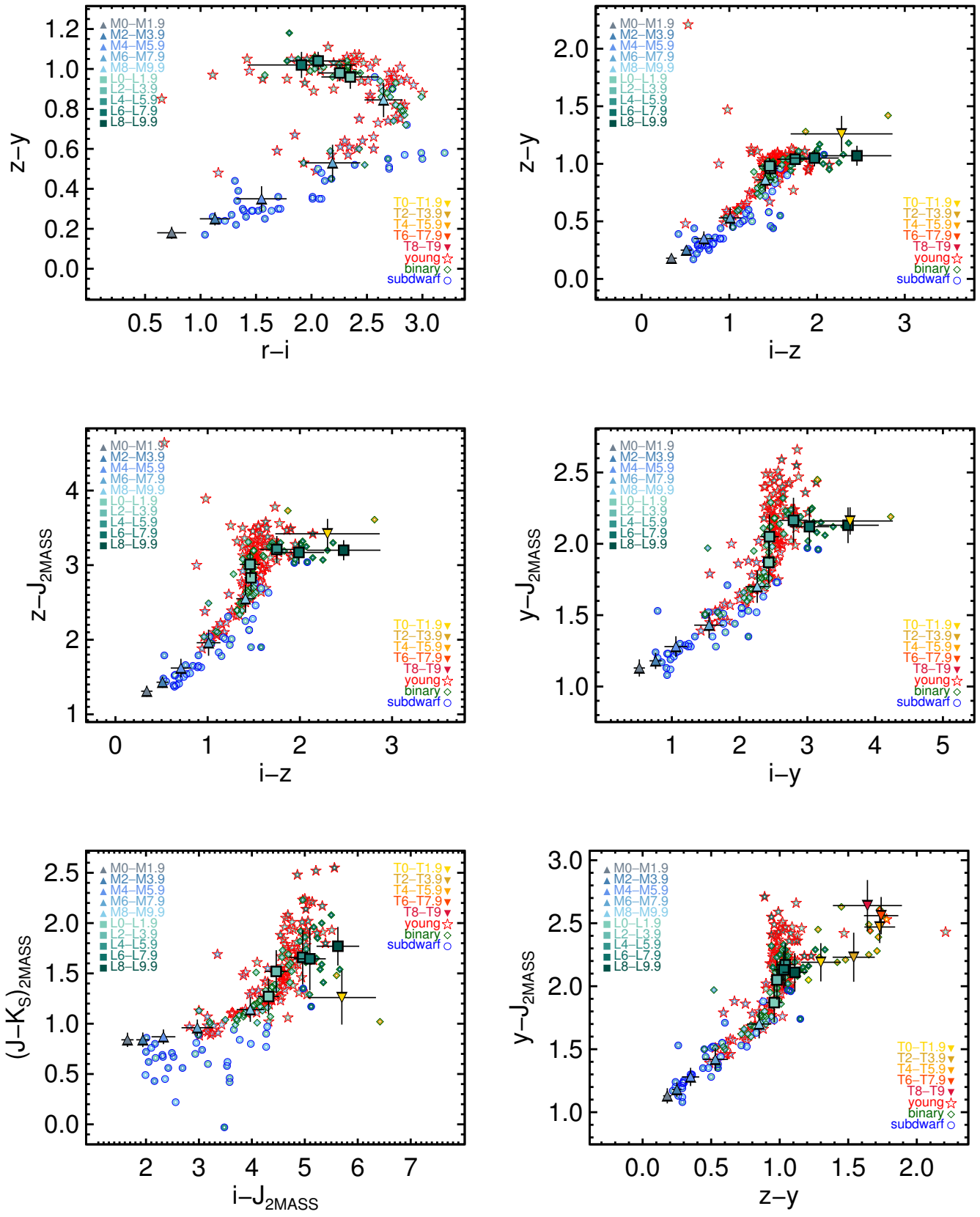

Figure 8. Color-color plots for known young objects, binaries, and subdwarfs in our PS1-detected catalog, using the same format as in Figure 6. Median colors and error bars for normal field objects from Figure 7 are overplotted for reference.

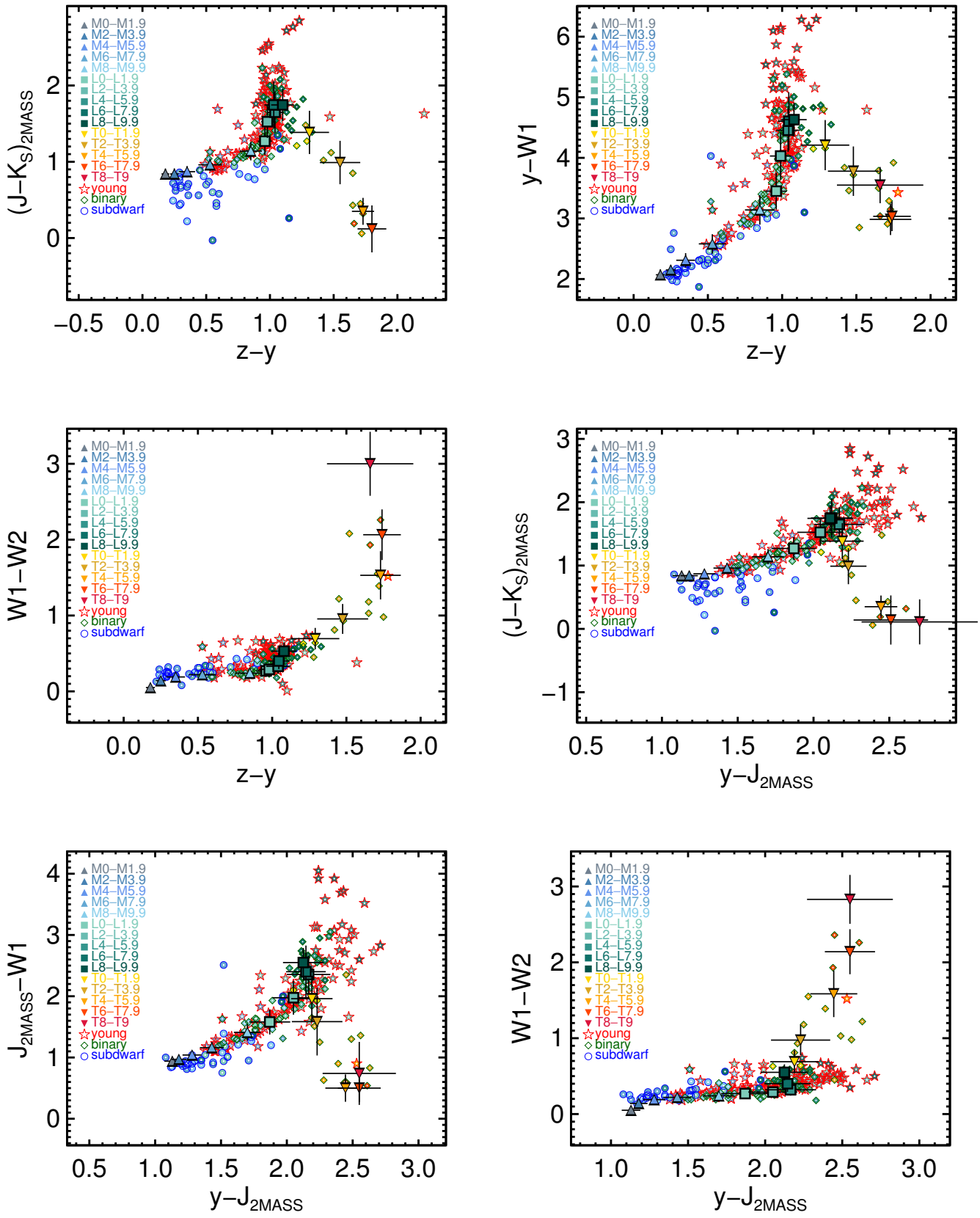

Figure 8. continued.

Table 7. Positions and Proper Motions of M, L, and T Dwarfs from the Pan-STARRS1 3π Survey

Discovery Name	Spectral Type[a,b] Opt	NIR	Adopted	Gravity[b] Opt	NIR	Binary	Young[c]	PS1 Mean Position[d] α_{J2000} (deg)	δ_{J2000} (deg)	Epoch (MJD)
SDSS J000013.54+255418.6	T5	T4.5	T4.5	···	···	···	···	0.056404	25.905390	55326.38
SDSS J000112.18+153535.5	···	L3.7 INT-G	L3.7 INT-G	···	INT-G	···	Y	0.301174	15.592647	55751.22
WISEA J000131.93−084126.9	···	L1 pec (blue)	L1 pec (blue)	···	···	···	···	0.383131	−8.690953	55632.76
SDSS J000250.98+245413.8	···	L5.5	L5.5	···	···	···	···	0.712466	24.903796	55329.42
2MASSI J0003422−282241	M7.5	M7: FLD-G	M7.5	···	FLD-G	···	···	0.927389	−28.378608	56101.40
2MASS J00044144−2058298	M8	···	M8	···	···	···	···	1.175450	−20.974699	55856.59
2MASS J00054844−2157196	M9	···	M9	···	···	···	···	1.454358	−21.955896	55717.70
ULAS J000613.24+154020.7	···	L9	L9	···	···	···	···	1.555349	15.672403	56032.02
SDSS J000614.06+160454.5	L0	···	L0	···	···	···	···	1.558610	16.081687	55734.32

PS1 Proper Motion $\mu_\alpha \cos\delta$ (mas yr^{-1})	$\mathrm{err}_{\mu_\alpha \cos\delta}$ (mas yr^{-1})	μ_δ (mas yr^{-1})	$\mathrm{err}_{\mu_\delta}$ (mas yr^{-1})	μ (mas yr^{-1})	err_μ (mas yr^{-1})	PA_μ (deg)	$\mathrm{err}_{\mathrm{PA}_\mu}$ (deg)	χ^2_ν	N_{ep}	Δt (yr)
−17.9	6.0	121.5	3.1	122.8	3.2	351.6	2.8	1.5	28	15.2
137.4	7.4	−180.5	3.6	226.8	5.3	142.7	1.6	2.1	34	14.1
337.9	2.8	−302.2	3.6	453.3	3.2	131.8	0.4	0.9	46	15.8
19.9	17.9	−46.4	9.5	50.5	11.1	156.8	18.7	1.1	28	15.2
285.5	1.9	−142.8	1.6	319.2	1.8	116.6	0.3	1.8	67	16.1
751.3	2.3	93.7	3.0	757.1	2.3	82.9	0.2	2.8	74	15.1
712.1	3.8	−125.7	4.5	723.1	3.8	100.0	0.4	2.9	66	14.9
84.3	41.4	−34.2	19.1	91.0	36.5	112.1	22.2	1.0	16	3.9
3.5	5.0	−40.1	4.9	40.3	4.9	175.0	7.2	0.8	40	17.2

PS1 v_{tan} π (mas)	err_π (mas)	dist[e] (pc)	err_{dist} (pc)	v_{tan} (km s^{-1})	σ_{tan} (km s^{-1})	Literature Proper Motion $\mu_\alpha \cos\delta$ (mas yr^{-1})	$\mathrm{err}_{\mu_\alpha \cos\delta}$ (mas yr^{-1})	μ_δ (mas yr^{-1})	$\mathrm{err}_{\mu_\delta}$ (mas yr^{-1})	References[f] (π; μ_{lit})
70.80	1.90	14.12	0.38	8.2	0.3	−19.1	1.5	126.7	1.3	41; 41
···	···	24.34	2.93	26.2	3.2	135.2	10.7	−169.6	13.7	–; 54
···	···	61.40	10.26	131.9	22.1	331.0	14.0	−299.0	14.0	–; 90
···	···	53.33	6.54	12.8	3.2	···	···	···	···	–; –
25.70	0.93	38.91	1.41	58.9	2.2	280.8	0.9	−141.5	0.8	130; 130
···	···	18.94	3.14	68.0	11.3	825.5	75.7	−9.2	75.5	–; 68
···	···	25.43	4.22	87.2	14.5	703.0	24.0	−119.0	4.0	–; 74
···	···	43.24	5.35	18.7	7.8	92.9	23.3	−73.8	23.3	–; 72
···	···	103.52	17.46	19.8	4.1	−5.0	19.0	−40.0	19.0	–; 138

[a] Spectral types taken from the literature (Section 2.4). When both optical and near-IR types are available, we adopt the optical type for M and L dwarfs and the near-IR type for T dwarfs. Most spectral types have an uncertainty of ±0.5 subtypes; ":" = ±1 subtype; "::" = ±2 or more subtypes. "sd" = subdwarf; "esd" = extreme subdwarf (Gizis 1997).

[b] β, γ, and δ indicate classes of increasingly low gravity based on optical (Kirkpatrick 2005; Cruz et al. 2009) or near-infrared (Gagné et al. 2015c) spectra. FLD-G indicates near-infrared spectral signatures of field-age gravity, INT-G indicates intermediate gravity, and VL-G indicates very low gravity (Allers & Liu 2013a).

[c] Young objects identified by low-gravity classifications or other spectroscopic evidence for youth, membership in star-forming regions or young moving groups, or companionship to a young star (Section 2.5).

[d] The mean PS1 position is the position calculated for the weighted mean epoch, in which the epochs are weighted by the rms of the R.A. and Decl. astrometric uncertainties.

[e] Distances were calculated from trigonometric parallaxes when available. If no parallax was available, we calculated photometric distances using i_{P1} magnitudes for spectral types M0–M5 and $W2$ magnitudes (when available) for spectral types M6 and later.

[f] References for spectral type, gravity, and binarity are given in Table 1.

[g] Although classified as FLD-G, the spectrum shows hints of intermediate gravity (as described in Aller et al. 2016).

[h] The R.A. and Decl. proper motion components listed in Table 2 of Lodieu et al. (2012b) appear to be reversed. We quote the corrected order here.

References—(1) Aberasturi et al. (2014), (2) Albert et al. (2011), (3) Aller et al. (2016), (4) Allers et al. (2009), (5) Andrei et al. (2011), (6) Artigau et al. (2011), (7) Bardalez Gagliuffi et al. (2014), (8) Baron et al. (2015), (9) Bartlett (2007), (10) Beamín et al. (2013), (11) Béjar et al. (2008), (12) Best et al. (2015), (13) Bihain et al. (2013), (14) Bouvier et al. (2008), (15) Bowler et al. (2013), (16) Burgasser et al. (2003b), (17) Burgasser et al. (2004), (18) Burgasser et al. (2007), (19) Burgasser et al. (2008a), (20) Burgasser et al. (2008c), (21) Burgasser et al. (2012), (22) Burgasser et al. (2015), (23) Burgasser et al. (2016), (24) Burningham et al. (2013), (25) Caballero (2007), (26) Cardoso et al. (2015), (27) Casewell et al. (2008), (28) Castro et al. (2013), (29) Costa et al. (2005), (30) Costa et al. (2006), (31) Dahn et al. (2002), (32) Dahn et al. (2008), (33) Deacon et al. (2005), (34) Deacon & Hambly (2007), (35) Deacon et al. (2009), (36) Deacon et al. (2011), (37) Deacon et al. (2012b), (38) Deacon et al. (2014), (39) Dieterich et al. (2014), (40) Dittmann et al. (2014), (41) Dupuy & Liu (2012), (42) Dupuy & Kraus (2013), (43) Dupuy et al. (2015), (44) Faherty et al. (2009), (45) Faherty et al. (2010), (46) Faherty et al. (2012), (47) Faherty et al. (2013), (48) Faherty et al. (2016), (49) Finch & Zacharias (2016), (50) Folkes et al. (2012), (51) Forbrich et al. (2016), (52) Gagné et al. (2014a), (53) Gagné et al. (2014b), (54) Gagné et al. (2015b), (55) Gatewood & Coban (2009), (56) Gauza et al. (2015), (57) Gelino et al. (2014), (58) Gizis et al. (2011a), (59) Gizis et al. (2013), (60) Gizis et al. (2015), (61) Hambly et al. (2001), (62) Harrington et al. (1993), (63) Henry et al. (2006), (64) Høg et al. (2000), (65) Jameson et al. (2008), (66) Kellogg et al. (2016), (67) Kendall et al. (2004), (68) Kendall et al. (2007a), (69) Kirkpatrick et al. (2010), (70) Kirkpatrick et al. (2011), (71) Kirkpatrick et al. (2014), (72) Lawrence et al. (2012), (73) Leggett et al. (2012), (74) Lépine et al. (2002b), (75) Lépine & Shara (2005), (76) Lépine et al. (2009), (77) Lépine & Gaidos (2011), (78) Liu et al. (2011), (79) Liu et al. (2013a), (80) Liu et al. (2013b), (81) Lodieu et al. (2005), (82) Lodieu et al. (2006), (83) Lodieu et al. (2012c), (84) Lodieu et al. (2012b), (85) Lodieu et al. (2012a), (86) Lodieu et al. (2013), (87) Lodieu (2013), (88) Lodieu et al. (2014), (89) Luhman et al. (2012), (90) Luhman & Sheppard (2014), (91) Luyten (1979), (92) Manjavacas et al. (2013), (93) Marocco et al. (2010), (94) Marocco et al. (2013), (95) Marsh et al. (2013), (96) McCaughrean et al. (2004), (97) Monet et al. (1992), (98) Monet et al. (2003), (99) Muzic et al. (2012), (100) Phan-Bao et al. (2008), (101) Phan-Bao (2011), (102) Pokorny et al. (2004), (103) Radigan et al. (2008), (104) Reid (2003), (105) Riedel et al. (2014), (106) Roeser et al. (2010), (107) Sahlmann et al. (2014), (108) Sahlmann et al. (2015), (109) Sahlmann et al. (2016), (110) Salim & Gould (2003), (111) Schilbach et al. (2009), (112) Schmidt et al. (2007), (113) Schmidt et al. (2010), (114) Schneider et al. (2016b), (115) Scholz et al. (2009), (116) Scholz et al. (2014), (117) Schweitzer et al. (1999), (118) Seifahrt et al. (2010), (119) Sheppard & Cushing (2009), (120) Shkolnik et al. (2012), (121) Smart et al. (2013), (122) Smith et al. (2014b), (123) Smith et al. (2014a), (124) Stern et al. (2007), (125) Thompson et al. (2013), (126) Tinney et al. (1995), (127) Tinney (1996), (128) Tinney et al. (2003), (129) van Altena et al. (1995), (130) van Leeuwen (2007), (131) Vrba et al. (2004), (132) Wang et al. (2014b), (133) Weinberger et al. (2016), (134) West et al. (2008), (135) Wright et al. (2013), (136) Zapatero Osorio et al. (2014), (137) Zhang et al. (2009), (138) Zhang et al. (2010).

Note—This table is available in its entirety in machine-readable form in the online journal. A portion is shown here for guidance regarding its form and content. The full table contains 9,938 rows. Columns 2–8 are the same as in Table 1, and are repeated here for reference.

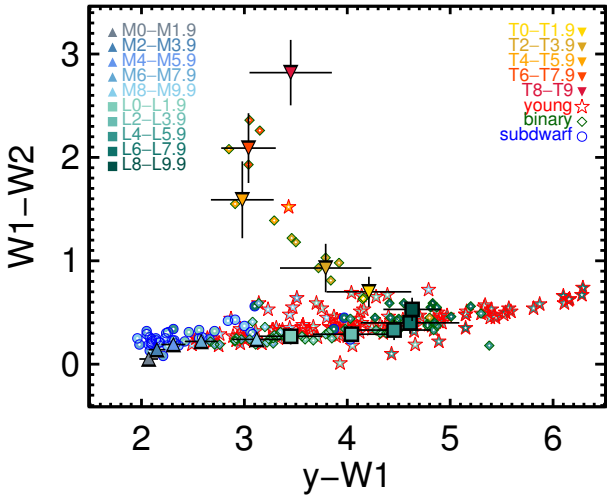

Figure 8. continued.

where π is the parallax, and p_α and p_δ are the parallax factors in R.A. and Decl., respectively. This is also, by construction, the position at which the covariance with the proper motion is minimized, and is therefore the best position given the set of observations. In cases where no proper motion is measured, the mean position coordinates are weighted means of the individual epochs. For objects with a 2MASS or Gaia detection, these are included in determining the mean epoch and position.

4.1.3. *Calculation for fast-moving objects*

The PS1 database builds astronomical objects from individual detections at different epochs by grouping detections within 1" of each other. In cases where two distinct objects are detected within 1" of each other at a single epoch, detections at other epochs are associated with the closer of the two objects (see Magnier et al., 2017, in prep, for details). This procedure is successful for stationary and slow-moving point sources, but for an object with a proper motion large enough to move $\gtrsim$1" over the four-year timespan of PS1, the detections may not all be grouped together in the PS1 database. In our ultracool catalog, we found that objects with proper motions $\gtrsim$ 200 mas yr^{-1} were often split into two or more "partial objects" in the PS1 database, identifiable by their proximity on the sky, astrometric consistency with proper motions from the literature, and consistent photometry. These partial objects often had significantly different proper motion measurements, but offered no *a priori* way to determine which (if any) of the measurements was correct. This motivated us to recalculate the proper motions for fast-moving objects, using an automated procedure to identify all the detections along the paths of motion. While our primary goal was to improve our proper motions of fast-moving objects, we performed the recalculation for all objects of spectral type M6 and later in our catalog.

To determine where to search for detections for each object, we used the PS1 and 2MASS positions in the follow manner. We calculated the distance between the PS1 and 2MASS positions, and generated a search box for the PS1 data based on the implied proper motion of the distance divided by a baseline of 12 years. We added 4" in quadrature to 5 years times the implied proper motion and used the resulting value for the length of a square box. We searched the PS1 and 2MASS databases for all detections within this box around the PS1 position. In cases where the 2MASS and PS1 positions were more than 2" apart, we also searched around the 2MASS position within a 1" box. Once we identified candidate detections, we determined the path on the sky from the 2MASS to the PS1 positions, and if the 2MASS–PS1 distance was more than 3", we excluded any points that were more than 1" away from the path. For objects in our catalog with no associated 2MASS detection, we used the best available proper motion from the literature to predict a 2MASS position by projecting backward 10 years from the PS1 position. For objects with no associated 2MASS detection and no literature proper motion, we simply searched in a 4" box around the PS1 position. Finally, we searched the Gaia DR1 database for detections within 1" of the PS1 position, and included the astrometry from a Gaia match if one was found.

We then calculated proper motions using the method summarized in Section 4.1.1 for objects having at least seven

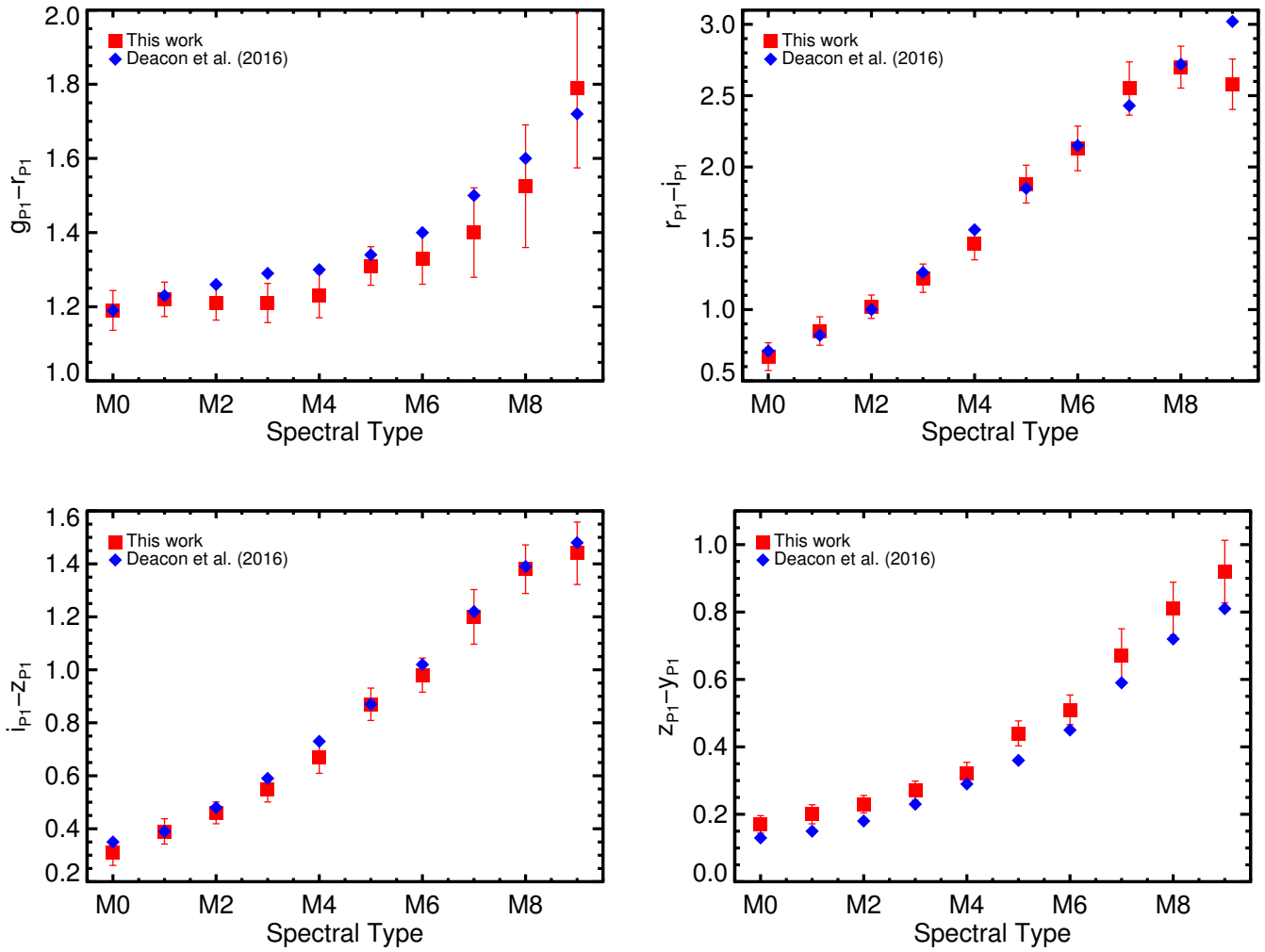

Figure 9. The colors of M dwarfs as a function of spectral type, compared with the colors derived from the SED templates of Deacon et al. (2016). Our colors are generally quite consistent with those of D16, with most differences small and likely the result of differences in our input samples. The blueward turn in $r_{P1} - i_{P1}$ at spectral type M9 was not identified by D16 because of their use of $g_{P1} - i_{P1}$ as a proxy for spectral type, which does not clearly distinguish between the late-M spectral subtypes.

detections (to ensure robust astrometric fits). We applied the same minimum quality cut as we used for the PS1 database proper motions, rejecting those for which either (or both) of $\mu_\alpha \cos\delta$ and μ_δ has an error greater than 100 mas yr^{-1} and $\mu/\sigma_\mu < 3$. Our recalculations produced proper motions for 2365 objects. These included 64 objects that do not have a proper motion in the PS1 database, most of which are moving faster than 200 mas yr^{-1}, demonstrating the success of our method. The largest proper motion for objects in our catalog reported in the PS1 database is 1567 mas yr^{-1}, but our recalculated measurements include 16 objects with greater proper motions, up to a maximum of 3506 mas yr^{-1} (SSSPM J1444−2019). The recalculation was unable to fit a proper motion to the identified detections for 154 objects. 41 of the objects for which the recalculation failed do have PS1 database proper motions, but these are mostly poor measurements ($\sigma_\mu \gtrsim 40$ mas yr^{-1}) for faint objects ($y \gtrsim 20$ mag) with few detections ($N \lesssim 10$).

Figure 10 compares our recalculated proper motions and errors to the values in the PS1 database. The recalculated proper motions are strongly consistent with the database measurements, and the errors for the recalculated proper motions are lower for 89% of the objects, with a median improvement of 33% in precision. We examined all objects for which the recalculated $\mu_\alpha \cos\delta$ or μ_δ differed by more than three times the error on the corresponding value in the PS1 database, and identified only six cases in which the recalculation produced a result clearly inconsistent with the separation between the PS1 and 2MASS positions or with a literature measurement. In each of these six cases, a nearby

object appears to have significantly contaminated the proper motion calculation. We rejected the recalculated values for these six objects. In all other cases of significant discrepancy the recalculated proper motion was consistent with a value in the literature (except for one object with no literature value), confirming that our recalculation improved the accuracy of these proper motions.

For our catalog (Table 7), we adopt the recalculated proper motions by default. We also present mean positions from our recalculations, which incorporate the 2MASS and Gaia positions used in the calculations. We use the PS1 database proper motions and positions only for the six contaminated recalculations described above and in cases where our recalculation was unable to fit a proper motion. In these cases we retained the PS1 database astrometry, and we flag these objects in Table 7. We also recalculated chip photometry for each object along with proper motion, but we did not apply the rigorous outlier-clipping procedure used for the PS1 database photometry, so by default we use the database photometry in our catalog. We use our recalculated photometry only in cases where the database reports photometry of insufficient quality or none at all, provided that our recalculated chip photometry passes the quality standards described in Section 3.1.2.

4.2. *Characteristics*

For the remainder of Section 4, we restrict our discussion to objects with spectral types M6 and later in order to focus our kinematic analysis on ultracool dwarfs near the Sun. Early-M dwarfs are visible at distances well beyond the solar neighborhood ($\gtrsim$200 pc) where large-scale galactic motions dominate the kinematics, entailing a discussion that is beyond the scope of this paper. We report PS1 proper motions for a total of 2,369 M6–T9 dwarfs, the largest set of uniformly-calculated proper motions for L and T dwarfs published to date. We note that the proper motions in our catalog do not comprise a clearly-defined sample and reflect biases inherited from the programs that discovered the objects (Section 2.7), but our proper motions nevertheless serve as a large and illustrative sample of the local ultracool population.

Figure 11 shows the time baselines and number of epochs used for the ultracool proper motions in our catalog. Most of our proper motions were calculated using a 2MASS position and have time baselines spanning 13–17 years. Proper motions using only PS1 astrometry have time baselines spanning $1-5$ years (data taken 2009–2014). For about one-quarter of our sample (593 objects), a Gaia DR1 (Lindegren et al. 2016) position was included in our proper motion.

Figures 12 and 13 show the proper motion distributions for our PS1 ultracool catalog. We find median values of $\mu_\alpha \cos\delta = -8.6$ mas yr^{-1} and $\mu_\delta = -42.0$ mas yr^{-1}. Our distributions are similar to those found in previous work on ultracool proper motions, including the Brown Dwarf Kinematics Project (BDKP; Faherty et al. 2009, 2012) and the BANYAN All-Sky Survey (BASS) Input Sample (Gagné et al. 2015b). Our median proper motion error of 3.5 mas yr^{-1} (Figure 13) is a factor of $\approx$5 smaller than that of BDKP and $\approx$2.5 smaller than BASS. The high precision of the PS1 measurements is a consequence of the high astrometric precision of PS1, the large number of epochs ($N > 20$ for 89% of proper motions), as well as the long time baseline for objects with a 2MASS position.

Figure 14 compares our PS1 proper motions to those of objects in common from BDKP, BASS, and other literature sources. Our proper motions are consistent with previously published values, especially the BDKP and BASS catalogs which are within 2σ for 90% of objects. In addition, we see no systematic offset between our measurements and those from BDKP and BASS. We do see a slight offset from other published proper motions (from multiple sources), suggesting that the PS1 proper motions are overall slightly smaller. Nevertheless, 90% of our values are consistent at 2.6σ or less with these other literature sources.

4.3. *Kinematics*

We calculated distances and tangential velocities for our catalog, which are listed in Table 7. The distances were determined from parallaxes in the literature when possible. When no parallax was available, we used $i_{\rm P1}$ photometry and the SED templates from D16 for M0–M5 dwarfs. D16 do not quote uncertainties for their SED templates, so based on the apparent scatter in their color transformations we adopt an uncertainty of 0.2 mag, and we add this in quadrature with the photometry errors to determine distance errors. For M6 and later-type dwarfs, we use $W2$ photometry with the spectral type-absolute magnitude polynomial and rms from Dupuy & Liu (2012) to calculate photometric distances and errors.

Figure 15 shows the distribution of $v_{\rm tan}$ among our single M6–T9 dwarfs, highlighting the young objects (Section 2.5) and subdwarfs. The peak of the $v_{\rm tan}$ distribution is in the $10-20$ km s^{-1} range, consistent with the distribution found by Faherty et al. (2009, hereinafter F09) for their 20 pc volume-limited ultracool sample. More than 90% of our sample has $v_{\rm tan} < 75$ km s^{-1}, indicating a very high probability of membership in the thin disk population (Dupuy

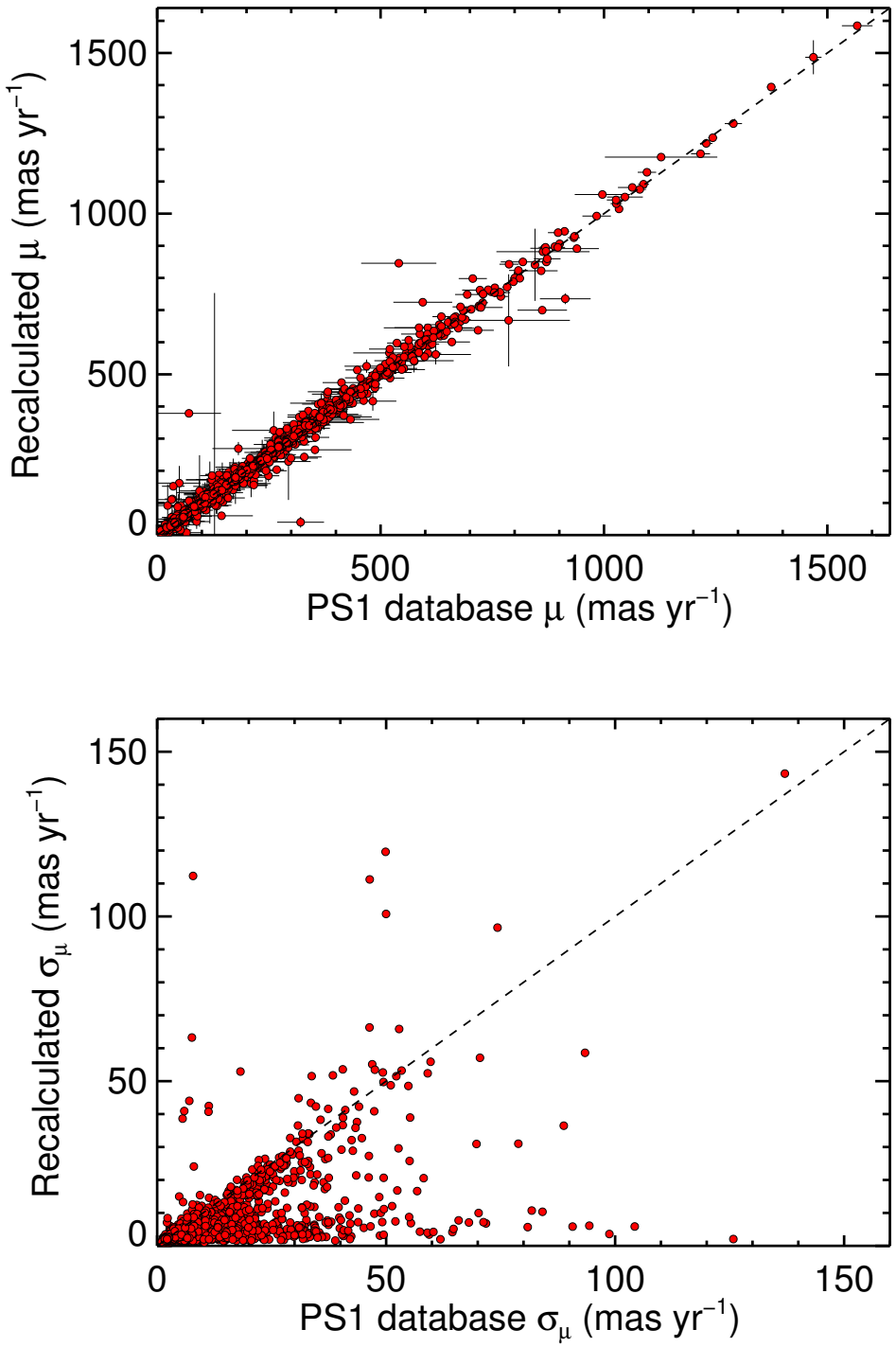

Figure 10. Comparison of the recalculated and PS1 database proper motions (*top*) and errors (*bottom*) for the M6–T9 dwarfs in our PS1 ultracool catalog. The dashed lines indicate equal values. The recalculated proper motions are strongly consistent with the database values, and in the cases of large discrepancy the recalculated proper motions are invariably consistent with literature values (except for six cases of clear contamination by a nearby object). The errors for the recalculated proper motions are lower for 89% of the objects, with a median reduction of 33%.

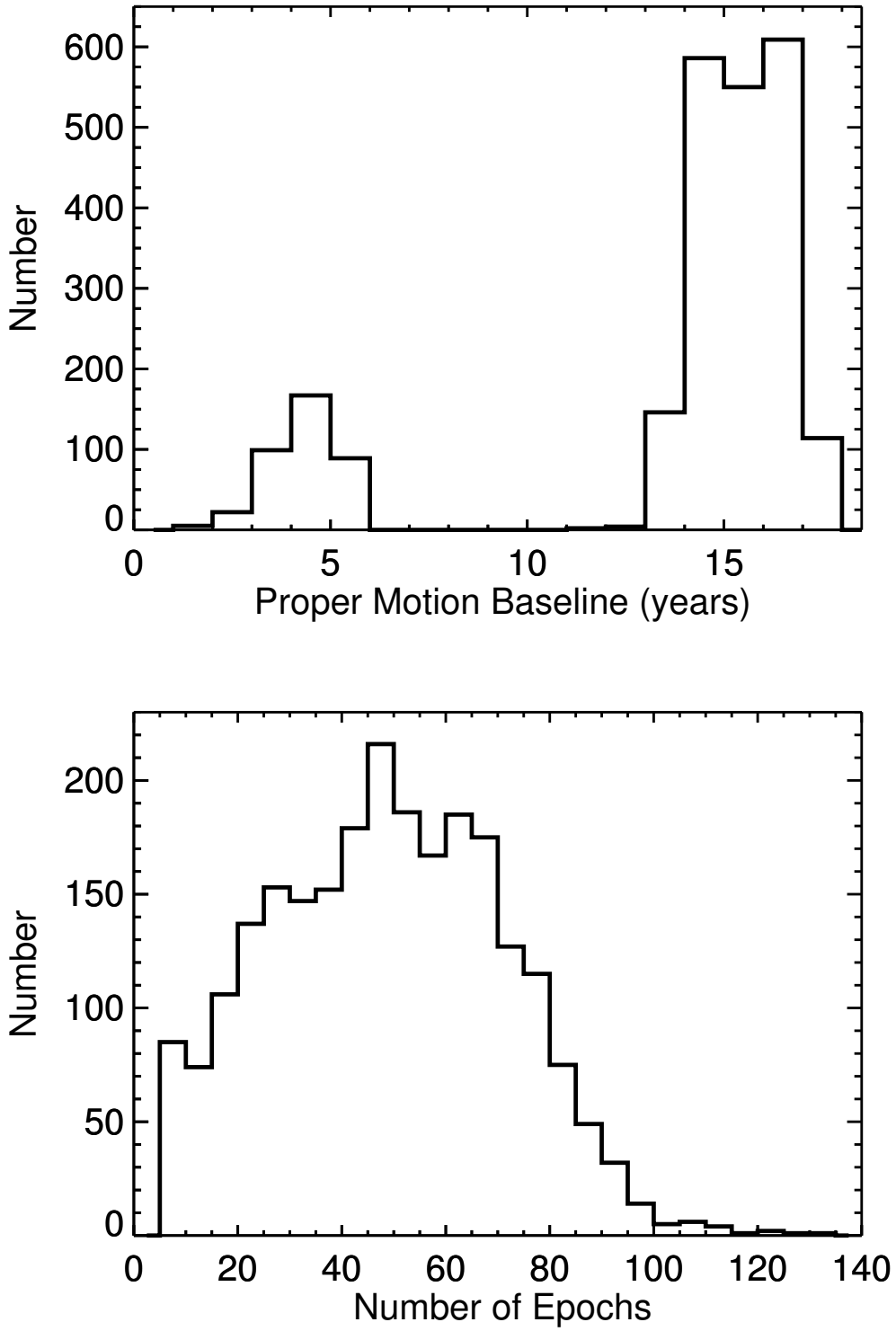

Figure 11. Distributions of the time baselines (*top*) and number of epochs (*bottom*) used to calculate the proper motions of the M6–T9 dwarfs in our PS1 ultracool catalog. For most objects (baselines ≈13-17 years) a 2MASS position was used in the motion fit. Baselines less than 10 years indicate that only PS1 astrometry was used. When available (for about one-quarter of the objects), a Gaia DR1 position was also included.

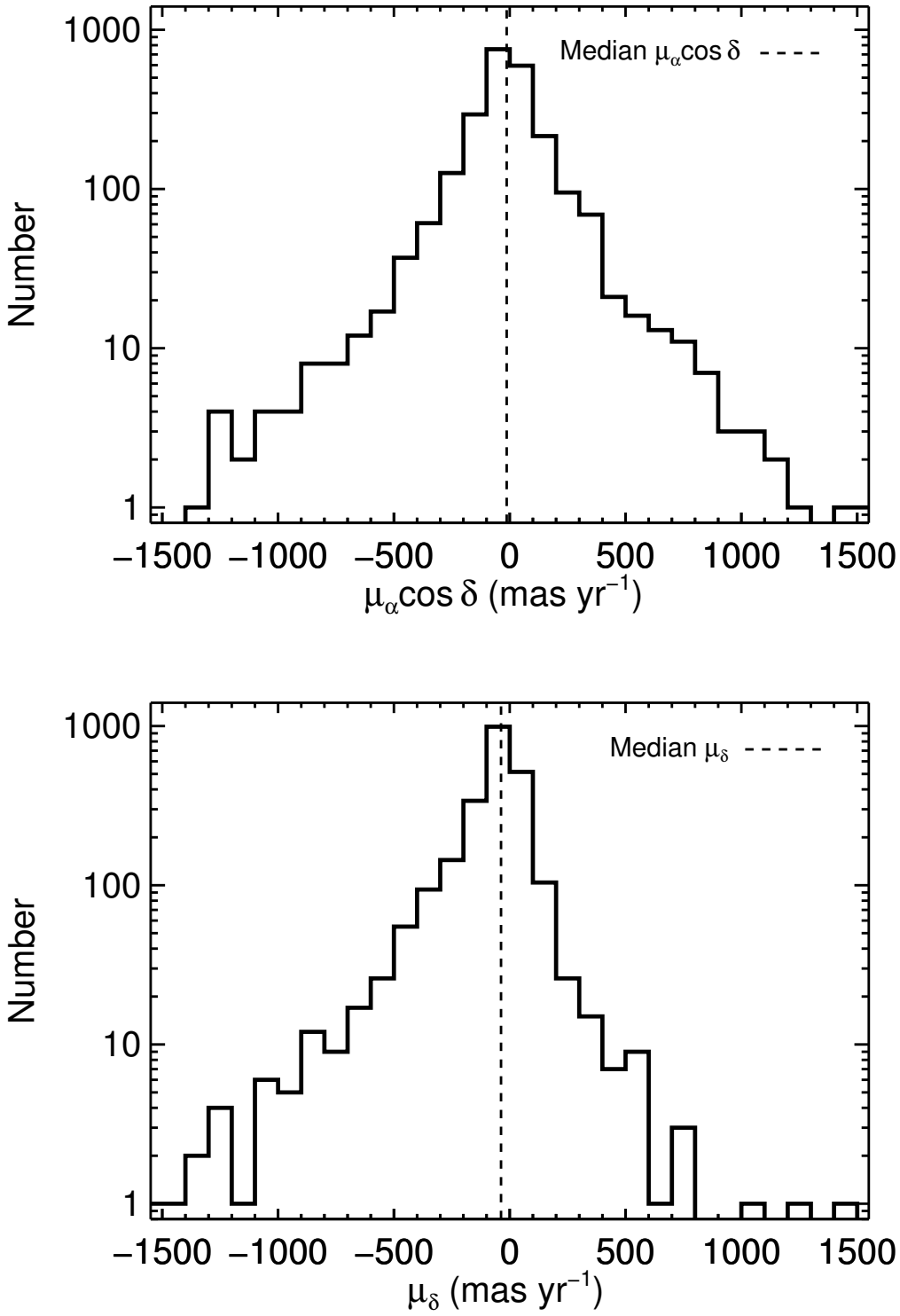

Figure 12. Distributions of the R.A. (*top*) and Decl. (*bottom*) proper motion components of the M6–T9 dwarfs in our PS1 ultracool catalog. The vertical dashed lines indicate the median values. The distributions are similar to those found in previous ultracool surveys (Schmidt et al. 2010; Faherty et al. 2012; Gagné et al. 2015b).

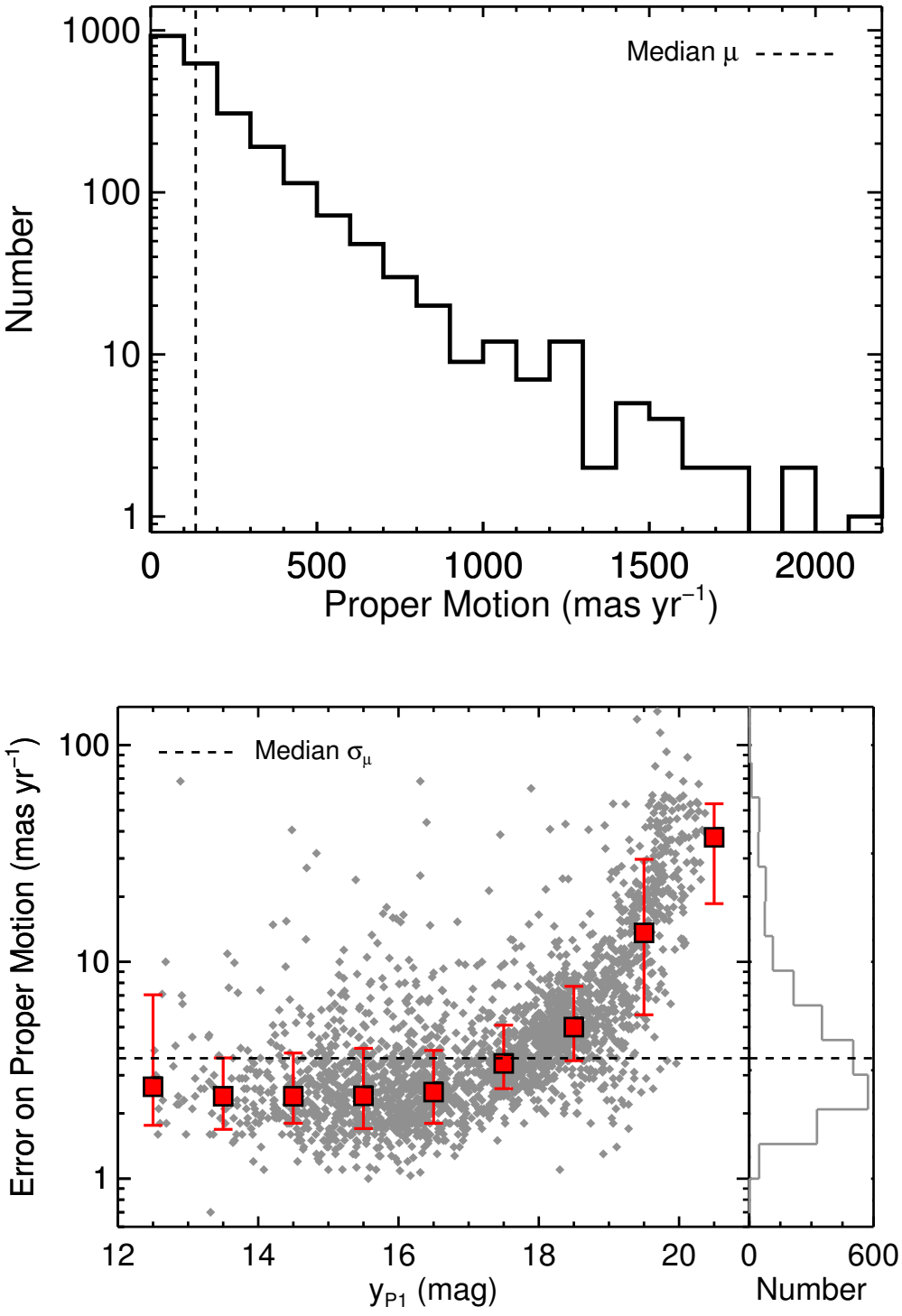

Figure 13. Distribution of the total proper motions (*top*) and proper motion errors as a function of y_{P1} (*bottom*) for the M6–T9 dwarfs in our PS1 ultracool catalog. The dashed lines indicate the median values. The large red squares indicate median errors for bins of one magnitude in y_{P1}, with error bars showing 68% confidence limits. values for bins of two spectral subtypes. Our errors are a factor of ≈5 smaller than those in Faherty et al. (2012) and ≈2.5 smaller than those in Gagné et al. (2015b).

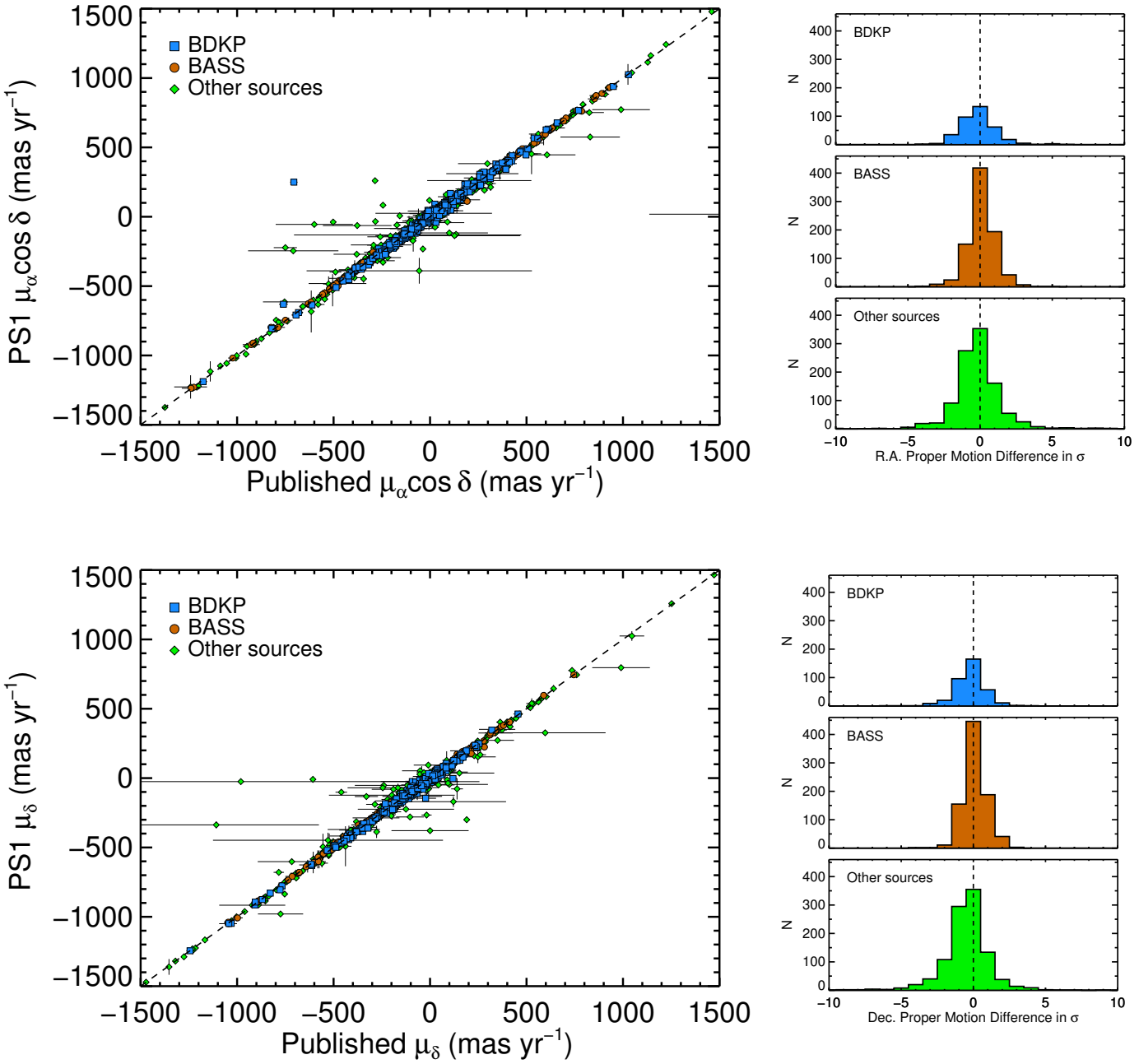

Figure 14. *Left*: Comparison of our PS1 proper motions in R.A. (*top*) and Decl. (*bottom*) with other results in the literature, highlighting the large BDKP and BASS catalogs. 90% of our proper motions are within 2σ of the BDKP and BASS measurements, and within 2.6σ of other literature values. *Right*: Histograms showing differences in R.A. and Decl. proper motions (computed as PS1 value − literature value). The histograms show no systematic offset between our PS1 proper motions and those of the BDKP and BASS catalogs, but suggest that the PS1 proper motions tend to be slightly smaller than those from other literature sources.

& Liu 2012). Figure 15 shows that the young objects and subdwarfs are members of distinct kinematic populations, consistent with the findings of Faherty et al. (2012). Almost all young objects have $v_{\rm tan}$ less than 60 km s^{-1}, slower on average than the rest of the thin-disk population. On the other hand, all but one subdwarf have $v_{\rm tan}$ greater than 60 km s^{-1} and comprise 88% of the objects with $v_{\rm tan} > 200$ km s^{-1}, extending to much higher velocities than other objects. Their high $v_{\rm tan}$ implies the subdwarfs are members of the older thick disk or halo populations as expected for low-metallicity objects.

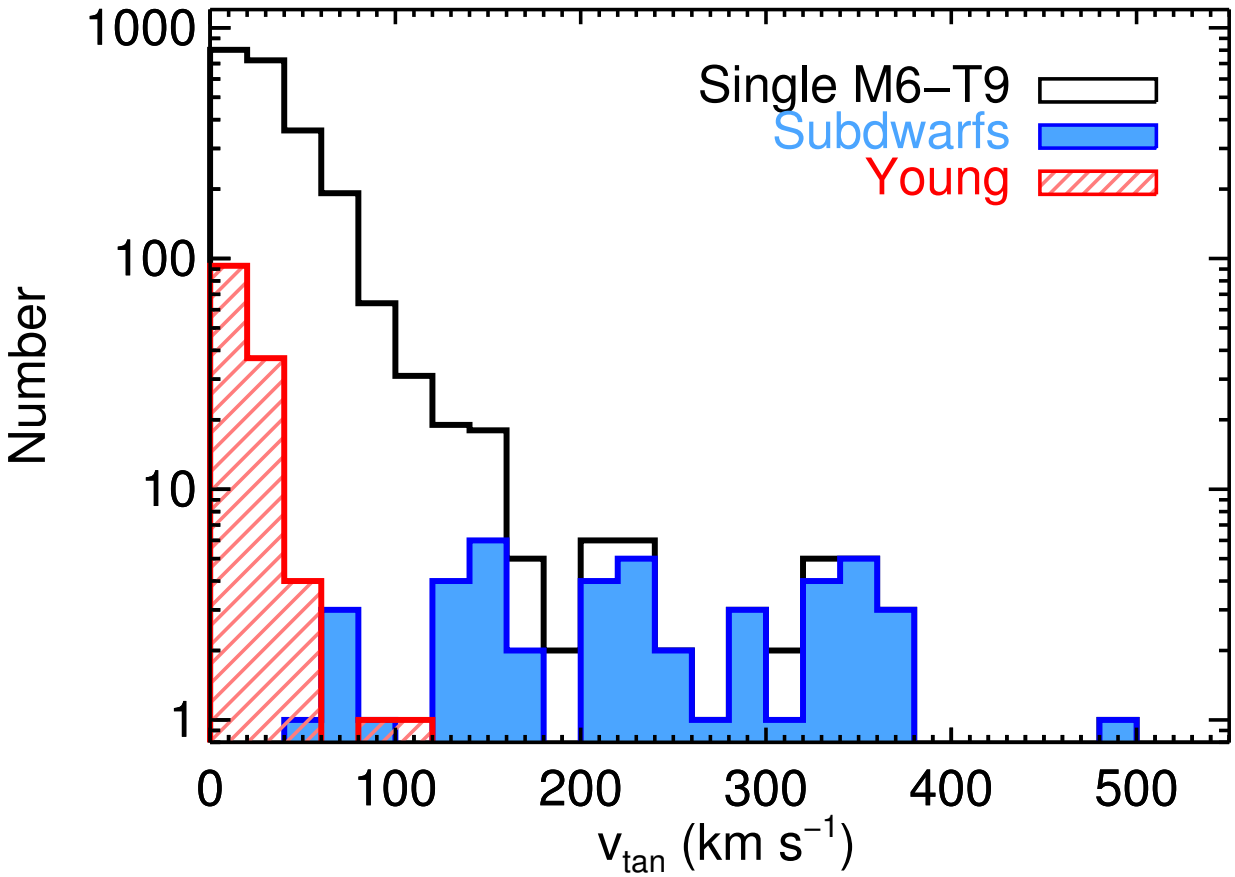

Figure 15. Distribution of tangential velocities for the single M6–T9 dwarfs in our catalog (black outline). Over 90% of objects have $v_{\rm tan} < 75$ km s^{-1} indicating membership in the thin disk population (Dupuy & Liu 2012). The solid blue histogram highlights the subdwarfs in our catalog, which have the high $v_{\rm tan}$ values typical of members of the older thick disk and halo populations. The hatched red histogram shows young objects in our catalog, which typically have smaller $v_{\rm tan}$ values than field-age objects.

F09 and Schmidt et al. (2010, hereinafter S10) used $(J-K_S)_{\rm 2MASS}$ colors, tangential velocities, and velocity dispersions to identify young populations of late-M and L dwarfs with kinematics distinct from the field population. F09 found that red outliers in their sample have lower $v_{\rm tan}$ and $\sigma_{\rm tan}$ (dispersion in $v_{\rm tan}$), while blue outliers have higher $v_{\rm tan}$ and $\sigma_{\rm tan}$. S10 found that this correlation between $(J-K_S)_{\rm 2MASS}$ and velocity dispersion extends throughout the field population. Both studies link the reddest objects to young populations (low-velocity thin disk) and the bluest objects to older populations (thick disk and halo). To examine the relationship between $v_{\rm tan}$ and color differences in our catalog, we use the $\delta_{J-K_S} = ((J-K_S) - (J-K_S)_{med})/\sigma_{J-K_S}$ defined by S10, where $(J-K_S)_{med}$ and σ_{J-K_S} are the median and rms $J-K_S$ colors, respectively, for each spectral type (Table 4). δ_{J-K_S} therefore gives us a spectral type-independent measurement of the extent to which an object's $J-K_S$ color differs from the median, where a negative δ_{J-K_S} value means the object is bluer than the median color.

In Figure 16, we compare $v_{\rm tan}$ to δ_{J-K_S} for single M6–T9 dwarfs. We calculated median $v_{\rm tan}$ values for bins of 1σ in δ_{J-K_S}. We excluded subdwarfs and young objects from the medians in order to assess the color dependence of $v_{\rm tan}$ for the generic ultracool field population. We show these median $v_{\rm tan}$ in Figure 16, and we overplot the subdwarfs and young objects for comparison. The blue outliers are mostly subdwarfs with $v_{\rm tan} > 100$ km s^{-1} while the red outliers are primarily young objects with $v_{\rm tan} < 10$ km s^{-1}, supporting the link between color outliers and age found by F09 and S10. Excluding the subdwarfs and young objects, the field population in our catalog shows a trend toward higher $v_{\rm tan}$ for bluer-than-median objects that is consistent with the $\sigma_{\rm tan}$ trend identified by S10, but we see no correlation between $v_{\rm tan}$ and $J-K_S$ color for redder objects. We also explored whether this trend held true across the full

spectral type range of our sample, because color variations in different spectral types will have different physical causes (e.g., different types of condensate clouds). We calculated the same median $v_{\rm tan}$ values for narrower ranges of spectral type (M6–M9.5, L0–L3.5, L4–L8.5, L9–T3.5, and T4–T9). Figure 16 also shows these medians, which makes clear the that the trend toward higher $v_{\rm tan}$ for bluer field objects is a late-M and L dwarf phenomenon but does not apply to T dwarfs.

We also explored the direct relationship between spectral type and tangential velocity, as any correlation would imply an age trend in ultracool spectral types. Figure 17 shows $v_{\rm tan}$ as a function of spectral type. We include median $v_{\rm tan}$ values for bins of two spectral subtypes, excluding subdwarfs and young objects from the medians but overplotting them for reference. We see no evidence for a dependence of $v_{\rm tan}$ on spectral type for ultracool dwarfs.

5. A BINARY DISCOVERED IN PS1

During outlier inspection we discovered a visual binary resolved for the first time by PS1. 2MASS J09033514−0637336 (hereinafter 2MASS J0903−0637), discovered and assigned a spectral type of M7 by Cruz et al. (2003), is clearly resolved in individual $r_{\rm P1}$, $i_{\rm P1}$, $z_{\rm P1}$, and $y_{\rm P1}$ warp images. Using the $i_{\rm P1}$ warp images, we measure a difference in flux of 0.10 ± 0.03 mag and a separation of 1.14 ± 0.02 arcsec for 2MASS J0903−0637. We detect no change in separation or position angle over the four-year span of the PS1 survey. 2MASS J0903−0637 has a proper motion from PS1 of 63.9 ± 3.4 mas yr^{-1}; if one of the two components were actually a stationary background object, it is likely that we would see a change in the separation and/or orientation of this binary. Using the $i_{\rm P1}$ photometry for 2MASS J0903−0637 and the absolute magnitude for M7 dwarfs from D16, and correcting for a binary with the measured 0.10 mag flux ratio, we calculate a photometric distance of 60.9 ± 5.7 pc. This places the projected binary separation at 69.5 ± 6.6 AU. As expected given the small angular separation, the binary is unresolved in 2MASS and *WISE* images, and therefore was not previously identified as a binary.

6. SUMMARY

We present a catalog of 9,938 M, L, and T dwarfs with photometry and proper motions from the Pan-STARRS1 3π Survey. This catalog contains all known L and T dwarfs as of 2015 December having well-measured photometry in at least one of the five PS1 bands ($g_{\rm P1}r_{\rm P1}i_{\rm P1}z_{\rm P1}y_{\rm P1}$), including 1,257 L dwarfs and 350 T dwarfs. The catalog also contains 457 late-M dwarfs chosen to represent the diversity of the nearby population, including low-gravity objects, high proper motion objects, young moving group members, known or suspected binaries, and wide companions to more massive stars, along with a large sample of 7,874 field M dwarfs identified by SDSS. We cross-matched our catalog with 2MASS and AllWISE to obtain photometry spanning ≈0.55 to 12 μm. We carefully vetted the detections in PS1, 2MASS, and AllWISE to ensure their association with previously identified M, L, and T dwarfs.

We use two types of photometry from PS1 in our catalog: chip photometry (highest accuracy) for most objects and warp photometry (greater depth) for faint, slow-moving objects. We identified a number of false detections (i.e., measurements of background noise) at the warp limiting magnitude for objects in our catalog, and we describe a method for screening warp detections to ensure they are real.

We use the photometry along with parallaxes from the literature to create empirical SEDs for field ultracool dwarfs covering $g_{\rm P1}$ to $W3$ bands. We determine typical colors of M0–T9 dwarfs, and we present numerous color-spectral type and color-color diagrams, along with median colors for each spectral subtype. We separate binaries, young objects, and subdwarfs from the rest of the field population, and we compare the colors of the different groups. Our catalog includes 492 L dwarfs detected in $r_{\rm P1}$, the largest sample of L dwarfs detected in this optical band. $r_{\rm P1}$ L dwarf colors show striking features, including a sharp blueward turn at the M/L transition and a handful of young objects with colors bluer than the average for their spectral type.

We calculate proper motions for our catalog using multiple-epoch astrometry from PS1 along with 2MASS and Gaia when available. Our method allows us to link the epochs of fast-moving objects that are split into more than one "object" in PS1, improving the precision of our proper motions compared to the PS1 database for 89% of the M6 and later dwarfs in our catalog and producing measurements for 64 objects lacking proper motions in PS1. Our catalog contains proper motions for 9,813 objects with a median precision of 3.5 mas yr^{-1}, tied to the Gaia DR1 reference frame. The catalog includes proper motions for a total of 2,394 M6–T9 dwarfs, including 409 objects with no previously published values and 1,140 measurements that improve upon previous literature values. Our catalog incorporates the largest set of homogeneous proper motions for L and T dwarfs published to date.

We assess the kinematics of the late-M, L, and T dwarfs in our sample and find evidence that bluer field-age late-M and L dwarfs (i.e., not subdwarfs) have higher tangential velocities, consistent with the trend towards higher $\sigma_{\rm tan}$ for bluer L dwarfs found by S10. More work is needed using well-defined (i.e., volume-limited) samples with accurate

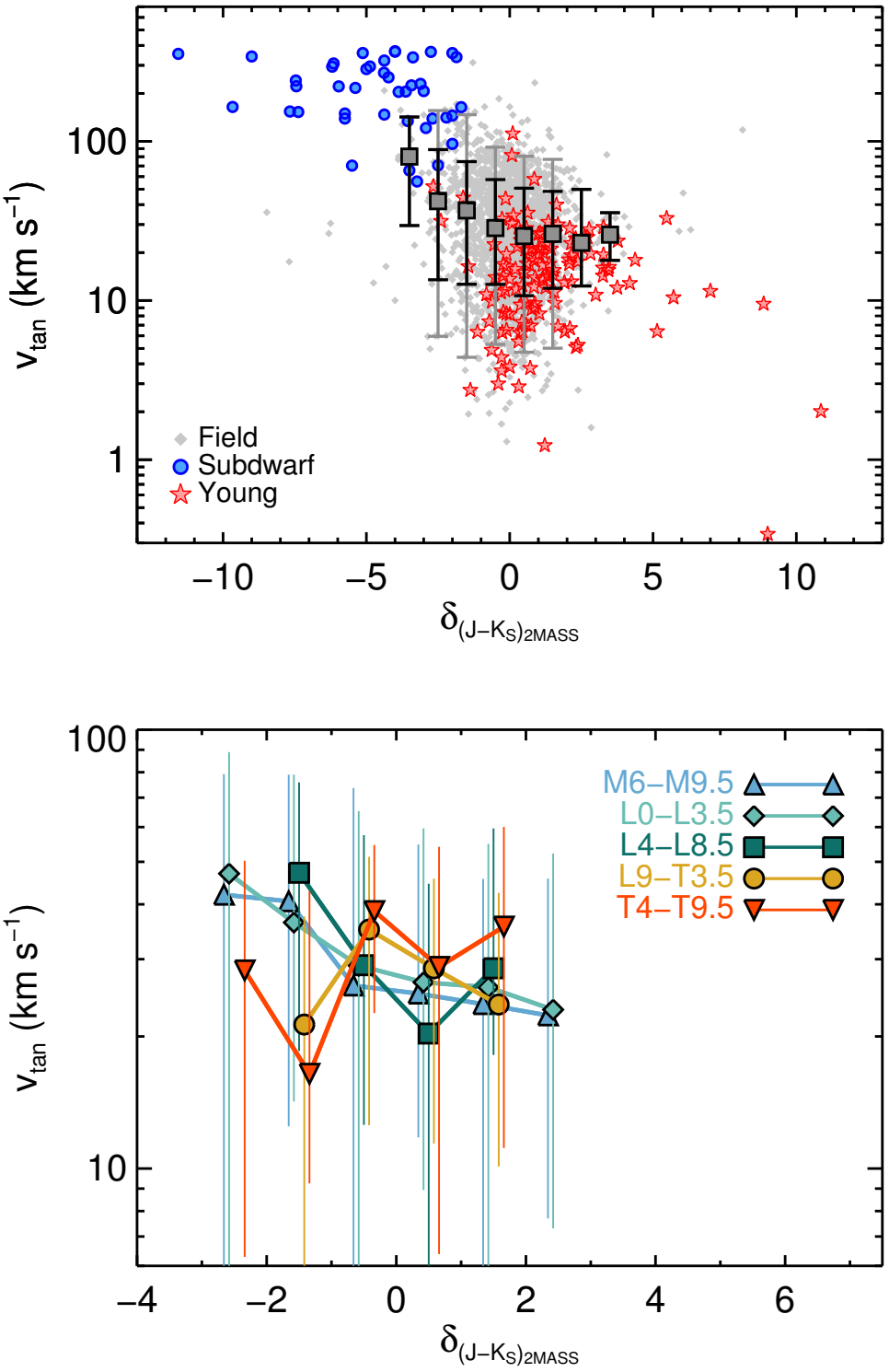

Figure 16. *Top*: Tangential velocity as a function of $\delta_{(J-K_S)_{2MASS}}$ (the number of standard deviations by which an object's $(J-K_S)_{2MASS}$ color differs from the median $(J-K_S)_{2MASS}$ for its spectral type) for single M6–T9 dwarfs. The large gray symbols indicate median v_{tan} values for 1σ bins of δ_{J-K_S}, with dark and light error bars marking 68% and 95% confidence intervals, respectively. The medians do not include subdwarfs or young objects, but we overplot these with blue circles and red stars, respectively, for comparison. The blue end of the field population tends toward higher v_{tan}, but on the red end there is no correlation with v_{tan}. *Bottom*: The same median v_{tan} values for bins of δ_{J-K_S} as in the top plot, split into five spectral type ranges (see legend). The δ_{J-K_S} bins are the same for each spectral type, and the median symbols have been offset slightly for visibility. The colored lines indicate the rms for each δ_{J-K_S} bin. The trend toward higher v_{tan} for bluer objects holds true for the late-M and L dwarfs, but not for T dwarfs

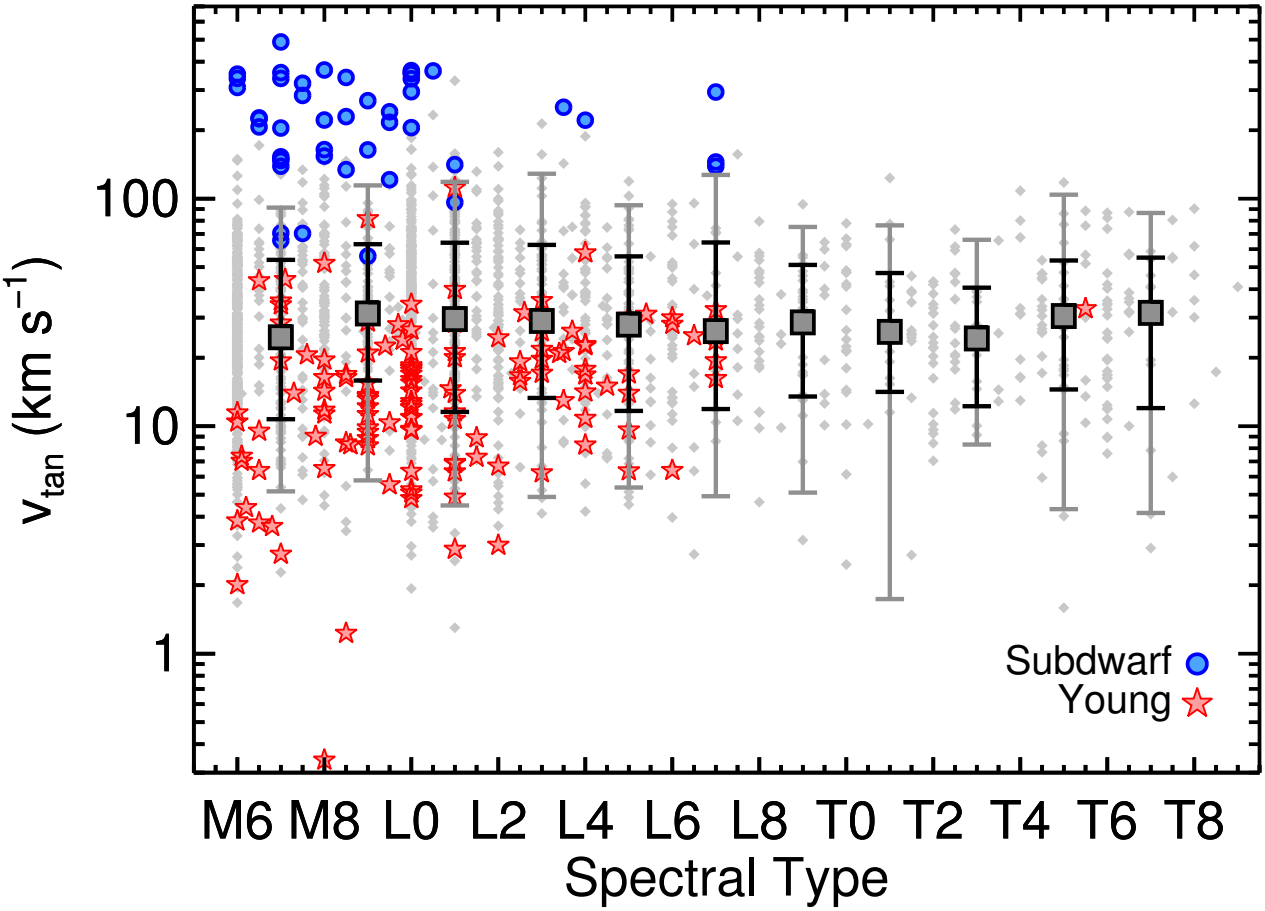

Figure 17. Tangential velocity as a function of spectral type for the single M6–T9 dwarfs in our catalog, using the same format as in Figure 16. Large gray symbols indicate median $v_{\rm tan}$ values for bins of two spectral subtypes, excluding subdwarfs and young objects. We find no correlation between spectral type and $v_{\rm tan}$ in our catalog.

distances to precisely characterize the relationship between colors and kinematics for nearby ultracool dwarfs.

The Pan-STARRS1 Surveys (PS1) have been made possible through contributions of the Institute for Astronomy, the University of Hawaii, the Pan-STARRS Project Office, the Max-Planck Society and its participating institutes, the Max Planck Institute for Astronomy, Heidelberg and the Max Planck Institute for Extraterrestrial Physics, Garching, The Johns Hopkins University, Durham University, the University of Edinburgh, Queen's University Belfast, the Harvard-Smithsonian Center for Astrophysics, the Las Cumbres Observatory Global Telescope Network Incorporated, the National Central University of Taiwan, the Space Telescope Science Institute, the National Aeronautics and Space Administration under Grant No. NNX08AR22G issued through the Planetary Science Division of the NASA Science Mission Directorate, the National Science Foundation under Grant No. AST-1238877, the University of Maryland, Eotvos Lorand University (ELTE), and the Los Alamos National Laboratory. This publication makes use of data products from the Wide-field Infrared Survey Explorer, which is a joint project of the University of California, Los Angeles, and the Jet Propulsion Laboratory/California Institute of Technology, and NEOWISE, which is a project of the Jet Propulsion Laboratory/California Institute of Technology. *WISE* and NEOWISE are funded by the National Aeronautics and Space Administration. This research has made use of the 2MASS data products; the UKIDSS data products; the VISTA data products; NASA's Astrophysical Data System; and the Database of Ultracool Parallaxes, maintained by Trent Dupuy at https://www.cfa.harvard.edu/∼tdupuy/plx. This research has made extensive use of

the SIMBAD and Vizier databases operated at CDS, Strasbourg, France. This work was greatly facilitated by many features of the TOPCAT software written by Mark Taylor (http://www.starlink.ac.uk/topcat/). WMJB received support from NSF grant AST09-09222. WMBJ, MCL, and EAM received support from NSF grant AST-1313455.

Facility: Pan-STARRS1

REFERENCES

Aberasturi, M., Burgasser, A. J., Mora, A., et al. 2014, AJ, 148, 129
Aganze, C., Burgasser, A. J., Faherty, J. K., et al. 2016, AJ, 151, 46
Albert, L., Artigau, E., Delorme, P., et al. 2011, AJ, 141, 203
Allen, P. R., Burgasser, A. J., Faherty, J. K., & Kirkpatrick, J. D. 2012, AJ, 144, 62
Allen, P. R., Koerner, D. W., McElwain, M. W., Cruz, K. L., & Reid, I. N. 2007, AJ, 133, 971
Allen, P. R., Koerner, D. W., Reid, I. N., & Trilling, D. E. 2005, ApJ, 625, 385
Aller, K. M., Kraus, A. L., Liu, M. C., et al. 2013, ApJ, 773, 63
Aller, K. M., Liu, M. C., Magnier, E. A., et al. 2016, ApJ, 821, 120
Allers, K. N., & Liu, M. C. 2013a, ApJ, 772, 79
Allers, K. N., & Liu, M. C. 2013b, in Brown Dwarfs Come of Age, Mem. S.A.It., 84, 1089
Allers, K. N., Liu, M. C., Dupuy, T. J., & Cushing, M. C. 2010, ApJ, 715, 561
Allers, K. N., Liu, M. C., Shkolnik, E. L., et al. 2009, ApJ, 697, 824
Alves de Oliveira, C., Moraux, E., Bouvier, J., et al. 2013, A&A, 549, 123
Andrei, A. H., Smart, R. L., Penna, J. L., et al. 2011, AJ, 141, 54
Artigau, E., Doyon, R., Lafreniere, D., et al. 2006, ApJ, 651, L57
Artigau, E., Lafreniere, D., Doyon, R., et al. 2011, ApJ, 739, 48
Bardalez Gagliuffi, D. C., Gelino, C. R., & Burgasser, A. J. 2015, AJ, 150, 163
Bardalez Gagliuffi, D. C., Burgasser, A. J., Gelino, C. R., et al. 2014, ApJ, 794, 143
Baron, F., Lafreniere, D., Artigau, E., et al. 2015, ApJ, 802, 37
Barrado Y Navascués, D., Zapatero Osorio, M. R., Martín, E. L., et al. 2002, A&A, 393, L85
Bartlett, J. L. 2007, PhD Thesis
Basri, G., Mohanty, S., Allard, F., et al. 2000, ApJ, 538, 363
Beamín, J. C., Minniti, D., Gromadzki, M., et al. 2013, A&A, 557, L8
Becklin, E. E., & Zuckerman, B. 1988, Nature, 336, 656
Béjar, V. J. S., Zapatero Osorio, M. R., Pérez Garrido, A., et al. 2008, ApJ, 673, L185
Bernard, E. J., Ferguson, A. M. N., Schlafly, E. F., et al. 2014, MNRAS, 442, 2999
Bessell, M. S. 1991, AJ, 101, 662
Best, W. M. J., Liu, M. C., Magnier, E. A., et al. 2013, ApJ, 777, 84
—. 2015, ApJ, 814, 118
Bihain, G., Rebolo, R., Zapatero Osorio, M. R., Béjar, V. J. S., & Caballero, J. A. 2010, A&A, 519, 93
Bihain, G., Scholz, R.-D., Storm, J., & Schnurr, O. 2013, A&A, 557, 43
Boeshaar, P. C. 1976, Ph.D. Thesis Ohio State Univ.
Boudreault, S., & Lodieu, N. 2013, MNRAS, 434, 142
Bouvier, J., Kendall, T., Meeus, G., et al. 2008, A&A, 481, 661
Bouy, H., Brandner, W., Martín, E. L., et al. 2003, AJ, 126, 1526
Bowler, B. P., Liu, M. C., & Dupuy, T. J. 2010, ApJ, 710, 45
Bowler, B. P., Liu, M. C., Shkolnik, E. L., & Dupuy, T. J. 2013, ApJ, 774, 55
Burgasser, A. J. 2004, ApJ, 614, L73
—. 2007, AJ, 134, 1330
Burgasser, A. J., Cruz, K. L., Cushing, M., et al. 2010a, ApJ, 710, 1142
Burgasser, A. J., Cruz, K. L., & Kirkpatrick, J. D. 2007, ApJ, 657, 494
Burgasser, A. J., Dhital, S., & West, A. A. 2009a, AJ, 138, 1563
Burgasser, A. J., Geballe, T. R., Leggett, S. K., Kirkpatrick, J. D., & Golimowski, D. A. 2006a, ApJ, 637, 1067
Burgasser, A. J., & Kirkpatrick, J. D. 2006, ApJ, 645, 1485
Burgasser, A. J., Kirkpatrick, J. D., Cruz, K. L., et al. 2006b, ApJS, 166, 585
Burgasser, A. J., Kirkpatrick, J. D., Liebert, J., & Burrows, A. S. 2003a, ApJ, 594, 510
Burgasser, A. J., Kirkpatrick, J. D., & Lowrance, P. J. 2005a, AJ, 129, 2849
Burgasser, A. J., Kirkpatrick, J. D., McElwain, M. W., et al. 2003b, AJ, 125, 850
Burgasser, A. J., Kirkpatrick, J. D., Reid, I. N., et al. 2003c, ApJ, 586, 512
Burgasser, A. J., Liu, M. C., Ireland, M. J., Cruz, K. L., & Dupuy, T. J. 2008a, ApJ, 681, 579
Burgasser, A. J., Looper, D. L., Kirkpatrick, J. D., Cruz, K. L., & Swift, B. J. 2008b, ApJ, 674, 451
Burgasser, A. J., Looper, D. L., & Rayner, J. T. 2010b, AJ, 139, 2448
Burgasser, A. J., Luk, C., Dhital, S., et al. 2012, ApJ, 757, 110
Burgasser, A. J., & McElwain, M. W. 2006, AJ, 131, 1007
Burgasser, A. J., McElwain, M. W., & Kirkpatrick, J. D. 2003d, AJ, 126, 2487
Burgasser, A. J., McElwain, M. W., Kirkpatrick, J. D., et al. 2004, AJ, 127, 2856
Burgasser, A. J., Reid, I. N., Leggett, S. K., et al. 2005b, ApJ, 634, L177
Burgasser, A. J., Sitarski, B. N., Gelino, C. R., Logsdon, S. E., & Perrin, M. D. 2011, ApJ, 739, 49
Burgasser, A. J., Tinney, C. G., Cushing, M. C., et al. 2008c, ApJ, 689, L53
Burgasser, A. J., Witte, S., Helling, C., et al. 2009b, ApJ, 697, 148
Burgasser, A. J., Kirkpatrick, J. D., Brown, M. E., et al. 1999, ApJ, 522, L65
Burgasser, A. J., Wilson, J. C., Kirkpatrick, J. D., et al. 2000a, AJ, 120, 1100
Burgasser, A. J., Kirkpatrick, J. D., Cutri, R. M., et al. 2000b, ApJ, 531, L57
Burgasser, A. J., Kirkpatrick, J. D., Brown, M. E., et al. 2002, ApJ, 564, 421
Burgasser, A. J., Kirkpatrick, J. D., Burrows, A. S., et al. 2003e, ApJ, 592, 1186
Burgasser, A. J., Gillon, M., Melis, C., et al. 2015, AJ, 149, 104
Burgasser, A. J., Lopez, M. A., Mamajek, E. E., et al. 2016, ApJ, 820, 32
Burningham, B., Pinfield, D. J., Lucas, P. W., et al. 2010a, MNRAS, 406, 1885
Burningham, B., Leggett, S. K., Lucas, P. W., et al. 2010b, MNRAS, 404, 1952
Burningham, B., Lucas, P. W., Leggett, S. K., et al. 2011, MNRASL, 414, L90

Burningham, B., Cardoso, C. V., Smith, L., et al. 2013, MNRAS, 433, 457
Burrows, A. S., Sudarsky, D., & Hubeny, I. 2006, ApJ, 640, 1063
Caballero, J. A. 2007, ApJ, 667, 520
Cardoso, C. V., Burningham, B., Smart, R. L., et al. 2015, MNRAS, 450, 2486
Casewell, S. L., Jameson, R. F., & Burleigh, M. R. 2008, MNRAS, 390, 1517
Castro, P. J., & Gizis, J. E. 2012, ApJ, 746, 3
Castro, P. J., Gizis, J. E., Harris, H. C., et al. 2013, ApJ, 776, 126
Chiu, K., Fan, X., Leggett, S. K., et al. 2006, AJ, 131, 2722
Chiu, K., Liu, M. C., Jiang, L., et al. 2008, MNRASL, 385, L53
Close, L. M., Potter, D., Brandner, W., et al. 2002a, ApJ, 566, 1095
Close, L. M., Siegler, N., Freed, M., & Biller, B. 2003, ApJ, 587, 407
Close, L. M., Siegler, N., Potter, D., Brandner, W., & Liebert, J. 2002b, ApJ, 567, L53
Cohen, M., Wheaton, W. A., & Megeath, S. T. 2003, AJ, 126, 1090
Costa, E., Méndez, R. A., Jao, W. C., et al. 2005, AJ, 130, 337
—. 2006, AJ, 132, 1234
Crifo, F., Phan-Bao, N., Delfosse, X., et al. 2005, A&A, 441, 653
Cruz, K. L., Burgasser, A. J., Reid, I. N., & Liebert, J. 2004, ApJ, 604, L61
Cruz, K. L., Kirkpatrick, J. D., & Burgasser, A. J. 2009, AJ, 137, 3345
Cruz, K. L., & Reid, I. N. 2002, AJ, 123, 2828
Cruz, K. L., Reid, I. N., Liebert, J., Kirkpatrick, J. D., & Lowrance, P. J. 2003, AJ, 126, 2421
Cruz, K. L., Reid, I. N., Kirkpatrick, J. D., et al. 2007, AJ, 133, 439
Cushing, M. C., Kirkpatrick, J. D., Gelino, C. R., et al. 2014, AJ, 147, 113
Cushing, M. C., & Vacca, W. D. 2006, AJ, 131, 1797
Cushing, M. C., Kirkpatrick, J. D., Gelino, C. R., et al. 2011, ApJ, 743, 50
Cutri, R. M., Skrutskie, M. F., Van Dyk, S., et al. 2003, VizieR On-line Data Catalog, II/246, 0
—. 2006, Explanatory Supplement to the 2MASS All Sky Data Release
Cutri, R. M., Wright, E. L., Conrow, T., et al. 2014, VizieR On-line Data Catalog, II/328
Dahn, C. C., Liebert, J., & Harrington, R. S. 1986, AJ, 91, 621
Dahn, C. C., Harris, H. C., Vrba, F. J., et al. 2002, AJ, 124, 1170
Dahn, C. C., Harris, H. C., Levine, S. E., et al. 2008, ApJ, 686, 548
Dawson, P., Scholz, A., Ray, T. P., et al. 2014, MNRAS, 442, 1586
Day-Jones, A. C., Marocco, F., Pinfield, D. J., et al. 2013, MNRAS, 430, 1171
Deacon, N. R., & Hambly, N. C. 2007, A&A, 468, 163
Deacon, N. R., Hambly, N. C., & Cooke, J. A. 2005, A&A, 435, 363
Deacon, N. R., Hambly, N. C., King, R. R., & McCaughrean, M. J. 2009, MNRAS, 394, 857
Deacon, N. R., Liu, M. C., Magnier, E. A., et al. 2011, AJ, 142, 77
—. 2012a, ApJ, 755, 94
—. 2012b, ApJ, 757, 100
—. 2014, ApJ, 792, 119
Deacon, N. R., Kraus, A. L., Mann, A. W., et al. 2016, MNRAS, 455, 4212
Delfosse, X., Tinney, C. G., Forveille, T., et al. 1999, A&AS, 135, 41
—. 1997, A&A, 327, L25
Delorme, P., Willott, C. J., Forveille, T., et al. 2008, A&A, 484, 469
Dieterich, S. B., Henry, T. J., Jao, W.-C., et al. 2014, AJ, 147, 94
Dittmann, J. A., Irwin, J. M., Charbonneau, D., & Berta-Thompson, Z. K. 2014, ApJ, 784, 156
Dobbie, P. D., Kenyon, F., Jameson, R. F., et al. 2002, MNRAS, 329, 543
Dupuy, T. J., Forbrich, J., Rizzuto, A., et al. 2016, ApJ, 827, 23
Dupuy, T. J., & Kraus, A. L. 2013, Science, 341, 1492
Dupuy, T. J., & Liu, M. C. 2012, ApJS, 201, 19
Dupuy, T. J., Liu, M. C., & Bowler, B. P. 2009, ApJ, 706, 328
Dupuy, T. J., Liu, M. C., Bowler, B. P., et al. 2010, ApJ, 721, 1725
Dupuy, T. J., Liu, M. C., Leggett, S. K., et al. 2015, ApJ, 805, 56
Epchtein, N., Deul, E., Derriere, S., et al. 1999, A&A, 349, 236
Faherty, J. K., Burgasser, A. J., Cruz, K. L., et al. 2009, AJ, 137, 1
Faherty, J. K., Burgasser, A. J., West, A. A., et al. 2010, AJ, 139, 176
Faherty, J. K., Rice, E. L., Cruz, K. L., Mamajek, E. E., & Núñez, A. 2013, AJ, 145, 2
Faherty, J. K., Burgasser, A. J., Walter, F. M., et al. 2012, ApJ, 752, 56
Faherty, J. K., Riedel, A. R., Cruz, K. L., et al. 2016, ApJS, 225, 10
Fan, X., Knapp, G. R., Strauss, M. A., et al. 2000, AJ, 119, 928
Finch, C. T., & Zacharias, N. 2016, AJ, 151, 160
Folkes, S. L., Pinfield, D. J., Jones, H. R. A., et al. 2012, MNRAS, 427, 3280
Forbrich, J., Dupuy, T. J., Reid, M. J., et al. 2016, ApJ, 827, 22
Forveille, T., Beuzit, J. L., Delorme, P., et al. 2005, A&A, 435, L5
Freed, M., Close, L. M., & Siegler, N. 2003, ApJ, 584, 453
Gagné, J., Burgasser, A. J., Faherty, J. K., et al. 2015a, ApJL, 808, L20
Gagné, J., Lafreniere, D., Doyon, R., et al. 2014a, ApJL, 792, L17
Gagné, J., Lafreniere, D., Doyon, R., Malo, L., & Artigau, E. 2014b, ApJ, 783, 121
—. 2015b, ApJ, 798, 73
Gagné, J., Faherty, J. K., Cruz, K. L., et al. 2015c, ApJS, 219, 33
Gatewood, G., & Coban, L. 2009, AJ, 137, 402
Gauza, B., Bejar, V. J. S., Pérez Garrido, A., et al. 2015, ApJ, 804, 96
Gauza, B., Béjar, V. J. S., Rebolo, R., et al. 2012, MNRAS, 427, 2457
Geballe, T. R., Knapp, G. R., Leggett, S. K., et al. 2002, ApJ, 564, 466
Geißler, K., Metchev, S. A., Kirkpatrick, J. D., Berriman, G. B., & Looper, D. L. 2011, ApJ, 732, 56
Gelino, C. R., Kirkpatrick, J. D., Cushing, M. C., et al. 2011, AJ, 142, 57
Gelino, C. R., Smart, R. L., Marocco, F., et al. 2014, AJ, 148, 6
Giampapa, M. S., & Liebert, J. 1986, ApJ, 305, 784
Giclas, H. L., Burnham, R., & Thomas, N. G. 1967, Bulletin / Lowell Observatory ; no. 138, 7
Gillon, M., Jehin, E., Lederer, S. M., et al. 2016, Nature, 533, 221
Gilmore, G., Reid, I. N., & Hewett, P. 1985, MNRAS, 213, 257
Gizis, J. E. 1997, AJ, 113, 806
—. 2002, ApJ, 575, 484
Gizis, J. E., Allers, K. N., Liu, M. C., et al. 2015, ApJ, 799, 203
Gizis, J. E., Burgasser, A. J., Berger, E., et al. 2013, ApJ, 779, 172
Gizis, J. E., Burgasser, A. J., Faherty, J. K., Castro, P. J., & Shara, M. M. 2011a, AJ, 142, 171
Gizis, J. E., Kirkpatrick, J. D., & Wilson, J. C. 2001, AJ, 121, 2185

Gizis, J. E., Monet, D. G., Reid, I. N., Kirkpatrick, J. D., & Burgasser, A. J. 2000a, MNRAS, 311, 385
Gizis, J. E., Monet, D. G., Reid, I. N., et al. 2000b, AJ, 120, 1085
Gizis, J. E., & Reid, I. N. 1997, PASP, 109, 849
Gizis, J. E., Reid, I. N., Knapp, G. R., et al. 2003, AJ, 125, 3302
Gizis, J. E., Troup, N. W., & Burgasser, A. J. 2011b, ApJL, 736, L34
Gizis, J. E., Faherty, J. K., Liu, M. C., et al. 2012, AJ, 144, 94
Goldman, B., Marsat, S., Henning, T., Clemens, C., & Greiner, J. 2010, MNRAS, 405, 1140
Goldman, B., Röser, S., Schilbach, E., et al. 2013, A&A, 559, A43
Golimowski, D. A., Leggett, S. K., Marley, M. S., et al. 2004, AJ, 127, 3516
Gomes, J. I., Pinfield, D. J., Marocco, F., et al. 2013, MNRAS, 431, 2745
Green, G. M., Schlafly, E. F., Finkbeiner, D. P., et al. 2014, ApJ, 783, 114
Hall, P. B. 2002, ApJ, 564, L89
Hambly, N. C., MacGillivray, H. T., Read, M. A., et al. 2001, MNRAS, 326, 1279
Harrington, R. S., Dahn, C. C., Kallarakal, V. V., et al. 1993, AJ, 105, 1571
Hawley, S. L., Covey, K. R., Knapp, G. R., et al. 2002, AJ, 123, 3409
Henry, T. J., Jao, W.-C., Subasavage, J. P., et al. 2006, AJ, 132, 2360
Henry, T. J., & Kirkpatrick, J. D. 1990, ApJ, 354, L29
Henry, T. J., Subasavage, J. P., Brown, M. A., et al. 2004, AJ, 128, 2460
Høg, E., Fabricius, C., Makarov, V. V., et al. 2000, A&A, 355, L27
Huelamo, N., Ivanov, V. D., Kurtev, R., et al. 2015, A&A, 578, A1
Irwin, M., McMahon, R. G., & Reid, I. N. 1991, MNRAS, 252, 61P
Jameson, R. F., Casewell, S. L., Bannister, N. P., et al. 2008, MNRAS, 384, 1399
Kaiser, N., Burgett, W., Chambers, K., et al. 2010, Proc. SPIE, 7733, 12
Kellogg, K., Metchev, S. A., Gagné, J., & Faherty, J. 2016, ApJL, 821, L15
Kellogg, K., Metchev, S. A., Geißler, K., et al. 2015, AJ, 150, 182
Kendall, T. R., Delfosse, X., Martín, E. L., & Forveille, T. 2004, A&A, 416, L17
Kendall, T. R., Jones, H. R. A., Pinfield, D. J., et al. 2007a, MNRAS, 374, 445
Kendall, T. R., Mauron, N., Azzopardi, M., & Gigoyan, K. 2003, A&A, 403, 929
Kendall, T. R., Tamura, M., Tinney, C. G., et al. 2007b, A&A, 466, 1059
Kirkpatrick, J. D. 2005, ARAA, 43, 195
Kirkpatrick, J. D., Beichman, C. A., & Skrutskie, M. F. 1997a, ApJ, 476, 311
Kirkpatrick, J. D., Dahn, C. C., Monet, D. G., et al. 2001a, AJ, 121, 3235
Kirkpatrick, J. D., Henry, T. J., & Irwin, M. J. 1997b, AJ, 113, 1421
Kirkpatrick, J. D., Henry, T. J., & Liebert, J. 1993, ApJ, 406, 701
Kirkpatrick, J. D., Henry, T. J., & McCarthy, D. W. J. 1991, ApJS, 77, 417
Kirkpatrick, J. D., Henry, T. J., & Simons, D. A. 1995, AJ, 109, 797
Kirkpatrick, J. D., Liebert, J., Cruz, K. L., Gizis, J. E., & Reid, I. N. 2001b, PASP, 113, 814
Kirkpatrick, J. D., McGraw, J. T., Hess, T. R., Liebert, J., & McCarthy, D. W. J. 1994, ApJS, 94, 749
Kirkpatrick, J. D., Reid, I. N., Liebert, J., et al. 1999, ApJ, 519, 802
—. 2000, AJ, 120, 447
Kirkpatrick, J. D., Cruz, K. L., Barman, T. S., et al. 2008, ApJ, 689, 1295
Kirkpatrick, J. D., Looper, D. L., Burgasser, A. J., et al. 2010, ApJS, 190, 100
Kirkpatrick, J. D., Cushing, M. C., Gelino, C. R., et al. 2011, ApJS, 197, 19
Kirkpatrick, J. D., Gelino, C. R., Cushing, M. C., et al. 2012, ApJ, 753, 156
Kirkpatrick, J. D., Schneider, A. C., Fajardo-Acosta, S., et al. 2014, ApJ, 783, 122
Kirkpatrick, J. D., Kellogg, K., Schneider, A. C., et al. 2016, ApJS, 224, 36
Knapp, G. R., Leggett, S. K., Fan, X., et al. 2004, AJ, 127, 3553
Koen, C. 2013, MNRAS, 428, 2824
Koerner, D. W., Kirkpatrick, J. D., McElwain, M. W., & Bonaventura, N. R. 1999, ApJ, 526, L25
Kraus, A. L., & Hillenbrand, L. A. 2009, ApJ, 703, 1511
Lachapelle, F.-R., Lafreniere, D., Gagné, J., et al. 2015, ApJ, 802, 61
Law, N. M., Hodgkin, S. T., & Mackay, C. D. 2006, MNRAS, 368, 1917
Lawrence, A., Warren, S. J., Almaini, O., et al. 2007, MNRAS, 379, 1599
—. 2012, VizieR On-line Data Catalog, II/314, 0
Leggett, S. K. 1992, ApJS, 82, 351
Leggett, S. K., Allard, F., Berriman, G., Dahn, C. C., & Hauschildt, P. H. 1996, ApJS, 104, 117
Leggett, S. K., Geballe, T. R., Fan, X., et al. 2000, ApJ, 536, L35
Leggett, S. K., Golimowski, D. A., Fan, X., et al. 2002, ApJ, 564, 452
Leggett, S. K., Saumon, D., Marley, M. S., et al. 2012, ApJ, 748, 74
Leinert, C., Weitzel, N., Richichi, A., Eckart, A., & Tacconi-Garman, L. E. 1994, A&A, 291, L47
Lépine, S., & Gaidos, E. 2011, AJ, 142, 138
Lépine, S., Rich, R. M., Neill, J. D., Caulet, A., & Shara, M. M. 2002a, ApJ, 581, L47
Lépine, S., Rich, R. M., & Shara, M. M. 2003a, ApJ, 591, L49
—. 2003b, AJ, 125, 1598
Lépine, S., & Shara, M. M. 2005, AJ, 129, 1483
Lépine, S., Shara, M. M., & Rich, R. M. 2002b, AJ, 124, 1190
—. 2003c, ApJ, 585, L69
Lépine, S., Thorstensen, J. R., Shara, M. M., & Rich, R. M. 2009, AJ, 137, 4109
Liebert, J., Dahn, C. C., Gresham, M., & Strittmatter, P. A. 1979, ApJ, 233, 226
Liebert, J., & Gizis, J. E. 2006, PASP, 118, 659
Liebert, J., Kirkpatrick, J. D., Cruz, K. L., et al. 2003, AJ, 125, 343
Lindegren, L., Lammers, U., Bastian, U., et al. 2016, A&A, 595, A4
Liu, M. C., Dupuy, T. J., & Allers, K. N. 2013a, Astronomische Nachrichten, 334, 85
—. 2016, ApJ, 833, 96
Liu, M. C., Dupuy, T. J., & Leggett, S. K. 2010, ApJ, 722, 311
Liu, M. C., & Leggett, S. K. 2005, ApJ, 634, 616
Liu, M. C., Leggett, S. K., Golimowski, D. A., et al. 2006, ApJ, 647, 1393
Liu, M. C., Wainscoat, R., Martín, E. L., Barris, B., & Tonry, J. L. 2002, ApJ, 568, L107
Liu, M. C., Deacon, N. R., Magnier, E. A., et al. 2011, ApJL, 740, L32

Liu, M. C., Magnier, E. A., Deacon, N. R., et al. 2013b, ApJL, 777, L20
Lodieu, N. 2013, MNRAS, 431, 3222
Lodieu, N., Boudreault, S., & Béjar, V. J. S. 2014, MNRAS, 445, 3908
Lodieu, N., Deacon, N. R., & Hambly, N. C. 2012a, MNRAS, 422, 1495
Lodieu, N., Dobbie, P. D., Cross, N. J. G., et al. 2013, MNRAS, 435, 2474
Lodieu, N., Espinoza Contreras, M., Zapatero Osorio, M. R., et al. 2012b, A&A, 542, 105
Lodieu, N., Hambly, N. C., & Jameson, R. F. 2006, MNRAS, 373, 95
Lodieu, N., Hambly, N. C., Jameson, R. F., & Hodgkin, S. T. 2008, MNRAS, 383, 1385
Lodieu, N., Hambly, N. C., Jameson, R. F., et al. 2007a, MNRAS, 374, 372
Lodieu, N., Scholz, R.-D., & McCaughrean, M. J. 2002, A&A, 389, L20
Lodieu, N., Scholz, R.-D., McCaughrean, M. J., et al. 2005, A&A, 440, 1061
Lodieu, N., Zapatero Osorio, M. R., Martín, E. L., Solano, E., & Aberasturi, M. 2010, ApJL, 708, L107
Lodieu, N., Zapatero Osorio, M. R., Rebolo, R., Martín, E. L., & Hambly, N. C. 2009, A&A, 505, 1115
Lodieu, N., Pinfield, D. J., Leggett, S. K., et al. 2007b, MNRAS, 379, 1423
Lodieu, N., Burningham, B., Day-Jones, A. C., et al. 2012c, A&A, 548, 53
Looper, D. L., Kirkpatrick, J. D., & Burgasser, A. J. 2007, AJ, 134, 1162
Looper, D. L., Kirkpatrick, J. D., Cutri, R. M., et al. 2008, ApJ, 686, 528
Loutrel, N. P., Luhman, K. L., Lowrance, P. J., & Bochanski, J. J. 2011, ApJ, 739, 81
Lucas, P. W., Tinney, C. G., Burningham, B., et al. 2010, MNRASL, 408, L56
Luhman, K. L. 2013, ApJL, 767, L1
—. 2014, ApJ, 786, L18
Luhman, K. L., Mamajek, E. E., Allen, P. R., & Cruz, K. L. 2009, ApJ, 703, 399
Luhman, K. L., & Sheppard, S. S. 2014, ApJ, 787, 126
Luhman, K. L., Patten, B. M., Marengo, M., et al. 2007, ApJ, 654, 570
Luhman, K. L., Loutrel, N. P., McCurdy, N. S., et al. 2012, ApJ, 760, 152
Luyten, W. J. 1979, A Catalogue of Stars with Proper Motions Exceeding 0"2 Annually (NLTT Catalogue) (Minneapolis: Univ. Minnesota)
Mace, G. N. 2014, ProQuest Dissertations and Theses, 75-09(E), 1
Mace, G. N., Kirkpatrick, J. D., Cushing, M. C., et al. 2013, ApJS, 205, 6
Magnier, E. A., Schlafly, E., Finkbeiner, D., et al. 2013, ApJS, 205, 20
Manjavacas, E., Goldman, B., Reffert, S., & Henning, T. 2013, A&A, 560, 52
Marocco, F., Smart, R. L., Jones, H. R. A., et al. 2010, A&A, 524, 38
Marocco, F., Andrei, A. H., Smart, R. L., et al. 2013, AJ, 146, 161
Marocco, F., Jones, H. R. A., Day-Jones, A. C., et al. 2015, MNRAS, 449, 3651
Marsh, K. A., Wright, E. L., Kirkpatrick, J. D., et al. 2013, ApJ, 762, 119
Marshall, J. L. 2008, AJ, 135, 1000
Martín, E. L., Basri, G., Zapatero Osorio, M. R., Rebolo, R., & García López, R. J. 1998, ApJ, 507, L41
Martín, E. L., Brandner, W., & Basri, G. 1999a, Science, 283, 1718
Martín, E. L., Brandner, W., Bouvier, J., et al. 2000, ApJ, 543, 299
Martín, E. L., Delfosse, X., Basri, G., et al. 1999b, AJ, 118, 2466
Martín, E. L., Rebolo, R., & Magazzu, A. 1994, ApJ, 436, 262
Martín, E. L., Phan-Bao, N., Bessell, M., et al. 2010, A&A, 517, 53
Matsuoka, Y., Peterson, B. A., Murata, K. L., et al. 2011, AJ, 142, 64
McCarthy, M. F., Bertiau, F. C., & Treanor, P. J. 1964, Ricerche Astronomiche, 6, 571
McCaughrean, M. J., Close, L. M., Scholz, R.-D., et al. 2004, A&A, 413, 1029
McCaughrean, M. J., Scholz, R.-D., & Lodieu, N. 2002, A&A, 390, L27
McElwain, M. W., & Burgasser, A. J. 2006, AJ, 132, 2074
McGovern, M. R., Kirkpatrick, J. D., McLean, I. S., et al. 2004, ApJ, 600, 1020
Metchev, S. A., Kirkpatrick, J. D., Berriman, G. B., & Looper, D. L. 2008, ApJ, 676, 1281
Mohanty, S., & Basri, G. 2003, ApJ, 583, 451
Monet, D. G., Dahn, C. C., Vrba, F. J., et al. 1992, AJ, 103, 638
Monet, D. G., Levine, S. E., Canzian, B., et al. 2003, AJ, 125, 984
Montagnier, G., Ségransan, D., Beuzit, J. L., et al. 2006, A&A, 460, L19
Mugrauer, M., Seifahrt, A., Neuhäuser, R., & Mazeh, T. 2006, MNRASL, 373, L31
Murray, D. N., Burningham, B., Jones, H. R. A., et al. 2011, MNRAS, 414, 575
Muzic, K., Radigan, J., Jayawardhana, R., et al. 2012, AJ, 144, 180
Phan-Bao, N. 2011, Astronomische Nachrichten, 332, 668
Phan-Bao, N., & Bessell, M. S. 2006, A&A, 446, 515
Phan-Bao, N., Guibert, J., Crifo, F., et al. 2001, A&A, 380, 590
Phan-Bao, N., Bessell, M. S., Martín, E. L., et al. 2006, MNRASL, 366, L40
—. 2008, MNRAS, 383, 831
Pineda, J. S., Hallinan, G., Kirkpatrick, J. D., et al. 2016, ApJ, 826, 73
Pinfield, D. J., Burningham, B., Tamura, M., et al. 2008, MNRAS, 390, 304
Pokorny, R. S., Jones, H. R. A., Hambly, N. C., & Pinfield, D. J. 2004, A&A, 421, 763
Pope, B., Martinache, F., & Tuthill, P. 2013, ApJ, 767, 110
Probst, R. G., & Liebert, J. 1983, ApJ, 274, 245
Radigan, J., Jayawardhana, R., Lafreniere, D., et al. 2013, ApJ, 778, 36
Radigan, J., Lafreniere, D., Jayawardhana, R., & Doyon, R. 2008, ApJ, 689, 471
Rebolo, R., Zapatero Osorio, M. R., Madruga, S., et al. 1998, Science, 282, 1309
Reid, I. N. 2003, AJ, 126, 2449
Reid, I. N., & Cruz, K. L. 2002, AJ, 123, 2806
Reid, I. N., Cruz, K. L., & Allen, P. R. 2007, AJ, 133, 2825
Reid, I. N., Cruz, K. L., Kirkpatrick, J. D., et al. 2008, AJ, 136, 1290
Reid, I. N., & Gilmore, G. 1981, MNRAS, 196, 15P
Reid, I. N., & Gizis, J. E. 2005, PASP, 117, 676
Reid, I. N., Gizis, J. E., Kirkpatrick, J. D., & Koerner, D. W. 2001, AJ, 121, 489
Reid, I. N., Hawley, S. L., & Gizis, J. E. 1995, AJ, 110, 1838
Reid, I. N., Kirkpatrick, J. D., Gizis, J. E., et al. 2000, AJ, 119, 369

Reid, I. N., Kirkpatrick, J. D., Liebert, J., et al. 2002, AJ, 124, 519
Reid, I. N., Lewitus, E., Allen, P. R., Cruz, K. L., & Burgasser, A. J. 2006a, AJ, 132, 891
Reid, I. N., Lewitus, E., Burgasser, A. J., & Cruz, K. L. 2006b, ApJ, 639, 1114
Reid, I. N., & Walkowicz, L. M. 2006, PASP, 118, 671
Reid, I. N., Cruz, K. L., Laurie, S. P., et al. 2003a, AJ, 125, 354
Reid, I. N., Cruz, K. L., Allen, P., et al. 2003b, AJ, 126, 3007
—. 2004, AJ, 128, 463
Reiners, A., & Basri, G. 2006, AJ, 131, 1806
Reylé, C., & Robin, A. C. 2004, A&A, 421, 643
Rice, E. L., Faherty, J. K., & Cruz, K. L. 2010, ApJL, 715, L165
Riedel, A. R., Finch, C. T., Henry, T. J., et al. 2014, AJ, 147, 85
Rodono, M., Ciatti, F., & Vittone, A. 1980, AJ, 85, 298
Rodriguez, D. R., Zuckerman, B., Kastner, J. H., et al. 2013, ApJ, 774, 101
Roeser, S., Demleitner, M., & Schilbach, E. 2010, AJ, 139, 2440
Ruiz, M. T., Leggett, S. K., & Allard, F. 1997, ApJ, 491, L107
Ruiz, M. T., Wischnjewsky, M., Rojo, P. M., & Gonzalez, L. E. 2001, ApJS, 133, 119
Sahlmann, J., Lazorenko, P. F., Bouy, H., et al. 2016, MNRAS, 455, 357
Sahlmann, J., Lazorenko, P. F., Ségransan, D., et al. 2014, A&A, 565, A20
—. 2015, A&A, 577, A15
Salim, S., & Gould, A. 2003, ApJ, 582, 1011
Salim, S., Lépine, S., Rich, R. M., & Shara, M. M. 2003, ApJ, 586, L149
Saumon, D., & Marley, M. S. 2008, ApJ, 689, 1327
Schilbach, E., Röser, S., & Scholz, R.-D. 2009, A&A, 493, L27
Schlafly, E. F., Finkbeiner, D. P., Juric, M., et al. 2012, ApJ, 756, 158
Schlafly, E. F., Green, G., Finkbeiner, D. P., et al. 2014, ApJ, 789, 15
Schlieder, J. E., Bonnefoy, M., Herbst, T. M., et al. 2014, ApJ, 783, 27
Schmidt, S. J., Cruz, K. L., Bongiorno, B. J., Liebert, J., & Reid, I. N. 2007, AJ, 133, 2258
Schmidt, S. J., Hawley, S. L., West, A. A., et al. 2015, AJ, 149, 158
Schmidt, S. J., West, A. A., Hawley, S. L., & Pineda, J. S. 2010, AJ, 139, 1808
Schneider, A. C., Cushing, M. C., Kirkpatrick, J. D., et al. 2014, AJ, 147, 34
Schneider, A. C., Greco, J., Cushing, M. C., et al. 2016a, ApJ, 817, 112
Schneider, A. C., Melis, C., Song, I., & Zuckerman, B. 2011, ApJ, 743, 109
Schneider, A. C., Windsor, J., Cushing, M. C., Kirkpatrick, J. D., & Wright, E. L. 2016b, ApJL, 822, L1
Schneider, D. P., Greenstein, J. L., Schmidt, M., & Gunn, J. E. 1991, AJ, 102, 1180
Schneider, D. P., Knapp, G. R., Hawley, S. L., et al. 2002, AJ, 123, 458
Scholz, R.-D. 2010a, A&A, 515, 92
—. 2010b, A&A, 510, L8
—. 2014, A&A, 561, 113
Scholz, R.-D., Bihain, G., Schnurr, O., & Storm, J. 2011, A&A, 532, L5
—. 2012, A&A, 541, 163
Scholz, R.-D., Bihain, G., & Storm, J. 2014, A&A, 567, A43
Scholz, R.-D., Lehmann, I., Matute, I., & Zinnecker, H. 2004a, A&A, 425, 519
Scholz, R.-D., Lodieu, N., & McCaughrean, M. J. 2004b, A&A, 428, L25
Scholz, R.-D., & Meusinger, H. 2002, MNRAS, 336, L49
Scholz, R.-D., Meusinger, H., & Jahreiss, H. 2001, A&A, 374, L12
Scholz, R.-D., Storm, J., Knapp, G. R., & Zinnecker, H. 2009, A&A, 494, 949
Schweitzer, A., Scholz, R.-D., Stauffer, J., Irwin, M., & McCaughrean, M. J. 1999, A&A, 350, L62
Seifahrt, A., Reiners, A., Almaghrbi, K. A. M., & Basri, G. 2010, A&A, 512, A37
Sheppard, S. S., & Cushing, M. C. 2009, AJ, 137, 304
Shkolnik, E. L., Anglada-Escudé, G., Liu, M. C., et al. 2012, ApJ, 758, 56
Shkolnik, E. L., Liu, M. C., & Reid, I. N. 2009, ApJ, 699, 649
Siegler, N., Close, L. M., Burgasser, A. J., et al. 2007, AJ, 133, 2320
Siegler, N., Close, L. M., Cruz, K. L., Martín, E. L., & Reid, I. N. 2005, ApJ, 621, 1023
Siegler, N., Close, L. M., Mamajek, E. E., & Freed, M. 2003, ApJ, 598, 1265
Silvestri, N. M., Lemagie, M. P., Hawley, S. L., et al. 2007, AJ, 134, 741
Sivarani, T., Lépine, S., Kembhavi, A. K., & Gupchup, J. 2009, ApJL, 694, L140
Skrutskie, M. F., Cutri, R. M., Stiening, R., et al. 2006, AJ, 131, 1163
Skrzypek, N., Warren, S. J., Faherty, J. K., et al. 2015, A&A, 574, A78
Smart, R. L., Tinney, C. G., Bucciarelli, B., et al. 2013, MNRAS, 433, 2054
Smith, L., Lucas, P. W., Burningham, B., et al. 2014a, MNRAS, 437, 3603
Smith, L., Lucas, P. W., Bunce, R., et al. 2014b, MNRAS, 443, 2327
Stern, D., Kirkpatrick, J. D., Allen, L. E., et al. 2007, ApJ, 663, 677
Stone, J. M., Skemer, A. J., Kratter, K. M., et al. 2016, ApJL, 818, L12
Strauss, M. A., Fan, X., Gunn, J. E., et al. 1999, ApJ, 522, L61
Stumpf, M. B., Brandner, W., Bouy, H., Henning, T., & Hippler, S. 2010, A&A, 516, 37
Stumpf, M. B., Brandner, W., Köhler, R., Bouy, H., & Henning, T. 2009, COOL STARS, 1094, 561
Stumpf, M. B., Geißler, K., Bouy, H., et al. 2011, A&A, 525, 123
Theissen, C. A., & West, A. A. 2014, ApJ, 794, 146
Theissen, C. A., West, A. A., & Dhital, S. 2016, AJ, 151, 41
Thompson, M. A., Kirkpatrick, J. D., Mace, G. N., et al. 2013, PASP, 125, 809
Thorstensen, J. R., & Kirkpatrick, J. D. 2003, PASP, 115, 1207
Tinney, C. G. 1993a, ApJ, 414, 279
—. 1993b, AJ, 105, 1169
—. 1996, MNRAS, 281, 644
Tinney, C. G., Burgasser, A. J., & Kirkpatrick, J. D. 2003, AJ, 126, 975
Tinney, C. G., Burgasser, A. J., Kirkpatrick, J. D., & McElwain, M. W. 2005, AJ, 130, 2326
Tinney, C. G., Delfosse, X., Forveille, T., & Allard, F. 1998, A&A, 338, 1066
Tinney, C. G., Mould, J. R., & Reid, I. N. 1993, AJ, 105, 1045
Tinney, C. G., Reid, I. N., Gizis, J. E., & Mould, J. R. 1995, AJ, 110, 3014
Tonry, J. L., Stubbs, C. W., Lykke, K. R., et al. 2012, ApJ, 750, 99
Tremblin, P., Amundsen, D. S., Chabrier, G., et al. 2016, ApJL, 817, L19
Tsvetanov, Z. I., Golimowski, D. A., Zheng, W., et al. 2000, ApJ, 531, L61
van Altena, W. F., Lee, J. T., & Hoffleit, E. D., eds. 1995, The General Catalogue of Trigonometric [Stellar] Parallaxes (New haven, CT: Yale University Observatory)

van Biesbroeck, G. 1961, AJ, 66, 528
van Leeuwen, F. 2007, A&A, 474, 653
Vrba, F. J., Henden, A. A., Luginbuhl, C. B., et al. 2004, AJ, 127, 2948
Wang, P. F., Chen, W. P., Lin, C. C., et al. 2014a, ApJ, 784, 57
Wang, Y., Jones, H. R. A., Smart, R. L., et al. 2014b, PASP, 126, 15
Weinberger, A. J., Boss, A. P., Keiser, S. A., et al. 2016, AJ, 152, 24
West, A. A., Hawley, S. L., Bochanski, J. J., et al. 2008, AJ, 135, 785
Wilson, J. C., Kirkpatrick, J. D., Gizis, J. E., et al. 2001, AJ, 122, 1989
Wilson, J. C., Miller, N. A., Gizis, J. E., et al. 2003, in IAU Symp. 211, Brown Dwarfs, ed. E. L. Martín (San Francisco: ASP), 197
Wright, E. L., Eisenhardt, P. R. M., Mainzer, A. K., et al. 2010, AJ, 140, 1868
Wright, E. L., Skrutskie, M. F., Kirkpatrick, J. D., et al. 2013, AJ, 145, 84
York, D. G., Adelman, J., Anderson, J. E. J., et al. 2000, AJ, 120, 1579
Zapatero Osorio, M. R., Béjar, V. J. S., Martín, E. L., et al. 2000, Science, 290, 103
Zapatero Osorio, M. R., Béjar, V. J. S., Miles-Páez, P. A., et al. 2014, A&A, 568, 6
Zapatero Osorio, M. R., Béjar, V. J. S., Rebolo, R., Martín, E. L., & Basri, G. 1999, ApJ, 524, L115
Zhang, Z. H., Pokorny, R. S., Jones, H. R. A., et al. 2009, A&A, 497, 619
Zhang, Z. H., Pinfield, D. J., Day-Jones, A. C., et al. 2010, MNRAS, 404, 1817
Zhang, Z. H., Pinfield, D. J., Burningham, B., et al. 2013, MNRAS, 434, 1005